

UNIVERSITÀ DEGLI STUDI DI BERGAMO

DOCTORAL THESIS

Thermalisation of a coupled pendulum chain

Author:

Marta GRESELIN

Tutor:

Prof. Giovanni SALES

Co-tutor:

Prof. Roberto LEPORINI

*A thesis submitted in fulfillment of the requirements
for the degree of Doctor of Philosophy*

in the

Engineering and Applied Sciences

Università degli Studi di Bergamo

Abstract

Faculty Name
Engineering and Applied Sciences

Doctor of Philosophy

Thermalisation of a coupled pendulum chain

by Marta GRESELIN

Coupled pendula show complex and unpredictable collective motions and provide a suitable physical model for complex dynamical systems. Starting from the well-known Fermi-Pasta-Ulam experiment non-linearly coupled oscillators are expected to undergo spontaneous thermalisation, typical of multi-body systems with non-linear interactions, and have been studied in order to investigate energy equipartition and second principle of thermodynamics. By means of an automated video-tracking apparatus we have monitored both single and collective motions occurring in a chain of 24 non-linearly coupled pendula on varying the initial conditions (anharmonicity level, number and energy of excited pendula, etc.). Compared to the original FPU model our chain is highly and quickly dissipative and thermalises very early. The energy metric Ω [13], which is an indicator of the ergodic entropy, was studied: after an initial transitory phase, it decays as t^{-2} in all different initial configurations we investigated. Moreover, we have observed other noticeable phenomena, e.g. some chaotic behaviour and intrinsic localised modes.

Acknowledgements

Desidero ringraziare il prof. Salesi per avermi dato questa preziosa opportunità di crescita personale e professionale e tutte le persone che si sono spese concretamente per aiutarmi nel frattempo, anche nel compito di mamma.

Contents

Abstract	iii
Acknowledgements	v
1 Introduction to FPU	1
1.1 Objective and purpose of the present Thesis	1
1.2 The FPU problem	2
1.3 The FPU model	4
1.3.1 Connection to the KdV equation	5
1.3.2 Modal energy in FPU model	6
1.3.3 The paradox	6
1.3.4 Energy thresholds: Izrailev and Chirikov	7
1.3.5 Plank-like distributions: Bocchieri, Scotti and Loinger	7
1.3.6 Relaxation times	8
1.3.7 Critical specific energy and the “natural packet”	8
1.3.8 Latest findings	9
1.4 Second law of thermodynamics and equipartition theorem	10
1.5 Main steps of the experimental project	11
1.6 Thesis plan	12
2 Small oscillations	13
2.1 Introduction	13
2.2 Free oscillations	13
2.3 Forced oscillations	15
2.4 Damped oscillations	16
2.5 Forced damped oscillations	18
2.6 Anharmonic oscillations	18
3 Small oscillations for coupled pendula	21
3.1 Coupled pendula	21
3.1.1 Normal modes	22
3.1.2 Beats	22
3.2 Coupled pendula with external springs	23
3.3 Coupled pendula with discretised cable	24
4 Methods and Material	25
4.1 Mechanical system	25
4.2 Releasing mechanism	26
4.3 VideoTracking procedure	28
4.3.1 Video recording	28
4.3.2 Video editing	29
4.3.3 Video tracking	29

4.3.4	Data processing	30
4.4	Measurement protocol	32
5	Experimental results	33
5.1	Displacement x as a function of t	33
5.2	Chaos outbreak	43
5.3	Ω as a function of t	46
5.4	Envelopes of the time evolution	50
5.5	Horizontal analysis: amplitude	54
5.6	Fourier analysis	56
6	Physical interpretation of the results	67
6.1	Measurements	67
6.2	Time evolution of pendulum displacement	67
6.3	Omega	68
6.3.1	Thermalization and dissipation	70
6.4	Dissipation	70
6.5	Fourier Analysis	73
6.6	Relaxation time	75
6.7	Horizontal Analysis	76
6.8	Chaos	77
7	Conclusions	79
7.1	Summary	79
7.2	Further research	81
Appendix A	Equipment specifications	83
A.1	EclipseMagnetic M52172/24VDC datasheet	83
A.2	Mean Well RS-100-24 power supply datasheet	84
A.3	GoPro Hero4 Black datasheet	85
Appendices		83
Appendix B	SphereTracking Software	87
B.1	file AutoColorFilter.cpp	87
B.2	file Sphere.cpp	91
B.3	file Sphere.h (to be included for the compilation in C code)	93
Appendix C	Mathematica code	95
C.1	Load data	95
C.2	Potential energy U , mechanical energy E , energy metrics Ω	98
C.3	Plots export	99
C.4	Fourier analysis	99
References		104

List of Figures

1.1	energy plot for an α -model with 32 masses	3
1.2	ILM	4
3.1	coupled pendula	21
3.2	beats	23
3.3	time evolution of Ω	23
4.1	<i>24 coupled pendula</i>	25
4.2	<i>System sketch</i>	26
4.3	<i>Equipment sketch</i>	27
4.4	<i>Releasing mechanism</i>	27
4.5	<i>Example frame of the output file of the videotracking algorithm</i>	30
4.6	<i>Sphere detection order with a Logitech webcam recording video</i>	31
4.7	<i>The plot represents the trajectories of the 24 spheres, with as many 3rd order polinomial</i>	32
5.1	P08 50°: normalised displacement	33
5.2	P08 50°: normalised displacement	34
5.3	P08 50°: normalised displacements	35
5.4	P08 50°: normalised displacements	36
5.5	P08 10°: normalised displacements	37
5.6	P08 10°: normalised displacements	38
5.7	P08 10°: normalised displacements	39
5.8	P06-12-18 50°: normalised displacements	40
5.9	P06-12-18 50°: normalised displacements	41
5.10	P06-12-18 50°: normalised displacements	42
5.11	P08-16 50°: two runs overlap to show chaos outbreak	43
5.12	P08 50°: two runs overlap to show chaos outbreak	44
5.13	P08 50°: two runs overlap to show chaos outbreak	45
5.14	P08 50°	46
5.15	P16 50°	46
5.16	P08-16 50°	46
5.17	P06-12-18 50°	46
5.18	P3-06-09-12-15-18-21 50°	47
5.19	P06-12-18 40°	47
5.20	P08 30°	47
5.21	P08-16 30°	47
5.22	P04-08-12-16-20 30°	48
5.23	P03-06-09-12-15-18-21 30°	48
5.24	P09-12-15 20°	48
5.25	PAII 20°	48
5.26	P08 10°	49

5.27	P08-16 10°	49
5.28	P08 50°	50
5.29	P16 50°	50
5.30	P08 and P16 50°	50
5.31	P06-12-18 50°	51
5.32	P03-06-09-12-15-18-21 50°	51
5.33	P06-12-18 40°	52
5.34	P03-06-09-12-15-18-21 30°	52
5.35	P04-08-12-16-20 30°	52
5.36	P08-16 30°	53
5.37	P08 30°	53
5.38	P09-12-15 20°	53
5.39	PAll 20°	53
5.40	maximum pendula amplitude P08 50° (left) - P16 50° (right)	54
5.41	maximum pendula amplitude P08-16 50° (left) - P06-12-18 50° (right)	54
5.42	maximum pendula amplitude P03-06-09-12-15-18-21 50° (left) - P06-12-18 40° (right)	54
5.43	maximum pendula amplitude P08 30° (left) - P08-16 30° (right)	55
5.44	maximum pendula amplitude P04-08-12-16-20 30° (left) - P03-06-09-12-15-18-21 30° (right)	55
5.45	maximum pendula amplitude PAll 20° (left) - P09-12-15 20° (right)	55
5.46	maximum pendula amplitude P08 10° (left) - P08-16 10° (right)	55
5.47	P08 50°	56
5.48	P08 50°	57
5.49	P08 50°	58
5.50	P08 50° main Fourier peaks (left) and excited pendula main peaks (right)	59
5.51	P06-12-18 50° main Fourier peaks (left) and excited pendula main peaks (right)	60
5.52	P04-08-12-16-20 30° main Fourier peaks (left) and excited pendula main peaks (right)	61
5.53	PAll 20° - main Fourier peaks	62
5.54	P08-16 50° main Fourier peaks (left) and excited pendula main peaks (right)	63
5.55	P08-16 30° main Fourier peaks (left) and excited pendula main peaks (right)	63
5.56	P08-16 10° main Fourier peaks (left) and excited pendula main peaks (right)	63
6.1	P08 50° Main Fourier peaks 0 – 1 Hz (left) - 0.45 – 0.54 Hz zoom (right)	74
6.2	P16 50°	75
6.3	pendulum 4 damping rate in different runs P04-08-12-16-20 30° (left) - P08 30° (right)	76
A.1	<i>datasheet page 1/2</i>	85
A.2	<i>datasheet page 2/2</i>	86

List of Tables

5.1	P08 50° Main Fourier peaks	59
5.2	P06-12-18 50° Main Fourier peaks	60
5.3	P04-08-12-16-20 30° Main Fourier peaks	61
5.4	PAll 20° Main Fourier peaks	62
5.5	P08-16 50° Main Fourier peaks	64
5.6	P08-16 30° Main Fourier peaks	64
5.7	P08 10° Main Fourier peaks	65
6.1	Total energy of the chain as a function of time: 8th pendulum at 50 ° (left) and at 10° (right)	72
6.2	P08 50°: Main Fourier peaks	74

*Dedicato a mio nipote Pietro.
Perchè il coraggio che ha dimostrato in questi lunghi mesi
lo accompagni sempre.*

Chapter 1

Introduction to FPU

1.1 Objective and purpose of the present Thesis

Coupled pendulum chains are subject to collective chaotic, solitonic and ergodic motions and provide a classical model for quite different complex dynamical systems and phenomena, such as neural and IT networks, biological evolution of living being and ecosystems, flavour neutrino oscillation, chaotic gravitational systems, non-linear atomic- molecular interaction in elastic media and atomic lattice in solid state physics. Starting with the well-known computational simulation of the Fermi, Pasta and Ulam (FPU) experiment, coupled pendula has been associated to spontaneous thermalisation and ergodic recurrence of multi-body systems with non-linear interactions, in order to better investigate the statistical behaviour of the energy equipartition and of the second principle of thermodynamics. Quite differently from numerical simulations, in the FPU literature very few FPU experimental realisations are found [10, 27, 35]: one of them has been developed in the laboratories of the Engineering Department of the University of Bergamo. We monitor in space and time the individual and collective motion of a chain of 24 coupled pendula, on varying the initial conditions. The initial excitation energy is varied depending on the excited oscillator number and initial angle, the excited normal modes and the anharmonicity degree. The main activities of the project are: setup of the chain, design of the electromechanical releasing mechanism, optimisation of the videotracking algorithm, writing of the algorithm for experimental data processing (including regression and best fit techniques), measurement campaign, data analysis, system modelling and finally physical data interpretation. Neglecting the openness of any real system, the expected phenomena are in particular: thermalisation and energy equipartition, asymptotic synchronisation, chaos footprint, Intrinsic Localised Modes and possibly solitons. In particular we investigate the energy equipartition expected by the second principle of thermodynamics, the coexistence of oscillation modes at both small and large wavelengths, peculiar coherence and interference phenomena between oscillators and evidence of chaotic and non-linear behaviour typical of complex dynamic systems. We are also interested in investigating possible applications of the obtained results in different fields of applied physics and engineering. The expected results of the research are to achieve:

- an initial understanding of a specific implementation of the FPU model in a specific real case, at least from a phenomenological standpoint
- the optimisation of the measurement equipment in order to have an easy and automatic gathering mechanism, providing high sensitive and precise results for the physical quantities of interest

- the physical interpretation and the quantitative and conceptual analysis for the gathered data, the refinement of the corresponding theoretical model, the disclosure of the obtained research findings.

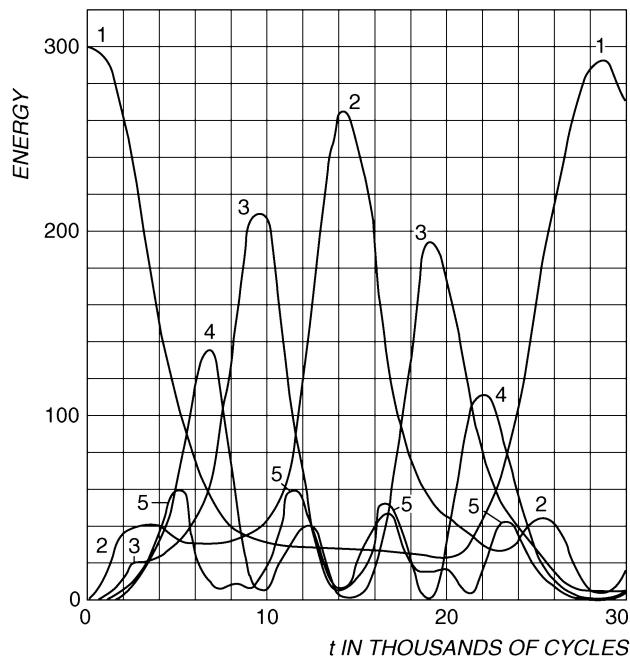
As a feedback it is possible to obtain informations on how to optimise the geometrical design of the system, the measurement instrument and the processing algorithms, as required by the physical quantities of interest.

1.2 The FPU problem

In May 1955, Los Alamos Scientific Laboratory (as it was then known) released the technical report LA-1940, titled “Studies of Nonlinear Problems: I.”, authored by Enrico Fermi, John Pasta and Stanislaw Ulam [15, 17, 16, 14, 46]. At that time this laboratory owned probably the most powerful machine available in the world to perform numerical calculation, the so called *Maniac* (Mathematical Analyzer Numerical Integrator and Computer) built for the nuclear bomb research going on. So the investigation of theoretical problems became also possible. Fermi had long been fascinated by a fundamental mystery of statistical mechanics that physicists call the “arrow of time”. Now imagine the beginning of a game of billiards with the 15 balls neatly racked up in a triangle and the cue ball hurtling in to send them careening all over the table. Fermi believed that the key was nonlinearity, the departure from the simple situation in which the output of a physical system is linearly proportional to the input. With Pasta and Ulam (and the help of the mathematician Tsingou), Fermi proposed to investigate what he assumed to be a very simple nonlinear dynamical system: a one dimensional chain composed of masses (in a number of 16 or 32 or 64) connected by springs with a pure longitudinal motion [9, 43]. In the FPU’s ideal setup, masses and springs were not subject to any friction or internal heating, oscillating forever without losing energy. The springs of this theoretical system were such as the restoring force they produced was not linearly proportional to the amount of compression or extension. Instead, FPU included nonlinear components in the mathematical relation between amount of deformation and the resulting restoring force: quadratic terms were present in the α model, while cubic terms in the β model. It was kind of a simplified model of a solid where the atoms are tied in the lattice structure. So the springs do not obey the Hooke law and the dynamic regime is non linear. As a consequence the system is, from a theoretical standpoint, “not-integrable”, non periodic and highly unpredictable. The key question FPU wanted to study was the time needed to reach the equilibrium. FPU’s premise was that the system could be started with the masses in just one simple mode of oscillation. With nonlinear springs different modes of oscillation can become excited. FPU expected that the system would “thermalise” over time: the vibrating masses would partition their energy equally among all the different allowed oscillation modes (FPU chain owns a finite number of oscillation modes, equal to the number of masses).

As an example this is the plot they published for the mechanical energy of each of the first 5 modes over 30 thousands cycles, for 32 masses when considering the α -model and an initial condition of a single sine wave (mode number 1). The higher modes were excited less than 30 on this arbitrary scale. They were absolutely astonished by the numerical results. Initially, energy was shared among several different modes. After more (simulated) time elapsed, the system returned to the same initial state, which is better known as a Poincarè recurrence.

One of the subtle effects of nonlinear physics was first observed in the 1830s by a young engineer named John Scott Russell. He was along a channel and he saw a

FIGURE 1.1: energy plot for an α -model with 32 masses

mass of water (moved by a boat) assuming the form of a large solitary elevation, a rounded, smooth and well-defined heap of water, which continued its course along the channel apparently without change of form or diminution of speed. In 1895, two Dutch physicists derived a nonlinear partial differential equation, now known as the Korteweg-de Vries (KdV) equation, that, they argued, could describe the results of Russell's experiments. This equation shows that the rate of change in time of the wave's height is governed by the sum of two terms: a nonlinear one (which gives rise to amplitude-dependent velocities) and a linear one (which causes wavelength-dependent dispersion). In particular, Korteweg and de Vries found a solitary-wave solution that matched the strange wave Russell had met.

In the early 1960s N. Zabusky and M. Kruskal [49, 37] of Princeton University generalised the FPU experiment to continuous chains, employing infinitesimally small springs and masses and obtaining from numerical simulations a near-recurrence and soliton-like solutions. To describe their solutions to the Korteweg-de Vries (KdV) equation, they invented what has become a widely used term for the solitary-wave phenomenon: soliton. Up to now many other scientists obtained energy equipartition over a sufficiently long time scale with both simulations and theoretical analysis. One of them is Eddie Cohen of Rockefeller University [7]: analysing FPU chain at high energy, they discovered that there are two thresholds as a function of energy for any oscillator. At the first threshold the system has a transition from a deterministic regularity to a weak chaos; at the second one chaos becomes strong and energy is forced to quickly distribute between different modes. They also found that equipartition happens sooner if mass number is higher and so, growing the number of non-linear oscillators, equipartition happens for any initial energy. The initial conditions of FPU simulation were below the chaos threshold and this could have interfered with the thermalisation process and the equipartition of initial energy.

Today FPU problem inspires research on many other non-linear systems. In solid state physics, they have been observed localised vibrational modes in perfect lattices. Those modes, called ILMs (Intrinsic Localised Modes) or discrete breathers,

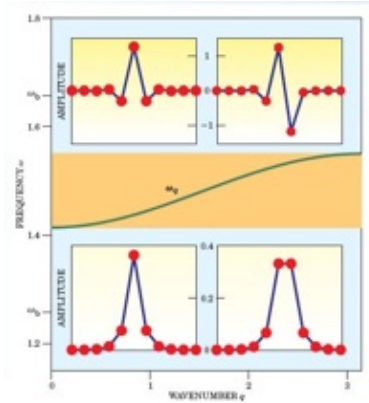


FIGURE 1.2: ILM

can appear in widely extended or highly non-linear lattices, by playing a rôle similar to the soliton in continuous physical systems. The main difference is that ILM don't have to move: they can vibrate in place. This was unveiled by Albert Sievers and Shozo Takeno in 1988 [48] and subsequently analysed by Sergej Flach in 2005 [12]. In solid state physics localisation phenomenon is generally explained as a consequence of an "extrinsic" chaos, that breaks the translational discrete invariance of the perfect lattice. This idea has been rejected in the '80s when ILM were discovered in periodic non-linear systems.

The breather term was first used for a specific solution of "sine-Gordon" equation (SGE), which is now one of the well-known solitonic equations

$$\frac{\partial^2 \theta}{\partial t^2} - \frac{\partial^2 \theta}{\partial x^2} + \sin \theta = 0 \quad (1.1)$$

Despite their non-linearity, those equations have analytical solutions, because they correspond to integrable hamiltonian systems. Let's consider the non-linear oscillators with very weak interaction. We can start them with different energies, in a way that most of the system energy is located in the first one. We can choose those excited states so that their frequencies are incommensurate. Then, after the initial state where both are at the maximum amplitude, they will never get in synch again. This property prevents first oscillator to get in resonance with the second and this makes it very difficult for energy to flow from one to the other. Let's consider a chain with a high number of oscillators. Just one vibrates with a relatively large amplitude, but with an incommensurate frequency with the other ones. The excited oscillator will hardly transfer its energy to the closest ones and for this reason it will maintain a large amplitude: this is an ILM. This property was formalised in Kolmogorov-Arnold-Moser theorem on non-linear dynamical systems.

1.3 The FPU model

The Fermi-Pasta-Ulam model represents a system of $N + 2$ equal particles on a line with mutual interactions between adjacent particles, provided by a potential of the form

$$V(r) = \frac{r^2}{2} + \alpha \frac{r^3}{3} + \beta \frac{r^4}{4}$$

As boundary conditions, the two extreme particles are fixed. The normalized Hamiltonian of the system is

$$H = \sum_i^N \left[\frac{p_i^2}{2} + \frac{(q_{i+1} - q_i)^2}{2} + \alpha \frac{(q_{i+1} - q_i)^3}{2} + \beta \frac{(q_{i+1} - q_i)^4}{2} \right]$$

For $\alpha = \beta = 0$ the system becomes linear and it can be reduced to a system of N independent harmonic oscillators (called *normal modes*) with well defined frequencies

$$\omega_j = 2 \sin[j\pi/(2(N + 1))], j = 1, \dots, N$$

The corresponding equation of motions read as follows:

$$\ddot{x}_j = (x_{j+1} + x_{j-1} - 2x_j) + \alpha[(x_{j+1} - x_j)^2 - (x_j - x_{j-1})^2]$$

or

$$\ddot{x}_j = (x_{j+1} - x_{j-1} - 2x_j)[1 + \alpha(x_{j+1} - x_{j-1})]$$

in the α -model and

$$\ddot{x}_j = (x_{j+1} + x_{j-1} - 2x_j) + \beta[(x_{j+1} - x_j)^3 - (x_j - x_{j-1})^3]$$

in the β -model.

1.3.1 Connection to the KdV equation

The continuum limit of the governing equations for the cable (with the quadratic force term) is the Korteveg-de Vries equation. If you define $c = \sqrt{\kappa/\rho}$ to be the wave speed, where $\kappa = k/h$ is the Young's module for the string and $\rho = m/h^3$ is the density, the previous equation for α -model (where k was equal to one due to normalisation) reads:

$$\ddot{x}_j = \frac{c^2}{h^2}(x_{j+1} - x_{j-1} - 2x_j)[1 + \alpha(x_{j+1} - x_{j-1})]$$

If $u(x, t)$ is the displacement of the string at position x and time t we pose $u(p_j, t) = x_j(t)$ where p_j are the equilibrium positions. Using the Taylor's theorem the last equation can be rewritten as follows

$$\begin{aligned} \left(\frac{x_{j+1} - x_{j-1} - 2x_j}{h^2} \right) &= \frac{u(x+h, t) + u(x-h, t) - 2u(x, t)}{h^2} = \\ &= u_{xx}(x, t) + \left(\frac{h^2}{12} \right) u_{xxxx}(x, t) + \mathcal{O}(h^4) \end{aligned}$$

Similarly, the second term in the third factor is:

$$\alpha(x_{j+1} - x_{j-1}) = 2\alpha h u_x(x, t) + \left(\frac{\alpha h^3}{3} \right) u_{xxx}(x, t) + \mathcal{O}(h^5)$$

Thus the continuous limit of the FPU system is:

$$\frac{1}{c^2} u_{tt} - u_{xx} = (2\alpha h) u_x u_{xx} + \left(\frac{h^2}{12} \right) u_{xxxx}(x, t) + \mathcal{O}(\alpha h^2, h^4)$$

Keeping the $\mathcal{O}(h^2)$ terms we obtain:

$$\frac{1}{c^2}u_{tt} - u_{xx} = (2\alpha h)u_x u_{xx} + \left(\frac{h^2}{12}\right)u_{xxxx}(x, t)$$

Considering the decomposition of traveling wave solutions (of the ordinary wave equation, to which this reduces when α, h vanish) and taking into account the right moving wave only, changing the coordinates to $\xi = x - ct$, $\tau = (\alpha h)ct$ and $y(\xi, \tau) = u(x, t)$, the equation becomes:

$$y_{\xi\tau} - \left(\frac{\alpha h}{2}\right)y_{\tau\tau} = -y_{\xi}y_{\xi\xi} - \left(\frac{h}{24\alpha}\right)y_{\xi\xi\xi\xi}$$

Taking the continuum limit, α/h tend to a constant and α and h tend to zero, putting $\delta = \lim_{h \rightarrow 0} \sqrt{u/(24\alpha)}$, then

$$y_{\xi\tau} = -y_{\xi}y_{\xi\xi} - \delta^2 y_{\xi\xi\xi\xi}.$$

Taking $v = y_{\xi}$ results in the KdV equation:

$$v_{\tau} + vv_{\xi} + \delta^2 v_{\xi\xi\xi} = 0.$$

1.3.2 Modal energy in FPU model

The total energy E then reduces to the sum $E = \sum_j E_j$ of the normal mode energies E_j , which are independent integrals of motion: $E_j(t) = E_j(0)$. When the nonlinear interaction is active, the normal mode energies are no longer integrals of motion and a standard arguments of classical statistical mechanics suggests that their time averages $E_j^*(t) = (1/t) \int_0^t E_j(\tau) d\tau$ should tend to a common value, thus realising what is usually called the equipartition of energy. More precisely this is expected to occur for almost all initial data with respect to the Gibbs measure, and in the thermodynamic limit, i.e. the limit of an infinite system with a finite non vanishing specific energy ϵ : $N \rightarrow \infty$, $E \rightarrow \infty$, $E/N \rightarrow \epsilon > 0$. In such a case, the common value of the time averages of the normal mode energies is identified with the temperature T by $E_j^*(t) \rightarrow k_B T$, where k_B is the Boltzmann constant. Correspondingly, the specific heat (defined as the derivative of energy with respect to temperature) turns out to be a constant, independent of temperature. The FPU problem consists in establishing whether the dynamics actually leads to equipartition. They considered initial data with energy given just to some low frequency modes. The thermalisation rate is the rate at which energy flows to the high frequency modes.

1.3.3 The paradox

In physics the question of equipartition of energy has a foundational meaning, being the one which gave rise to quantum mechanics. As a matter of fact it is experimentally found that equipartition of energy is obtained in the limit of high temperatures and/or low frequencies and it is not in the complementary region. As a reminder equipartition of energy means that mean energy is independent of frequency and specific heat is independent of temperature. Then in 1900 Planck found that the distribution of energy (per oscillator) U versus frequency ω at temperature T is given by

$$U(\omega, T) = \frac{\hbar\omega}{e^{\hbar\omega/k_B T} - 1} = k_B T \frac{x}{e^x - 1}$$

where

$$x = \frac{\hbar\omega}{k_B T}$$

is the relevant dimensionless parameter. The Planck's law can also be obtained by the usual arguments of statistical mechanics if energy is assumed to be quantized. This means that the energy of a harmonic oscillator can only assume values like $E_n = (n + \frac{1}{2})\hbar\omega$ where $n \geq 0$. If energy is not quantized, one instead recover the "classical" equipartition value $U(\omega, T) = k_B T$. So the FPU result appeared as a paradox.

1.3.4 Energy thresholds: Izrailev and Chirikov

In 1966 Izrailev and Chirikov [34] made a connection between the FPU problem and the modern results of perturbation theory, i.e. KAM theorem [36, 1, 40]. The point is that the perturbed system is proven to be qualitatively similar to the unperturbed one only if the perturbation is smaller than a certain threshold, which has to be estimated in the specific case. In the FPU model the unperturbed system is the linearised one with its N independent integrals and the perturbation is given by the total energy: in fact the relative "size" of the nonlinearity tends to zero with the total energy. So their idea was that the perturbed system would be qualitatively similar to the unperturbed one if the total energy is smaller than a critical energy, say E^c : the unexpected result obtained by Fermi was due to the initial energy small with respect to this threshold. This paradox would disappear at all if we could prove that this threshold vanishes in the thermodynamic limit. They conceived the idea that the threshold should depend on the choice of the initial data and in particular to an initial excitation of mode j there is a corresponding energy threshold E_j^c . According to their estimate, the energy threshold would tend to zero, at least for the case of large j . This result almost eliminates the paradox, because, at least for initial data with excitations of the high frequency modes, in the thermodynamic limit, one would always be above the threshold, so the system would have no relation with the unperturbed one and thus would evolve to equipartition. In 1997 Shepelyansky [47] stated that he accomplished the task to extend such a result to the case of small j , taking into account certain resonances not considered by Izrailev and Chirikov.

1.3.5 Plank-like distributions: Bocchieri, Scotti and Loinger

In 1970 in Milan the team of Bocchieri, Scotti and Loinger [2, 20], stimulated by Izrailev and Chirikov work, had the idea of checking numerically whether the specific critical energy $\epsilon^c = E^c/N$ vanishes in the thermodynamic limit or not. This was done using initial excitations of the lowest mode. The energy threshold was defined as the "final" stationary value of the time averages $E_j^*(t)$. It turned out that there was a critical energy above which there was an apparent equipartition, while it did not happen at lower energies. The critical energy E^c appeared to be proportional to N and this implies the existence of the specific critical energy $\epsilon > 0$. In other terms, it was suggested that there is a relevant set of initial data, which lead to "final" states not corresponding to equipartition of energy. The computations were performed with Lennard-Jones interatomic potential with Argon specific values: in this case the specific critical energy turned out to have of 4% of the depth of the potential well. In 1972 an investigation was done by Galgani and Scotti [20] of the distribution of energy for the "final" states that are found below the threshold for the low frequency excitations. The expression of the final values E_j^* in terms of the

corresponding frequencies ω_j is rather well fitted by Planck-like distributions of the form

$$E^*(\omega, E) = \frac{A\omega}{e^{\beta A\omega} - 1}$$

where β was depending on the total energy E as an inverse temperature should, while A parameter appeared to be constant. Using the Argon specific molecular parameters A turns out to have a value very close to Planck's constant. Shortly later Cercignani [5, 21] suggested there might be an analogy between energy thresholds and quantum zero-point energy.

1.3.6 Relaxation times

If we denote by “freezing” the FPU qualitative phenomenon when the final distribution of energy is near the initial one (i.e. equipartition is not reached) if the initial one corresponds to excitation of the very low frequency modes, this freezing is expected to hold just below some energy threshold. Then the point is now if such a freezing persists in the thermodynamic limit or not: if it does it is relevant for physics otherwise not. It looks like Izrailev and Chirikov believe this, while the Italian physicists do not. But there are two points to be discussed. A clear definition for the freezing with respect to the question of time involved, i.e. the size of the relaxation times in relation to the observation time. The second has to do with the meaning of the notion of “energy per oscillator”. Considering the first point, the perturbation theory is strongly related to observation time. Indeed in order to prove that a certain system is “similar” to another “unperturbed” one we have to preliminarily fix a time t up to which the similarity should hold: such a time is the counterpart of the physical observation time. It is now agreed by the scientific community that taking into account the observation time is a physically relevant requirements even in the FPU problem. Equipartition state can be seriously studied if involved observation time is accurately discussed. If experimental observation times are much shorter than relaxation times equipartition cannot be observed. The KAM theorem refers to infinite observation time. One can instead make reference to finite times: Nekhoroshev thought how to deal with them in an efficient way [41, 23]. For example crystals and polyatomic molecules as well as glasses and polymers might have a pretty rapid relaxation to a metaequilibrium state which should last for a long time, while the final relaxation to equipartition (Maxwell-Boltzmann equilibrium) might then occur on a much longer time scale [19]. For the second problem, Boltzmann pointed out that we cannot identify thermodynamic energy and mechanical energy. The observation time has to be declared in advance. The system has a certain mechanical energy given by the initial conditions and its thermodynamic energy is the fraction of the mechanical energy that the system can actually exchange with the measurement instrument up to the given observation time. So one might have equipartition of energy for the mechanical energy, but a Planck distribution for the exchangeable energy.

1.3.7 Critical specific energy and the “natural packet”

In a later work Galgani [22] showed that for initial data of the FPU type, the results depend on the specific energy ϵ . There exists a critical specific energy ϵ^c such that for $\epsilon > \epsilon^c$ equipartition is obtained within a time that increases as an inverse power of ϵ with decreasing ϵ . On the contrary, below the threshold, i.e. for $\epsilon < \epsilon^c$, two time scales are met: in a short time a “natural packet” is formed that extends

up to a maximal frequency $\bar{\omega}(\epsilon)$ proportional to $\epsilon^{1/4}$. Only on a much longer time scale equipartition is reached. As Galgani and its team suggested [4, 3], probably the FPU paradox cannot be eliminated because it has a deep physical meaning. Up to the “short” times classical mechanics might qualitatively agree with quantum mechanics and only later they differentiate. Indeed, according to quantum mechanics the Planck’s law is the final equilibrium distribution, while, apparently, according to classical mechanics it might describe a meta-equilibrium distribution which only over much longer glassy-like time scale would finally evolve to the “classical” Maxwell-Boltzmann equilibrium: it is a problem of time scales.

To summarise, in the last fifty years, investigating the FPU problem and similar systems, great progresses have been done on a wide area of open problems and original phenomena not completely understood in the fields of non linear dynamics, statistical mechanics and computational physics. The present project draws inspiration from this research line, which goes on all over the world by researchers with different scientific backgrounds and methodological approaches: anyway almost all of them are theoretical and numerical simulations rather than observation of a physical system in a laboratory.

1.3.8 Latest findings

Few years ago Miguel Onorato of the University of Turin published his research [42] which provides a large contribution to solve the FPU problem: he resorts to wave turbulence theory (interacting but not correlated waves), which can explain the continuous energy transfer between short waves and long waves, predicting in this way both the thermalisation mechanism and time rate. His approach was based on the nonlinear interaction of weakly nonlinear dispersive waves with the main assumption that irreversible transfer of energy in their spectrum is achieved by exact resonant wave-wave interactions. Such resonant interactions are the base for the so-called “wave turbulence theory” [50] and are responsible for the phenomenon of thermalization. Working in a Fourier space he obtains for the α -FPU system an evolution equation for the normal modes which has a Hamiltonian structure and is characterized by a quadratic nonlinearity, i.e. a three-wave interaction system. He shows that it is impossible to find nonzero wave numbers satisfying the resonant condition. He states that the equipartition phenomenon is not to be expected for the Fourier modes of the variables free to interact. He then builds a spectrum characterised only by free modes, through ad hoc canonical transformations that removes all non resonant interactions. To present a physical interpretation of the canonical transformation, the initial state of a α -FPU system initialised by a single mode k_0 would then be characterised by the generation of the higher harmonics of it. The reduced α -FPU model where three-wave interactions have been removed by the canonical transformation have different four-wave solutions: trivial resonances, responsible for frequency shift, but not for energy transfer between modes, and non-trivial quadruplets, that are not, by the way, interconnected, cannot be accounted for an effective energy mixing. So four-waves resonant interactions are isolated and no efficient mixing (and thermalization) can be achieved via a four-wave process: this result was first obtained Henrici and Kappeler in 2008 [28] following some ideas developed earlier by B. Rink [45, 44]. Five-wave interactions are nonresonant and can be removed as above. And finally six-wave resonant sextuplets are interconnected and they represent an efficient mechanism of spreading energy in the spectrum. Because of the existence of these exact resonant processes, equipartition is expected to take place. The estimate of the timescale of equipartition is achieved using the

kinetic equation, which describes the time evolution of the average spectral energy density. The time evolution turns out to be proportional $1/\epsilon^8$, where

$$\epsilon = \frac{\alpha}{m} \left(\frac{\gamma}{m} \right)^{1/4} \sqrt{\sum_k \omega_k |a_k(t=0)|^2}$$

In the latter γ is the coefficient of the linear term, a_k is the complex amplitude of a normal mode defined as

$$a_k = \frac{1}{2\omega_k} (P_k - i\omega_k Q_k)$$

Q_k are the Fourier amplitudes of the displacement variables and $P_k = \dot{Q}_k$. If $\epsilon = 0$ the system is linear and Onorato study covers the weakly nonlinear regime only, i.e. $\epsilon \ll 1$. So thermalisation should occur earlier for systems with stronger nonlinearities.

1.4 Second law of thermodynamics and equipartition theorem

In the following we recall the existing connection between the two laws we frequently mention and that are key in the physical interpretation of the behaviour of the system. In classical statistical mechanics a system of N molecules has a volume V and an internal energy between E and $E + \Delta$. Its dynamics is determined by the Hamiltonian $\mathcal{H}(p, q)$ from which the canonical equation of motions can be obtained. If we denote with $\sum(E)$ the states of the system at the energy E , defined by

$$\sum(E) = \int_{\mathcal{H}(p,q) < E} dpdq \quad (1.2)$$

and with $\Gamma(E)$ the space occupied in the phase space by the microcanonical ensemble, such that $\Gamma(E) = \sum(E + \Delta) - \sum(E)$, we call $\omega(E)$ the density of states of the system at the energy E , defined by $\omega(E) = \frac{\partial \sum(E)}{\partial E}$ and the following relation holds: $\Gamma(E) = \omega(E)\Delta$. The system is described by the physical quantity called entropy $S(E, V)$ which can be defined in different, but equivalent ways:

$$S = k \log \sum(E)$$

$$S = k \log \Gamma(E)$$

$$S = k \log \omega(E)$$

If we consider the first definition, we can notice that $\sum(E)$ is a not decreasing function of V and for this reason S is also a not decreasing function of V . In fact if the volume V grows, also the integral in 1.2 is performed on a larger domain of integration. This is exactly the *second law of thermodynamics*.

Then we calculate the ensemble average of $x_i \left(\frac{\partial \mathcal{H}}{\partial x_j} \right)$ we can write:

$$\begin{aligned} \langle x_i \frac{\partial \mathcal{H}}{\partial x_j} \rangle &= \frac{1}{\Gamma(E)} \int_{E < \mathcal{H} < E + \Delta} dp dq x_i \frac{\partial \mathcal{H}}{\partial x_j} = \\ &= \frac{\Delta}{\Gamma(E)} \frac{\partial}{\partial E} \int_{\mathcal{H} < E} dp dq x_i \frac{\partial \mathcal{H}}{\partial x_j} \end{aligned}$$

Noting that $\frac{\partial E}{\partial x_j} = 0$, the last integral can be rewritten as follows

$$\begin{aligned} &= \int_{\mathcal{H} < E} dp dq x_i \frac{\partial \mathcal{H}}{\partial x_j} = \int_{\mathcal{H} < E} dp dq x_i \frac{\partial}{\partial x_j} (\mathcal{H} - E) = \\ &= \int_{\mathcal{H} < E} dp dq \frac{\partial}{\partial x_j} [x_j (\mathcal{H} - E)] - \delta_{ij} \int_{\mathcal{H} < E} dp dq (\mathcal{H} - E) \end{aligned}$$

The first integral on the right side vanishes because it reduces to a surface integral over the boundary of the region defined by $\mathcal{H} < E$, and on this boundary $\mathcal{H} - E = 0$. Substituting the latest result into the previous equation we obtain

$$\begin{aligned} \langle x_i \frac{\partial \mathcal{H}}{\partial x_j} \rangle &= \frac{\delta_{ij}}{\omega(E)} \frac{\partial}{\partial E} \int_{\mathcal{H} < E} dp dq (E - \mathcal{H}) = \\ &= \frac{\delta_{ij}}{\omega(E)} \int_{\mathcal{H} < E} dp dq = \frac{\delta_{ij}}{\omega(E)} \sum(E) = \\ &= \delta_{ij} \frac{\sum(E)}{\partial \sum(E) / \partial E} = \delta_{ij} \left[\frac{\partial}{\partial E} \log \sum(E) \right]^{-1} = \\ &\quad \delta_{ij} \frac{k}{\partial S / \partial E} \end{aligned}$$

that is

$$\langle x_i \frac{\partial \mathcal{H}}{\partial x_j} \rangle = \delta_{ij} kT$$

This is the *generalized equipartition principle*.

1.5 Main steps of the experimental project

Neglecting its openness, the energy of the mechanical system described in Chapter 4, is expected to undergo thermalisation and equipartition of the available energy. As a matter of fact one of the main objectives of the research project reported in this thesis is to observe and study the time evolution of that system. A secondary aim of the research is to study the dynamics of nonlinearly coupled oscillators when dissipation is in place, particularly when short times are considered. In the following the main steps of the research project are listed:

- a scrutinised study of the scientific literature regarding the subject and the existing results and the design of a preliminary theoretical model of the physical process. This theoretical model is used to choose the best guidelines to build the experimental system (in terms of materials to be used, sizing criteria and technological equipment to be acquired) and the optimal conditions for measurement activities.
- the implementation of the experiment in the laboratory and the collection of the corresponding measurement data
- the analysis and physical interpretation of the results and the comparison between the outcomes of different runs

In order to achieve our goals we performed a number of intermediate steps detailed as follows:

- realisation of the oscillator chain and of the electromagnetic equipment used to automatically release pendula, which act as exciters of the chain in several different initial configurations; arrangement of the test execution, measurement activity and data gathering
- positioning of the GoPro Hero4 webcam (120fps framerate and fullHD Field of View) for recording the whole motion and tuning of the technique used in data acquisition through GoPro Hero4 webcam (120fps framerate and fullHD Field of View) for recording and subsequent videotracking
- execution of an extensive measurement campaign including anharmonic excitations (large angles), multiple pendula excitations (from 2 up to 24) and “inverse modes”, when in the same initial configuration excited pendula are alternately released on opposite sides of the system
- programming of the Mathematica code for data processing with a specific interest for (mean and integral) physical quantities related to energy, such as the “inverse metric” for thermalisation, as well as Fourier analysis. The analysis of the thermalisation kinetics allowed us to understand the temporal response of the system to the dissipative processes
- design of a physical model of the chain and of the interaction of the oscillators through the coupling cable, represented by a number of oscillators (a discretised version of the cable) connected by springs moving along a horizontal axis and sustaining pendula performing small oscillations in the same direction
- physical explanation of the collected data, of the overall system interaction with the surrounding environment and comparison with the theoretical model

1.6 Thesis plan

In Chapter 2 we first introduce the general theory of small oscillations: the simple case of free oscillations is treated first and then forced and damped oscillations are considered. Later on the anharmonic oscillations are covered in order to complete the previous picture.

In Chapter 3 a model is proposed to describe a system of coupled pendula and a preliminary result is given for the energy metric Ω to be later compared with experimental results. After this theoretical introduction, in Chapter 4 the experimental equipment is described: the setup of the chain is introduced as well as the electromagnetic mechanism use to excite pendula. Later on the videotracking methodology is described in detail. Device specifications can be found in Appendix A, while the videotracking source code in Appendix B and the processing algorithm developed with Mathematica in Appendix C. And finally the measurement protocol is illustrated.

Going further in Chapter 5 a selection of experimental result is given with a number of plots and tables produced by data processing.

Those results are discussed in detail in Chapter 6. First the physical quantities of interest are listed, then the analysis is given for those points: time evolution of displacement, energy metric evolution, dissipation process, chaos outbreak, decay time estimate, Fourier analysis and horizontal analysis of amplitudes.

Finally in Chapter 7 the main findings of the research are summarised and further possible investigation are proposed.

Chapter 2

Small oscillations

2.1 Introduction

Our system is composed of a chain of oscillators with a non linear coupling, subject to the gravity force, to air frictional force and to constrain reaction at the fixed ends of the chain.

2.2 Free oscillations

Real mechanical systems experience what are called *small oscillations* about a position of stable equilibrium. In the simplest case the system has only one degree of freedom. Here we consider small displacements from the equilibrium position. We can write the Lagrangian of the system executing small oscillations retaining the first non vanishing term in the expansion of potential energy $U(x)$ the form [38]:

$$L = \frac{1}{2}m\dot{x}^2 - \frac{1}{2}kx^2 \quad (2.1)$$

where x is the displacement from the equilibrium position and the minimum value for the potential energy is set to zero, i.e. $U(0) = 0$. The Euler-Lagrange equation of motion is

$$\ddot{x} + \omega^2 x = 0 \quad (2.2)$$

where

$$\omega = \sqrt{\frac{k}{m}}$$

is a fundamental characteristic of the oscillations, called (*angular*) *frequency*, independent of the initial conditions, but only dependent on the mechanical properties of the system itself. The linear homogeneous differential equation 2.2 has the following general solution:

$$x = A \cos(\omega t + \alpha) \quad (2.3)$$

where the arbitrary constants A and α are the *amplitude* and the *phase* determined by initial conditions. Solution 2.3 can also be written in a different form using a complex expression (which has a simpler use when differentiating):

$$x = \text{Re}[\tilde{A}e^{i\omega t}] \quad (2.4)$$

where

$$\tilde{A} = Ae^{i\alpha}$$

The energy of such a system is given by

$$E = \frac{1}{2}m\dot{x}^2 + \frac{1}{2}kx^2 = \frac{1}{2}m\omega^2 A^2$$

It has a constant value, which depends on the square of the amplitude.

If the system has more than one degree of freedom (assume n), this theory can be easily extended. The Lagrangian of a mechanical system oscillating with n degrees of freedom takes the form:

$$L = \sum_{i,j=1}^n \left(\frac{1}{2}m_{ij}\dot{x}_i\dot{x}_j - \frac{1}{2}k_{ij}x_ix_j \right) \quad (2.5)$$

where $m_{ij} = m_{ji}$ and $k_{ij} = k_{ji}$. The Euler-Lagrange equation is therefore:

$$\sum_{j=1}^n (m_{ij}\ddot{x}_j + k_{ij}x_j) = 0 \quad (2.6)$$

for $i = 1, \dots, n$. This is a system of n linear homogeneous differential equations with constant coefficients and can be solved using the method of characteristics. Taking into account eq. 2.4 we search for a set of n functions of the form:

$$x_j = \text{Re}[A_j e^{i\omega t}] \quad (2.7)$$

where constants A_j have to be determined. By substituting 2.7 in 2.6 we obtain a system of linear algebraic equations to be satisfied by A_j :

$$\sum_j (-\omega^2 m_{ij} + k_{ij}) A_k = 0$$

For this system to have non-zero solutions, the determinant of the coefficients must be zero:

$$|k_{ij} - \omega^2 m_{ij}| = 0 \quad (2.8)$$

This is the *characteristic equation* of order n in ω^2 : in general it has n different real positive roots ω_i , named as *characteristic frequencies* or *eigenfrequencies* of the system. The roots are real positive, because otherwise the system would not be conservative. If all ω_i are different, A_j are proportional to the minors of the determinant 2.8: we denote them with Δ_{ij} . The general solution can be written as the sum of the particular solutions $x_j = \Delta_{ij} C_i e^{i\omega_i t}$

$$x_j = \text{Re} \sum_i \Delta_{ij} C_i e^{i\omega_i t} \equiv \sum_i \Delta_{ij} \Theta_i \quad (2.9)$$

where

$$\Theta_i = \text{Re}[C_i e^{i\omega_i t}]$$

This means that each coordinate of the system changes in time as a superposition of n simple periodic oscillations Θ_i , each one with its own defined frequency, but arbitrary amplitude and phase. Coordinates Θ_i are new generalised coordinates, named *normal coordinates* undergoing the *normal oscillations* of the system. In normal coordinates the equations of motion become n independent equations:

$$\ddot{\Theta}_i + \omega_i^2 \Theta_i = 0$$

that is, that normal oscillations of the system are completely independent. In terms of normal coordinates the Lagrangian expressed reduces to a sum of Lagrangians describing one-dimensional oscillations with frequency ω_i (see 2.1):

$$L = \sum_i \frac{1}{2} (\dot{\Theta}_i^2 - \omega_i^2 \Theta_i^2)$$

2.3 Forced oscillations

So far we have considered only free oscillations. If the oscillating system undergoes a variable external force, it performs *forced* oscillations. We consider only weak forces acting on the system, so that the forced (not resonant) oscillations remain small. Let us consider the simple one dimensional case as in 2.1. This external force introduces a new potential energy term in the Lagrangian, which can be expressed as a power series of displacement x as follows:

$$U_e = U_e(0, t) - xF(t) + \mathcal{O}(x)$$

being

$$F(t) = - \left. \frac{\partial U_e(x, t)}{\partial x} \right|_{x=0}$$

Therefore the Lagrangian of the system writes

$$L = \frac{1}{2} m \dot{x}^2 - \frac{1}{2} k x^2 + xF(t) \quad (2.10)$$

giving the following equation of motion:

$$\ddot{x} + \omega^2 x = \frac{F(t)}{m} \quad (2.11)$$

where ω is the frequency of the free oscillations. The general solution of such non-homogeneous linear differential equation with constant coefficients is the sum of the general solution of the associated homogeneous equation and of a particular solution of the non-homogeneous one.

When the external force is a simple periodic function of time with frequency γ , such as $F(t) = f \cos(\gamma t + \beta)$ and $\gamma \neq \omega$, the general solution of the equation is

$$x = a \cos(\omega t + \alpha) + \left[\frac{f}{m(\omega^2 - \gamma^2)} \right] \cos(\gamma t + \beta)$$

Thus a system undergoing a periodic force performs a motion which is a combination of two oscillations, one with the intrinsic frequency ω of the system and one with the frequency γ of the force.

By contrast when $\gamma = \omega$, the general solution turns out to be endowed with a resonant term:

$$x = a \cos(\omega t + \alpha) + \frac{f}{2m\omega} t \sin(\omega t + \beta)$$

which makes the oscillation amplitude increasing linearly with time, so that the small oscillation approximation does not hold anymore. As γ approaches ω the general solution describes small oscillations of variable amplitude: the amplitude varies periodically with frequency $|\gamma - \omega|$ yielding the so-called *beats*. We can rewrite the

latter equation changing the variable ($\xi \equiv \dot{x} + i\omega x$) so obtaining

$$\frac{d\xi}{dt} - i\omega\xi = \frac{F(t)}{m} \quad (2.12)$$

This first-order non-homogeneous differential equation has the following general solution

$$\xi = e^{i\omega t} \left[\int_0^t \frac{1}{m} F(t) e^{-i\omega t} dt + \xi_0 \right]$$

where $\xi_0 = \xi(0)$. The function $x(t)$ is the imaginary part of $\frac{\xi}{\omega}$. The energy of a system performing forced oscillations is not conserved, since the force acting on the system provides energy which can be obtained as:

$$E = \frac{1}{2m} \left| \int_{-\infty}^{\infty} F(t) e^{-i\omega t} dt \right|^2$$

In other words the energy of the system depends of the modulus squared of the Fourier component of the force with the intrinsic frequency of the system. Now we can easily extend such forced oscillation theory to a n -dimensional oscillating system using normal coordinates, which can be treated as a set of independent 1-dimensional forced oscillations. The Lagrangian of the system can be written

$$L = L_0 + \sum_i F_i(t) x_i$$

where L_0 is the Lagrangian for free oscillations. In normal coordinates it becomes

$$L = \sum_i \frac{1}{2} m_i (\dot{\Theta}_i^2 - \omega_i^2 \Theta_i^2) + \sum_i f_i(t) \Theta_i$$

where

$$f_i(t) \equiv \sum_k F_k(t) \Delta_{ik}$$

The corresponding equations of motion are

$$\ddot{\Theta}_i + \omega_i^2 \Theta_i = \frac{f_i(t)}{m_i}$$

Each equation involves one single unknown function $\Theta_i(t)$.

2.4 Damped oscillations

The motion of the oscillating system we are studying, rather than in vacuum, can instead occur in a damping medium. The motion is retarded and the energy dissipated is converted into heat. If we assume the oscillations happen with a frequency small compared to those of the dissipative processes in the medium, we can assume the body to be subject to a *friction* force which depends only on the velocity. Moreover, if the velocity is small enough, we can express the frictional force as an expansion of velocity powers. The first non-zero term is the first order term and, neglecting the higher order terms, we can apply the Stokes law writing the frictional force as follows ($\alpha > 0$):

$$f_{fr} = -\alpha \dot{x}$$

The equation of motion now contains a new term

$$m\ddot{x} = -kx - \alpha\dot{x}$$

and can be rewritten as:

$$\ddot{x} + 2\lambda\dot{x} + \omega^2x = 0$$

where ω is as usual the free oscillation frequency and $\lambda = \alpha/2m$ is the so called *damping coefficient*. This second order homogeneous differential equation has different solutions depending on the ratio between λ and ω . If $\lambda < \omega$ (weak friction) the general solution can be written as:

$$x = ae^{-\lambda t} \cos(\omega't)$$

where $\omega' \equiv \sqrt{\omega^2 - \lambda^2}$. This solution describes the so-called *damped oscillations*, i.e. harmonic oscillations with exponentially decreasing amplitude with time constant λ . The frequency ω' is smaller than ω , from which we deduce that friction slows down motion. If $\lambda \ll \omega$ the mean energy of the system decreases according to

$$E = E_0e^{-2\lambda t}$$

where E_0 is the initial energy. On the contrary if $\lambda > \omega$ (strong friction) the system undergoes an *aperiodic damping*, i.e. approaches asymptotically the equilibrium position. We now extend this theory to n -dimensional systems. The frictional force has n components which are linear functions of the velocities and can be written as:

$$f_{fr,i} = - \sum_k \alpha_{ik} \dot{x}_k$$

It can be shown that $\alpha_{ik} = \alpha_{ki}$; for this reason we can rewrite

$$f_{fr,i} = - \frac{\partial F}{\partial \dot{x}_i}$$

where F is a quadratic form

$$F = \frac{1}{2} \sum_{ik} \alpha_{ik} \dot{x}_i \dot{x}_k$$

called *dissipative function*. Those frictional forces have to be added into the equation of motion 2.6 obtaining

$$\sum_k (m_{ik} \ddot{x}_k + k_{ik} x_k) = - \sum_k \alpha_{ik} \dot{x}_k \quad (2.13)$$

If we put $x_k = A_k e^{rt}$ in these equations we obtain:

$$\sum_k (m_{ik} r^2 + \alpha_{ik} r + k_{ik}) A_k = 0$$

The corresponding characteristic equation then is:

$$|m_{ik} r^2 + \alpha_{ik} r + k_{ik}| = 0$$

This is an equation in r of degree $2n$ with real coefficients: so all roots must have negative real parts, as the dissipative forces produce a decrease in the overall energy.

It can be shown that the time derivative of the mechanical energy of the system is directly related to the dissipative function F as follows:

$$\frac{dE}{dt} = -2F$$

This implies that F is a positive definite quadratic form.

2.5 Forced damped oscillations

Forced oscillations under friction for a one dimensional system are described by the equation of motion:

$$\ddot{x} + 2\lambda\dot{x} + \omega_0^2x = f(t)$$

where $f(t)$ is an external force depending on time. When there is a simple periodic external force, the general solution of the non homogeneous 2-order differential equation is of the form:

$$x = a \exp(-\lambda t) \cos(\omega_0 t + \alpha) + b \cos(\gamma t + \delta)$$

where the first term decreases exponentially with time leaving the second term. Exponential decrease depends on λ damping coefficient, while the asymptotic steady oscillations have an amplitude b which grows as γ approaches ω_0 , but does not become infinite (as in resonance without friction) and is inversely proportional to the λ coefficient. In order to consider an n -dimensional system we should take advantage of normal coordinates

$$\sum_k (m_{ik} \ddot{x}_k + \alpha_{ik} \dot{x}_k + k_{ik} x_k) = F(t) \quad (2.14)$$

2.6 Anharmonic oscillations

If we want to study oscillations at a higher level of approximation (anharmonic or non-linear oscillations), when we expand the potential and the kinetic energies of the system in terms of coordinates and velocities, we have to retain higher order terms. By doing this, some new phenomena are foreseen. If we write the Lagrangian considering expansion up to third-order terms, in the potential energy appears terms of degree three in the coordinates x_i and in the kinetic energy terms containing product of velocities and coordinates of the form $\dot{x}_i \dot{x}_j x_l$. Thus the Lagrangian is of the form:

$$L = \frac{1}{2} \sum_{i,k=1}^n (m_{ik} \dot{x}_i \dot{x}_k - k_{ik} x_i x_k) + \frac{1}{2} \sum_{i,k,l=1}^n l_{ikl} \dot{x}_i \dot{x}_k x_l - \frac{1}{3} \sum_{i,k,l=1}^n n_{ikl} x_i x_k x_l$$

where l_{ikl} and n_{ikl} are constant coefficients. If we express the Lagrangian in the normal coordinates of the linear approximation Θ_ω , being that coordinate transformation linear, we obtain the following result:

$$L = \frac{1}{2} \sum_{i=1}^n (\dot{\Theta}_i^2 - \omega_i^2 \Theta_i^2) + \frac{1}{2} \sum_{i,k,l=1}^n \lambda_{ikl} \dot{\Theta}_i \dot{\Theta}_k \Theta_l - \frac{1}{3} \sum_{i,k,l=1}^n \nu_{ikl} \Theta_i \Theta_k \Theta_l$$

where again λ_{ikl} and ν_{ikl} are constant coefficients. The equations of motion for this Lagrangian can be written in the form:

$$\ddot{\Theta}_i + \omega_i^2 \Theta_i = f_i(\Theta, \dot{\Theta}, \ddot{\Theta}) \quad (2.15)$$

where f_i are second-order homogeneous functions of the normal coordinates and of their time derivatives. If we use the method of successive approximations, we can express Θ_i as the sum:

$$\Theta_i = \Theta_i^{(1)} + \Theta_i^{(2)}$$

where $\Theta_i^{(2)}$ is very small compared to $\Theta_i^{(1)}$ and $\Theta_i^{(1)}$ satisfies:

$$\ddot{\Theta}_i^{(1)} + \omega_i^2 \Theta_i^{(1)} = 0$$

and thus are ordinary harmonic oscillations such as:

$$\Theta_i^{(1)} = a_i \cos(\omega_i t + \alpha_i)$$

If we retain just second-order terms in the right-hand side of equations 2.15, we obtain

$$\ddot{\Theta}_i^{(2)} + \omega_i^2 \Theta_i^{(2)} = f_i(\Theta^{(1)}, \dot{\Theta}^{(1)}, \ddot{\Theta}^{(1)}) \quad (2.16)$$

This is a set of inhomogeneous linear differential equations in which the right-hand side can be written as a sum of simple periodic functions.

$$\begin{aligned} \Theta_i^{(1)} \Theta_k^{(1)} &= a_i a_k \cos(\omega_i t + \alpha_i) \cos(\omega_k t + \alpha_k) = \\ &= \frac{1}{2} a_i a_k \{ \cos[(\omega_i + \omega_k)t + \alpha_i + \alpha_k] + \cos[(\omega_i - \omega_k)t + \alpha_i - \alpha_k] \} \end{aligned}$$

So the right-hand sides of equations 2.16 consist of terms corresponding to oscillations whose frequencies are the sums and differences of the eigen-frequencies of the system. In the second approximation, we conclude that additional oscillations with frequencies

$$\omega_i \pm \omega_k$$

are superimposed on the normal oscillations of the system (double frequency $2\omega_i$ and frequency zero are included). These are called *combination frequencies*. But in higher order approximation the fundamental frequencies are not the ones of the "unperturbed" case $\omega_i^{(0)}$. For this reason the method of successive approximations must be modified so that the periodic factors in the solutions shall contain the exact values of the frequency. As an example we consider an anharmonic oscillation in one dimension and we express the exact frequency as $\omega = \omega_0 + \omega^{(1)} + \omega^{(2)} + \dots$. If the Lagrangian is written as follows:

$$L = \frac{1}{2} m \dot{x}^2 - \frac{1}{2} m \omega_0^2 x^2 - \frac{1}{3} m \alpha x^3 - \frac{1}{4} m \beta x^4$$

and the corresponding equation of motion is:

$$\ddot{x} + \omega_0 x = -\alpha x^2 + \beta x^3$$

It turns out that $\omega^{(1)} = 0$ (in order for the resonance to be absent in the right-hand side), while

$$\omega^{(2)} = \left(\frac{3\beta}{8\omega_0} - \frac{5\alpha^2}{12\omega_0^3} \right) a^2$$

Finally the combination oscillation of the third order is of the kind $x = x^{(1)} + x^{(2)} + x^{(3)}$ where:

$$\begin{aligned}x^{(1)} &= a \cos \omega t \\x^{(2)} &= -\frac{\alpha a^2}{2\omega_0^2} + \frac{\alpha a^2}{6\omega_0^2} \cos 2\omega t \\x^{(3)} &= \frac{a^3}{16\omega_0^2} \left(\frac{\alpha^2}{3\omega_0^2} - \frac{1}{2}\beta \right) \cos 3\omega t\end{aligned}$$

Chapter 3

Small oscillations for coupled pendula

3.1 Coupled pendula

We now study the system made of the pendula with the same mass ($m_1 = m_2 = 1$) and length ($l_1 = l_2 = 1$) hanging at the same height. They undergo to the gravity force with $g = 1$ and are interconnected by a mass-less spring of elastic constant k and equilibrium length equal to distance d between the hanging points. This is a system of coupled pendula. For the sake of simplicity we take $d = 1$. Considering

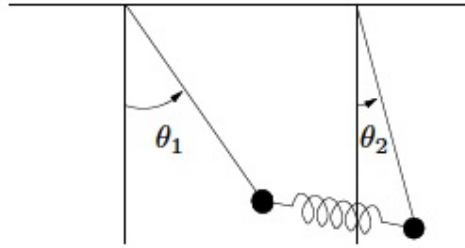


FIGURE 3.1: coupled pendula

small oscillations only, the system is described by the following Lagrangian:

$$L = \frac{1}{2}(\dot{\theta}_1^2 + \dot{\theta}_2^2) - \frac{1}{2}(\theta_1^2 + \theta_2^2 + k(\theta_1 - \theta_2)^2) \quad (3.1)$$

In fact if we consider a reference frame where the hanging points have coordinates $(0, 0)$ and $(0, d)$ respectively, pendulum positions are given by $P_1 = (\sin \theta_1, -\cos \theta_1)$ and $P_2 = (d + \sin \theta_2, -\cos \theta_2)$. Hence the elastic energy is given by:

$$\begin{aligned} U_{el}(\theta_1, \theta_2) &= \frac{1}{2}k \left(\sqrt{(d + \sin \theta_2 - \sin \theta_1)^2 + (-\cos \theta_2 + \cos \theta_1)^2} - d \right)^2 = \\ &= \frac{1}{2}k \left(\sqrt{d^2 + 2 + 2d(\sin \theta_2 - \sin \theta_1) - 2\cos(\theta_1 - \theta_2)} - d \right)^2 = \\ &= \frac{1}{2}kd^2 \left(\sqrt{(1 + 2d^{-1}(\theta_2 - \theta_1) - 2d^{-2}(\theta_1^2 + \theta_2^2 - 2\theta_1\theta_2) - 1)} - 1 \right)^2 + \mathcal{O}(\theta^2) = \\ &= \frac{1}{2}k(1 + \theta_2 - \theta_1 + \mathcal{O}(\theta^2) - 1)^2 + \mathcal{O}(\theta^2) \end{aligned}$$

Instead gravitational potential energy is given by

$$\begin{aligned} U_{gr} &= -\cos \theta_1 - \cos \theta_2 = -1 + \frac{1}{2}\theta_1^2 - 1 + \frac{1}{2}\theta_2^2 + \mathcal{O}(\theta^2) = \\ &= \text{const.} + \frac{1}{2}\theta_1^2 + \frac{1}{2}\theta_2^2 + \mathcal{O}(\theta^2) \end{aligned}$$

This demonstrate the given expression of the Lagrangian.

3.1.1 Normal modes

This system has two normal modes with frequencies $\omega_1 = 1$ and $\omega_2 = \sqrt{1 + 2k}$. In order to demonstrate this result the following coordinate change has to be defined:

$$Q_1 = \frac{\theta_1 + \theta_2}{2}, \quad Q_2 = \frac{\theta_1 - \theta_2}{2}$$

The Lagrangian 3.1 in those new coordinates rewrites:

$$L = \frac{1}{2}(\dot{Q}_1^2 + \dot{Q}_2^2) - \frac{1}{2}(\omega_1^2 Q_1^2 + \omega_2^2 Q_2^2)$$

where $\omega_1 = 1$ and $\omega_2 = \sqrt{1 + 2k}$. If $Q_2 = 0$ (i.e. $\theta_1 = \theta_2$), then the pendula oscillate in phase with frequency $\omega_1 = 1$ (no work done by the spring), while if $Q_1 = 0$, then the pendula oscillate with opposite phase and frequency $\omega_2 = \sqrt{1 + 2k}$.

3.1.2 Beats

If $k \ll 1$ energy is periodically transferred from first to second pendulum (*beats*). Indeed the following initial conditions can be considered:

$$\theta_1 = \theta_2 = 0, \quad \dot{\theta}_1 = v \quad \dot{\theta}_2 = 0$$

i.e. the whole initial energy is concentrated in the first pendulum as kinetic energy. Hence the initial condition in the new coordinates rewrites:

$$Q_1 = Q_2 = 0, \quad \dot{Q}_1 = \dot{Q}_2 = \frac{v}{\sqrt{2}}$$

and the following solution are obtained:

$$\theta_1(t) = v \cos \epsilon t \sin \omega t + \mathcal{O}(k)$$

$$\theta_2(t) = -v \cos \epsilon t \sin \omega t + \mathcal{O}(k)$$

where $\epsilon = (\omega_1 - \omega_2)/2 = k/2 + \mathcal{O}(k^2)$ and $\omega = (\omega_1 + \omega_2)/2 = 1 + k/2 + \mathcal{O}(k^2)$. The solutions describe an oscillation mode with period $T = 2\pi/\omega$, modulated by another sinusoidal curve with a much longer period $2\pi/\epsilon \gg 1$. When $t = 2\pi/\epsilon$, the motion of $\theta_1(t)$ is almost completely damped, while $\theta_2(t)$ reaches the maximum amplitude which is comparable with the initial amplitude of $\theta_1(t)$.

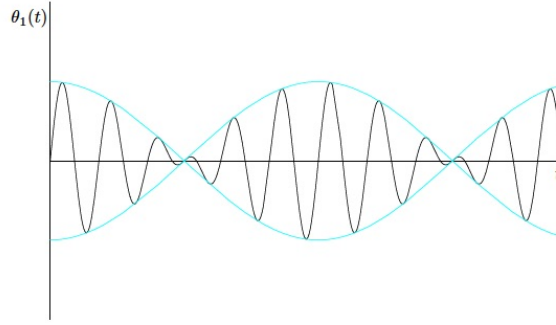


FIGURE 3.2: beats

3.2 Coupled pendula with external springs

In order to better approximate the system described in Chapter 4, the previous system has to include to more springs connecting the pendula with lateral walls (at a distance L). Moreover in general springs can contribute to internal forces with non linear terms (with α and β coefficients). As a consequence the Lagrangian 3.1 becomes:

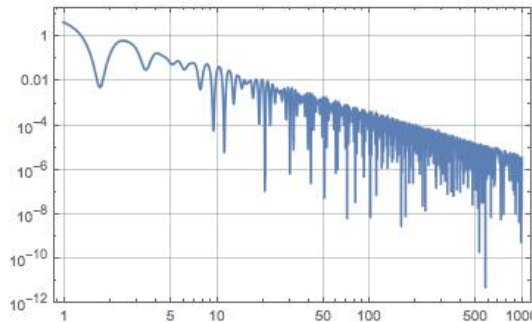
$$\begin{aligned}
 L = & \frac{1}{2}m (\dot{x}_1(t)^2 + \dot{x}_2(t)^2) - \frac{mg}{2l} (x_1(t)^2 + x_2(t)^2) - \\
 & - \frac{k}{2} (x_1(t)^2 + 2(x_2(t) - x_1(t))^2 + (L - x_2(t))^2) - \\
 & - \alpha (x_1(t)^3 + 2(x_2(t) - x_1(t))^3 + (L - x_2(t))^3) - \\
 & - \beta (x_1(t)^4 + 2(x_2(t) - x_1(t))^4 + (L - x_2(t))^4)
 \end{aligned}$$

The corresponding Eulero-Lagrange equations are the following:

$$\begin{aligned}
 -12l\beta x_1(t)^3 + 3lx_1(t)^2(\alpha + 8\beta x_2(t)) - x_1(t) (3kl + gm + 12l\alpha x_2(t) + 24l\beta x_2(t)^2) + \\
 + l (2kx_2(t) + 6\alpha x_2(t)^2 + 8\beta x_2(t)^3 - m\ddot{x}_1(t)) = 0 \\
 -\alpha (-3(L - x_2(t))^2 + 6(x_1(t) - x_2(t))^2) + k(L + 2x_1(t) - 3x_2(t)) - \frac{gm x_2(t)}{l} - \\
 -\beta (-4(L - x_2(t))^3 + 8(-x_1(t) + x_2(t))^3) - m\ddot{x}_2(t) = 0
 \end{aligned}$$

Solving the associated Cauchy problem, the energy metric Ω (see 6.3) can be calculated for different values of parameters α and β .

As an example for $\alpha = 1$ and $\beta = 0$ the bilogarithmic plot for Ω is given by:

FIGURE 3.3: time evolution of Ω

As it is shown, after a transient Ω behaviour can be approximated by a power law: in particular $\Omega \sim t^{-2}$. This result apply to a non-dissipative system. In a further research the contribution of dissipation in determining the time evolution of Ω has to be better investigated.

3.3 Coupled pendula with discretised cable

The coupled pendula considered until now, are suspended to a rigid body which does not act as a coupling device. A different system of coupled pendula is composed by a cable sustaining the pendula and the pendula themselves. Contrary to previous system, the cable can move and provides the coupling between the pendula. In order to take into account the coupling contribution provided by the cable, the mass of the cable is discretised. M is the pendulum mass, m the discrete mass of a segment of cable, l is the discrete length of the cable and L is the length of the pendulum. The following Lagrangian applies to a single pendulum connected to a cable composed by 3 segments (the 2 discrete mass M are concentrated at the segment extremes). The motion is projected on the horizontal direction of oscillation of both cable and pendulum.

$$L = \frac{1}{2}ml^2 \left(\dot{\alpha}(t)^2 \cos^2 \alpha(t) + (\dot{\alpha}(t) \cos \alpha(t) + \dot{\beta}(t) \cos^2 \beta(t)) + \right. \\ \left. + \frac{1}{2}M \left(\frac{l}{2}(2\dot{\alpha}(t) \cos \alpha(t) + \dot{\beta}(t) \cos \beta(t)) + L\dot{\phi}(t) \cos \phi(t) \right)^2 - \frac{MgL}{2}\phi(t)^2 \right)$$

This Lagrangian could be studied in a further stage of the research.

Chapter 4

Methods and Material

4.1 Mechanical system



FIGURE 4.1: 24 *coupled pendula*

The mechanical system depicted in figure 4.1 was designed and built in Dalmine laboratories. It consists of a large aluminium framework, the hosted pendulum chain and the releasing mechanism. The framework is 2 m long, 2 m high and 1 m deep and was built using 40 x 80 mm and 40 x 40 mm aluminium extrusions. It stands over four concrete blocks placed on the floor. A 5 m long 5 mm diameter braided steel cable (0.1 kg/m linear density) crosses the cage and hangs from two hooks in the short upper side of the cage; it is pretensioned with two 18.450 kg counterweights. On the internal part of the cage a long 1 mm nylon rope was used to hang each of the 24 pendula from the steel cable and to connect them all. Each pendulum has a length of 1.145 mm and is coupled with the other pendula by that rope, which transmits the interaction strains. Due to the pendula distributed mass, the steel cable assumes approximately a catenary shape when the system is at rest. For this reason the pendula have different height from soil: the externals are 90 cm high, while the centrals are 80 cm high. Each pendulum consists of a red coloured iron sphere: its mass is 480 g and its diameter is 5 cm. Each sphere has a boss with a 2 mm through hole where the nylon rope is inserted. We chose iron spheres, in order to use an electromagnetic releasing mechanism. Moreover we have chosen the red

colour for the pendula in order to better distinguish them from the background using video-tracking procedure to study the motion of the chain. This system, shown in the previous picture 4.1 is sketched in the following plot: The upper corners of

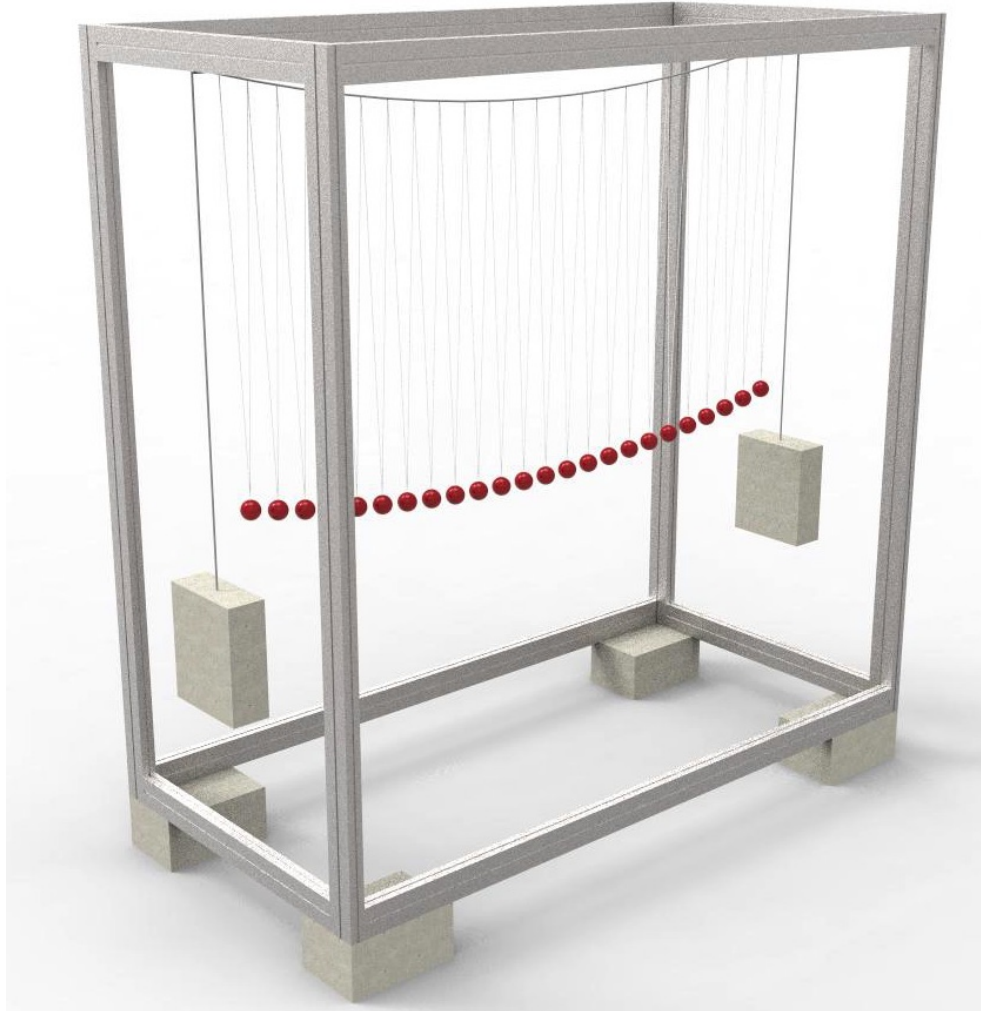


FIGURE 4.2: *System sketch*

the framework have been connected to floor using tie rods in order to minimise the energy lost by the system, because of vibrations of the framework itself.

4.2 Releasing mechanism

In order to release the required pendula at a specific angle at rest, we selected an EclipseMagnetics electromagnets model *M52172/24VDC*. They have a 25 mm diameter and a typical holding force of 150 N. This size is well suited for the iron sphere, while the holding force is pretty high compared to the pendulum weight (less than 5 N). But the magnetic pull decreases rapidly when the air gap grows; so it is pretty strong at the contact point, but it is not in the surrounding because of sphere curvature. See [A](#) for electromagnets specifications.

Those 24 electromagnets are connected in parallel to a Mean Well model RS-100-24 power supply (it produces a 24V DC voltage and offers a 108W rated power). See [A](#) for power supply specifications. When they are energised, they hold the pendula

which touch them.

Those electromagnets need to be moved on a vertical plane, depending on the selected initial angle. For that purpose they are fixed to an aluminium bar, which can be moved vertically along another aluminium frame. This mechanical structure is placed on 4 wheels: this allow to move the electromagnets horizontally, both inside (10° and 20°) and outside the cage (30° to 50°).

A number of electromagnets is used to hold the corresponding number of pendula to a desired initial excitation angle. When the initial configuration is ready, video-recording is started, the electromagnets are switched off and the excited pendula are released.



FIGURE 4.3: *Equipment sketch*



FIGURE 4.4: *Releasing mechanism*

4.3 VideoTracking procedure

4.3.1 Video recording

For that purpose we use a GoPro Hero4 Black webcam, fixed top-down in the upper part of the framework. This webcam is slightly displaced on one side of the chain: the position was chosen in order to take full advantage of the UltraWide FOV of the webcam covering a 50° oscillations of both sides of the chain and minimising the visibility of the cable and the consequent shadowing of the underlying pendula. In our setup the horizontal axis of the webcam is aligned with the chain (118.2°), while the vertical axis is aligned with the direction of the oscillation (69.5°): the position allows the webcam to see the chain in all planned initial configurations. In order to better distinguish the outermost spheres, that otherwise looks very close to one another due to perspective, we plugged into the webcam a Neewer(R) 52MM 0.45X Wide Angle High Definition Lens with Macro. <http://www.neewer.com/90083804.html> The webcam records in fullHD (1920x1080) with a frame rate of 120 fps. This high frame rate is useful in order to track the high speed motion of pendula released at high angles (from 50° to 30°), but is replaced by a slower frame rate (60 fps) when lower energy runs and slower pendula are considered. The webcam records the chain motion for 2 hours, since the excited pendula are released: recording is done on a Lexar 1000x microSDXC UHS-3 of capacity 128GB, which is officially tested by GoPro with Hero4, as shown in GoPro website:

<https://it.gopro.com/help/articles/Block/microSD-Card-Considerations>

That microSD offers up to 150MB/s read and 45MB/s write performance as stated by Lexar on their website:

<http://www.lexar.com/products/memory-cards/microsd/Lexar-Professional-1000x-microSDHC-microSDXC-UHS-II-Cards.html>

Despite the official data, we noticed the webcam replicates frame on a regular basis. When recording at 120 fps: analysing the video duplicated frames are detected and are estimated around to 20 to 25% (they are uniformly distributed over the recording). When recording at 60 fps, the replication rate is lower and it is higher in the very first phase than in the latter. Those replica are then automatically removed and this operation does not have relevant consequences on the obtained measurements.

The GoPro Hero4 webcam uses chaptering as a safety precaution: in fact it splits the footage in 3.9GB files (which corresponds to about 9 minutes of video at a time at the 120 fps and to about 18 minutes at 60 fps), in order to minimise data loss in case the file get corrupted for any reason. The produced files are named in sequence with a unique id of the recoding session and a progressive number for the specific file in that sequence: the segments can be easily and seamlessly rejoined in editing software such as GoPro Studio or VLC. In order for the webcam to record for 2 hours at highest frame rate and resolution settings, we removed the battery and we used an USB attachment to the external power. In order to avoid webcam overheating we also did not take advantage of the wireless connectivity to remotely start and stop recording activity.

4.3.2 Video editing

The following operations are needed in order to prepare a suitable video file to be used by the video-tracking algorithm described later. When recording is stopped, the file sequence stored in the microSD is imported on a pc (server) running Windows 10 using GoPro Quik v2.3 software. Then using GoPro Studio the video files are converted from their highly compressed format into the Digital Intermediate (DI) Cineform Codec, used by GoPro Studio for video editing. In the next stage VLC Command Line Interface is used to merge (option #gather is used) all the .avi files in the correct sequence in a single large .avi file. When this is done, VLC is used to convert the large .avi file (in the Cineform Codec) to smaller .mp4 file. In order to do so the Kolor CineForm HD plugin for VLC is needed, which allows to play CineForm encoded videos in VLC.

4.3.3 Video tracking

When the 2 hours video file of the run is ready, we need to extract the position of the 24 pendula in every frame. In order to achieve this goal, OpenCV libraries are used. OpenCV (Open Source Computer Vision) is a library of programming functions mainly aimed at real-time computer vision. The library is cross-platform and free for use under the open-source BSD license. Object video-tracking is one of main fields in computer vision. Due to the availability of 2D and 3D high quality and low cost webcams and to the growing need of automatic analysis of videos, there is a large interest on video-tracking advanced algorithms. One of the basic step in video analysis is detection of selected moving objects and their tracking frame by frame. Object tracking can be thought as the estimate of object trajectory on the image plane, by assigning coherent labels to objects in different frame of the same video. OpenCV's application areas are pretty wide and include motion tracking. Open source tutorial code written by Kyle Hounslow, University of British Columbia, and based on OpenCV is available for download at the following website and the object-tracking-tutorial was used.

<https://github.com/kylehounslow/opencv-tuts>

This C++ code was adapted to the specific needs of the experimental setup according to the recommendations provided in specific tutorials [29, 30, 31, 32, 33]. In particular, despite it can be used for real-time processing, it was adapted to post-process recorded videos and for this reason it was called "GoProTracking" algorithm. The first operation performed by the code is colour filtering from RGB colorspace (used by devices) to HSV (hue saturation value) colorspace (largely used in image processing). So each video frame is converted into HSV first and then the image is filtered in order to select the colours of interest between a MIN and MAX HSV threshold (it is a set of 6 values: min and max Hue, min and max Saturation and min and max Value). The thresholded image is a binary (black and white) image where the filtered object appears in white. Looking at the binary image and searching for the 1s, the filtered objects are found. Those HSV intervals can be narrow or large depending on the both the colour and the lightning of the object. Having narrow intervals is preferable, because it is unlikely to obtain noise in the HSV image. But even if the object of interest is monochrome, it is a 3D object and it is hard to uniformly illuminate it on all facets. This explains why the HSV intervals are easily large, even with monochrome objects. Our chain is monochrome opaque red, but objects to be tracked are spheres. This filtering methodology requires a good shading of the background in order for the objects to be tracked: the whole webcam FOV has to be checked so as to prevent

noise. For this purpose we used several white clothes/tissues and a white carpet to obtain a uniform background and to partially shade natural light and obtain a stable lighting. If there is noise left in the binary image, the software perform few morphological operations: small white spots in white space are “eroded” making them smaller or not existent and then larger white spaces are “dilated”, making them larger. Those operations are done using rectangular elements in order to be less computationally intensive. When colour filtering is done, the second operation performed by the code is contour finding. The contour is the outline of all objects found in the binary image and in this case it should look like a circle. Then the algorithm identifies the position in pixel of the center of each circle. The image is a 1920×1080 pixels. The x coordinate is the one following the motion, while the y coordinate should be approximately constant at all time, but, due to setup imprecisions as well as to fisheye image distortion, it does slightly change (of the order of few tens of pixel), but anyway it can be considered as the pendulum position along the chain. At this point the code uses some of the openCV drawing functions to draw crosshair on each tracked object, to print its coordinates in pixel next to it and the frame number on each frame. This enriched frame is appended to a new output .avi file, with a compression format CODEC DIV4 (MPEG4 modified for DIVX). At the same time a new line is added to a text file, where frame number is in the first column and then the following couple of columns show the x, y coordinates for each tracked object.

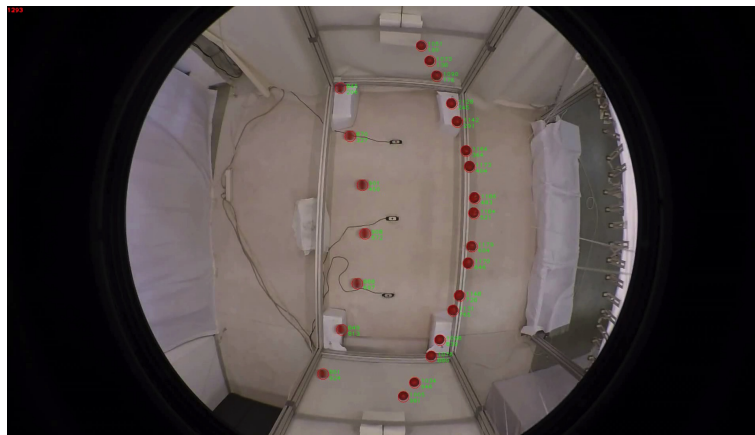


FIGURE 4.5: Example frame of the output file of the videotracking algorithm

4.3.4 Data processing

At this stage the text file with (t, x, y) coordinates is ready for processing. Two problems need to be solved:

- pixel coordinates have to be converted in meters and
- pendula ordering has to be correctly recognised despite fisheye effect: one of the fisheye distortion effects is to bend pendula trajectories (both in x and in y) in a such a way that the frame analysis can encounter the next pendulum before the expected one (pendula ordering is based on growing y), because the excited pendulum reach a position which has a lower y with respect to the non excited neighbour.

In order to better explain this effect consider the following frame of a Logitech webcam positioned on the floor and oriented upwards: when videotracking is performed, frame scan is started from the upper left corner down to lower right corner.

The first object found by the algorithm has coordinates (701, 76), while the second has (397, 77): the two y coordinates are very close and a higher excitation would produce a lower y coordinate for the excited pendulum with respect to the following one. In that case the algorithm would mix the data of the two pendula, producing spurious coordinate "jumps".

The data contained in the text file are imported in MS Excel: it is about $40 \cdot 10^6$

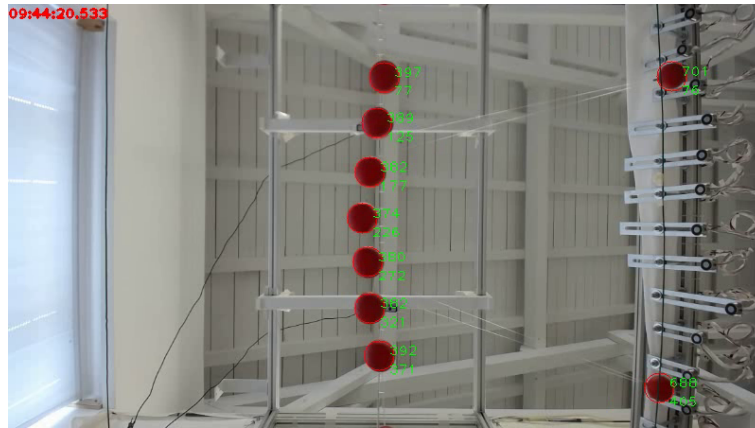


FIGURE 4.6: Sphere detection order with a Logitech webcam recording video

data. ¹ Rows with more than the expected 49 columns have to be dropped (one or more undesired objects have been tracked). On the other side, an ordering of the overall data with respect to the last columns is done in order to identify rows with less than 49 columns: those rows are dropped because at least one of desired pendula was not tracked. Now the file is ready to be further analysed. On average the number of deleted rows corresponds to about 5% percent of the overall data and therefore it can be considered negligible. The calibration procedure described in the following addresses both identified problems and it was repeated for each pendulum. A metric beam was placed horizontally just under the examined pendulum and it was aligned in the oscillation plane. Then while webcam recording was on, for few seconds we held the examined pendulum over specific positions along that metric beam, i.e. every 10 cm on each side of the chain starting from the rest position up to a 1.2 m distance. This short video was then analysed with the video-tracking algorithm in order to extract the pixel x, y coordinates of those known metric positions. Those 23 x coordinates with the corresponding known metric distances were analysed in Excel in order to deduce the best transformation converting pixel into meters. We found that a linear transformations is well suited to produce such a conversion ($R^2 = 0.999$). The same set of pixel x, y coordinates was used to trace the pendulum trajectory in the horizontal plane. With no fisheye effect, the trajectory is just a straight line, but the webcam and the macro lens introduce a fisheye effect which bends that line at the extremes. Again the 23 couples of data was analysed in Excel to obtain the best polynomial fitting of that curve: we found that a third order polynomial is appropriate in order to fit those data. The pixel coordinates found in the text file produced by the video-tracking algorithm are compared to those trajectories in order to recognise which pendulum they belong to. The video tracking results are then studied and analysed from a statistical and physical standpoint using Wolfram Mathematica.

¹ $7200 \text{ s} \times 120 \text{ fps} \times 48 \text{ coord}/f=40 \cdot 10^6 \text{ coord}$. This is for 120 fps recording. Half the value for 60 fps recordings.

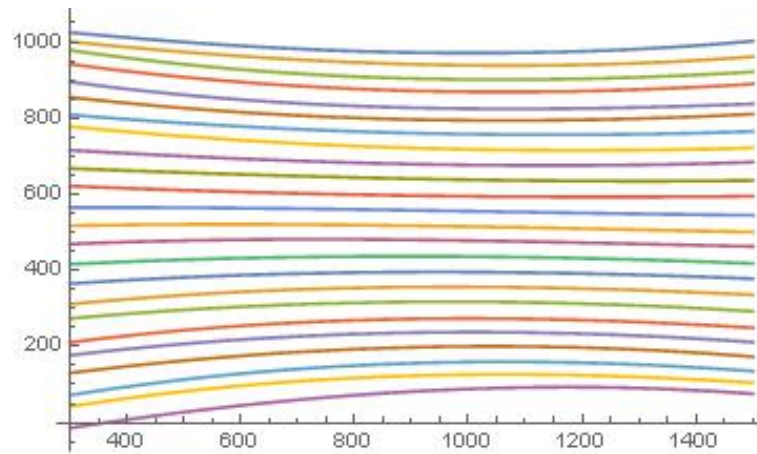


FIGURE 4.7: *The plot represents the trajectories of the 24 spheres, with as many 3rd order polynomials*

4.4 Measurement protocol

The measurement campaign followed a well defined protocol aimed to excite specific normal modes of the chain, in a wide frequency range. The pendula were excited to the following angles: 10° , 20° , 30° , 40° and 50° . Given a fixed excitation angle we studied the initial conditions corresponding to the following excited pendula (if not otherwise specified, normal mode excitation is considered):

- pendulum n. 8
- pendulum n. 16
- pendula n. 8 and 16
- pendula n. 8 and 16 (differential mode, i.e. opposite sides)
- pendula n. 6, 12 and 18
- pendula n. 4, 8, 12, 16 and 20
- pendula n. 9, 12 and 15
- pendula n. 3, 6, 9, 12, 15, 18 and 21

For the lowest angles (10° and 20°) other initial configurations were studied:

- all pendula
- pendula from 1 to 12 on one side and from 13 to 24 on the opposite side

for an overall number of 44 runs with different initial conditions. A couple of runs have been repeated with the same initial conditions to study the chaotic behaviour of the system.

Chapter 5

Experimental results

5.1 Displacement x as a function of t

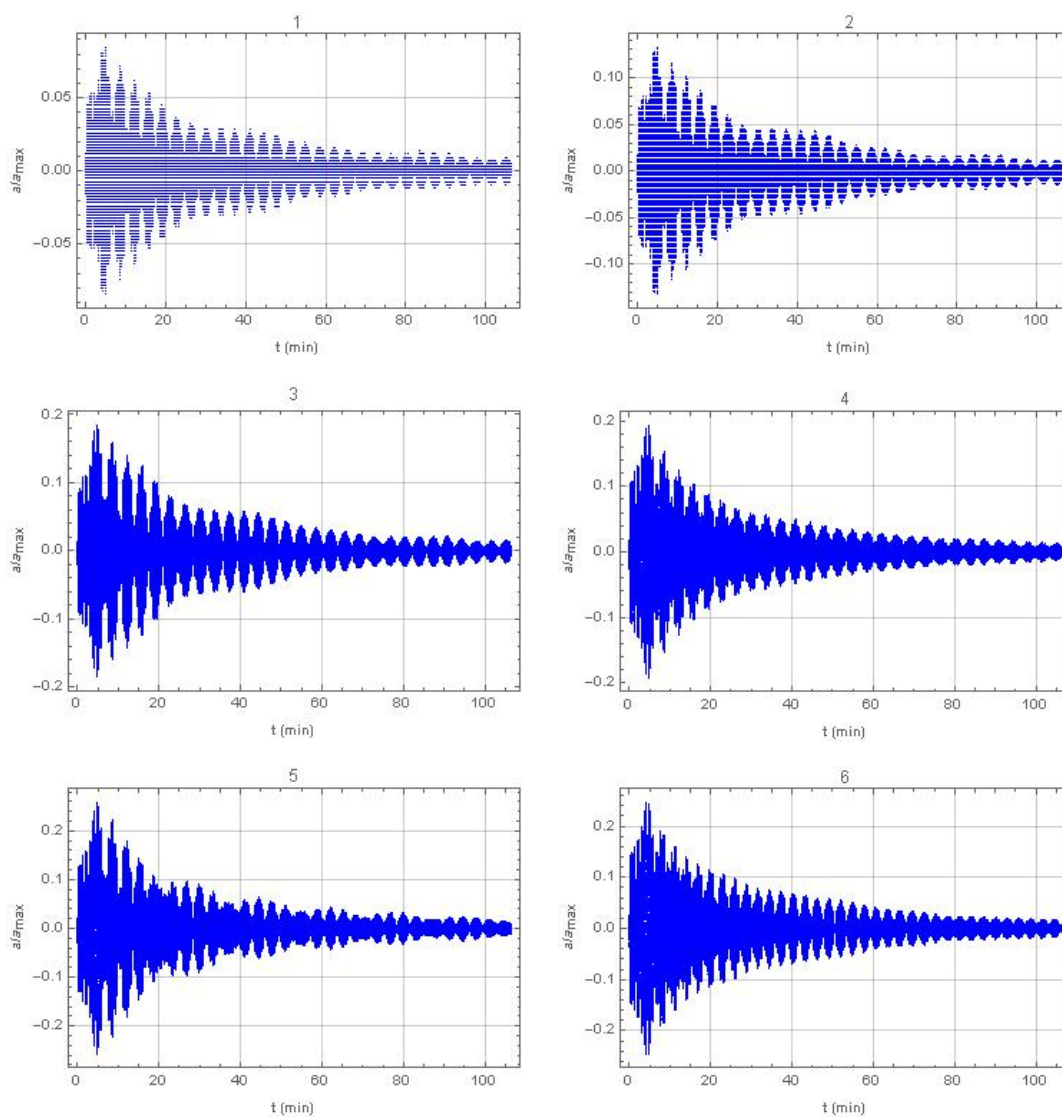


FIGURE 5.1: P08 50°: normalised displacement

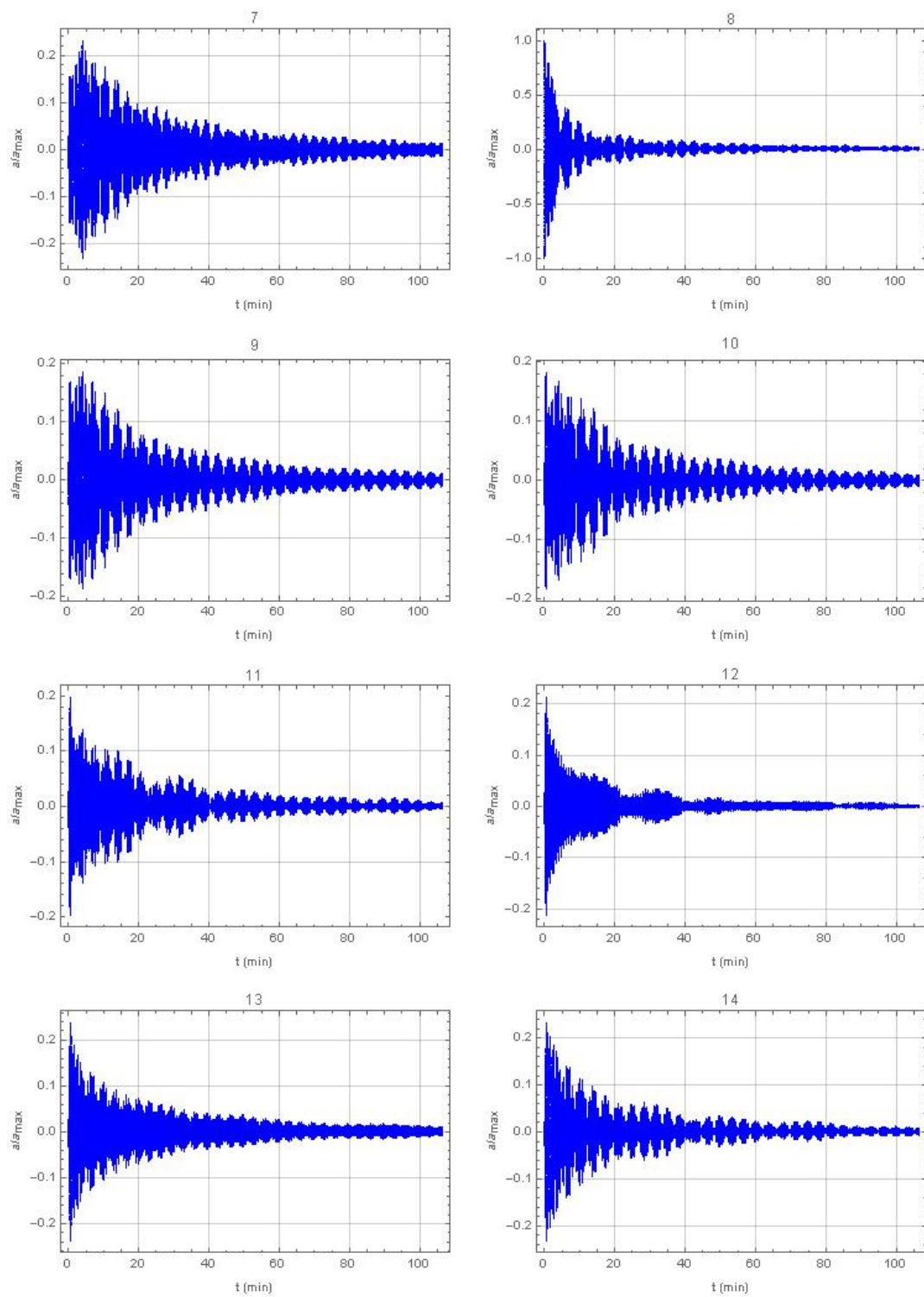


FIGURE 5.2: P08 50°: normalised displacement

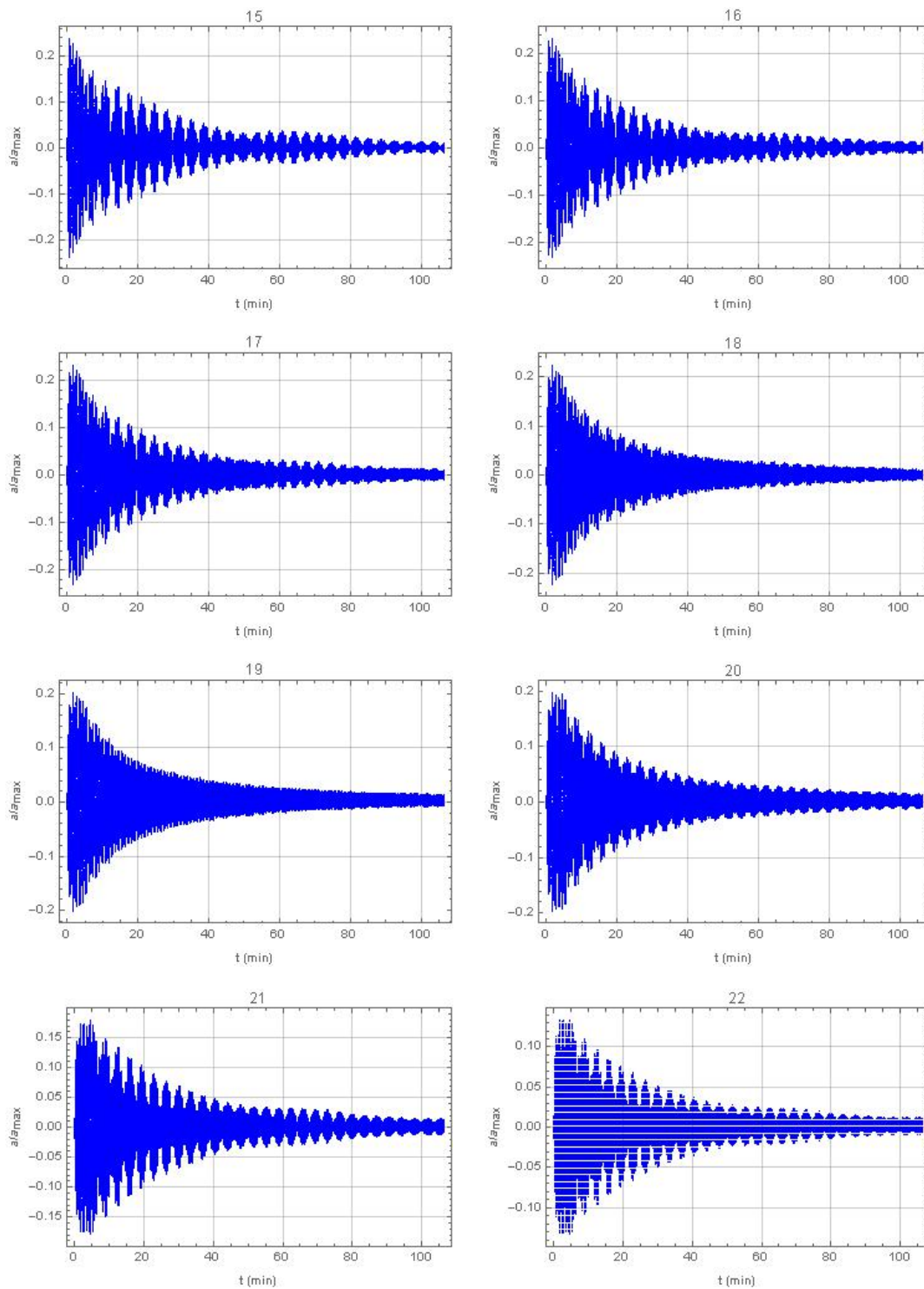


FIGURE 5.3: P08 50°: normalised displacements

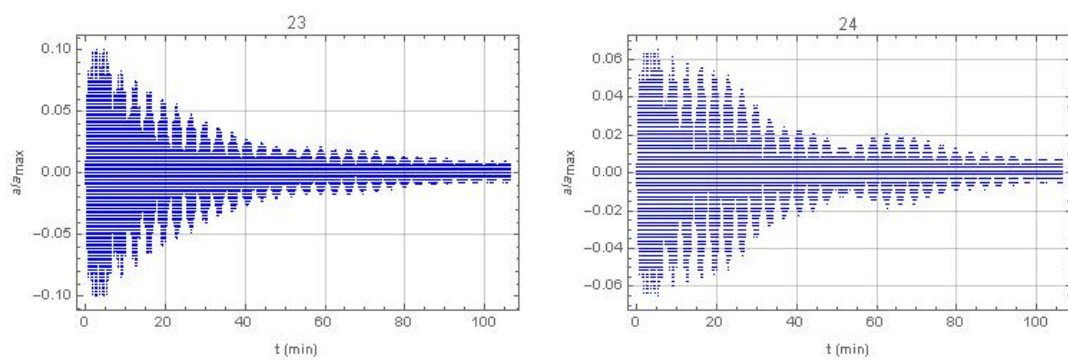


FIGURE 5.4: P08 50°: normalised displacements

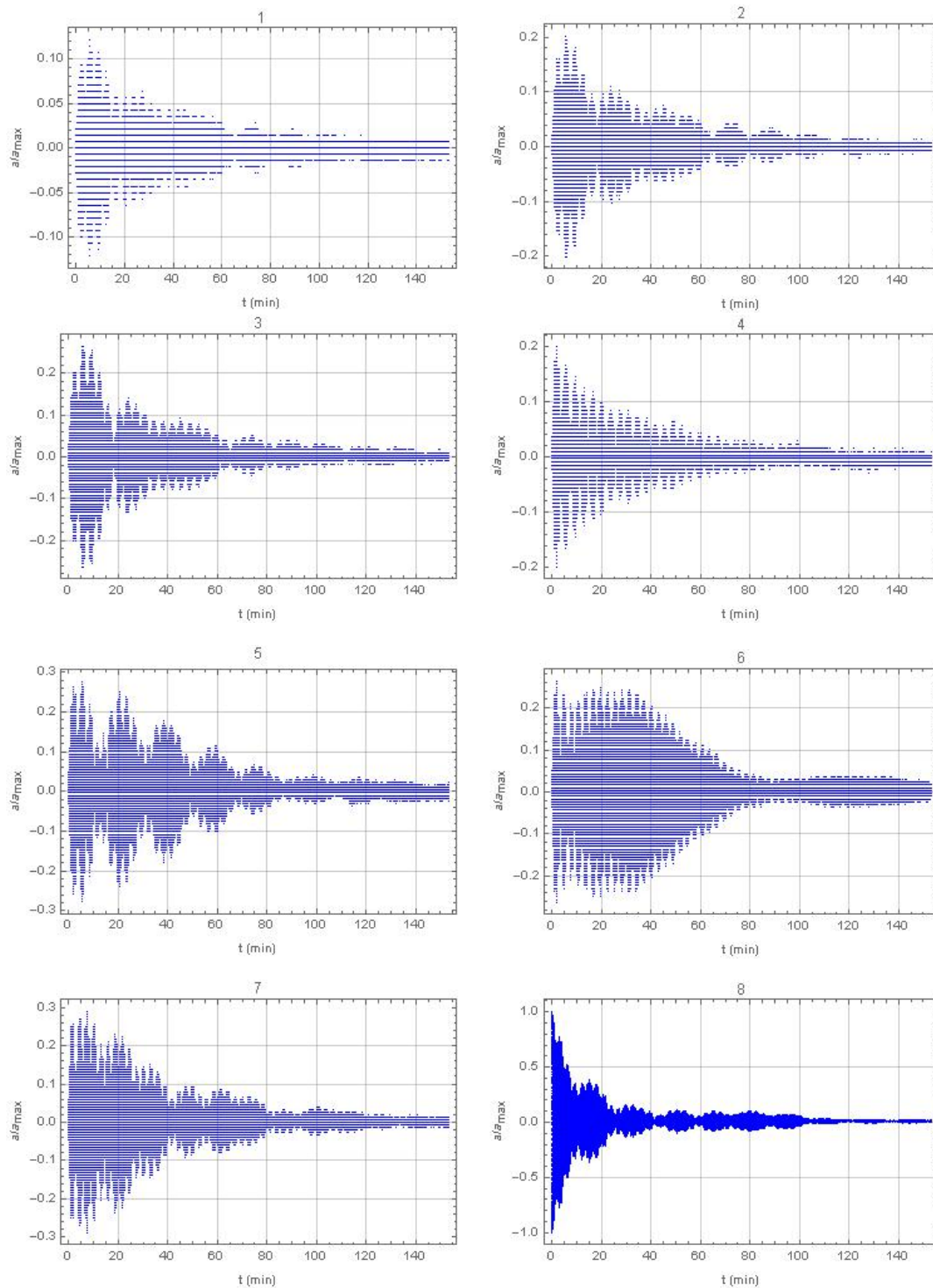
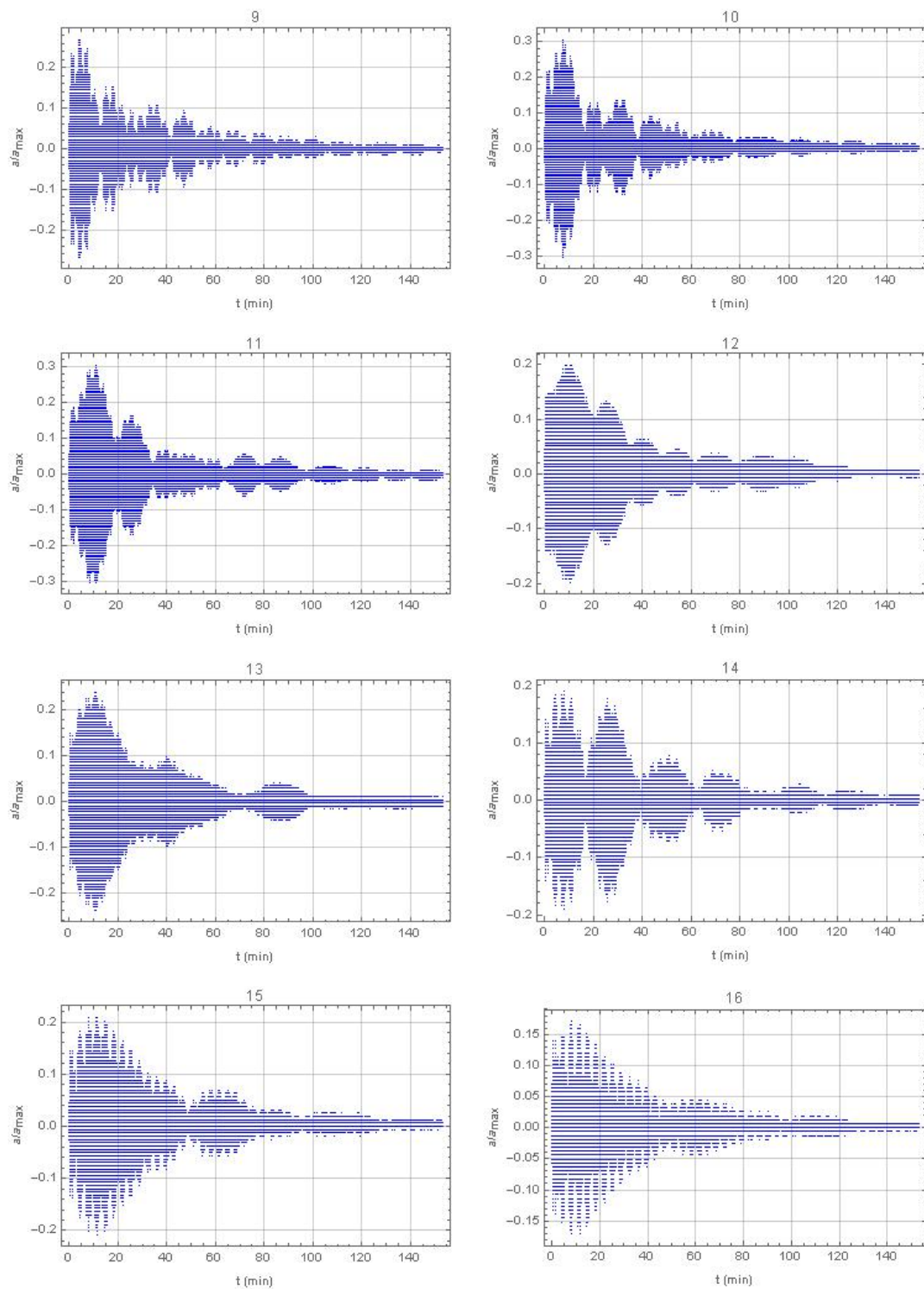


FIGURE 5.5: P08 10°: normalised displacements

FIGURE 5.6: P08 10° : normalised displacements

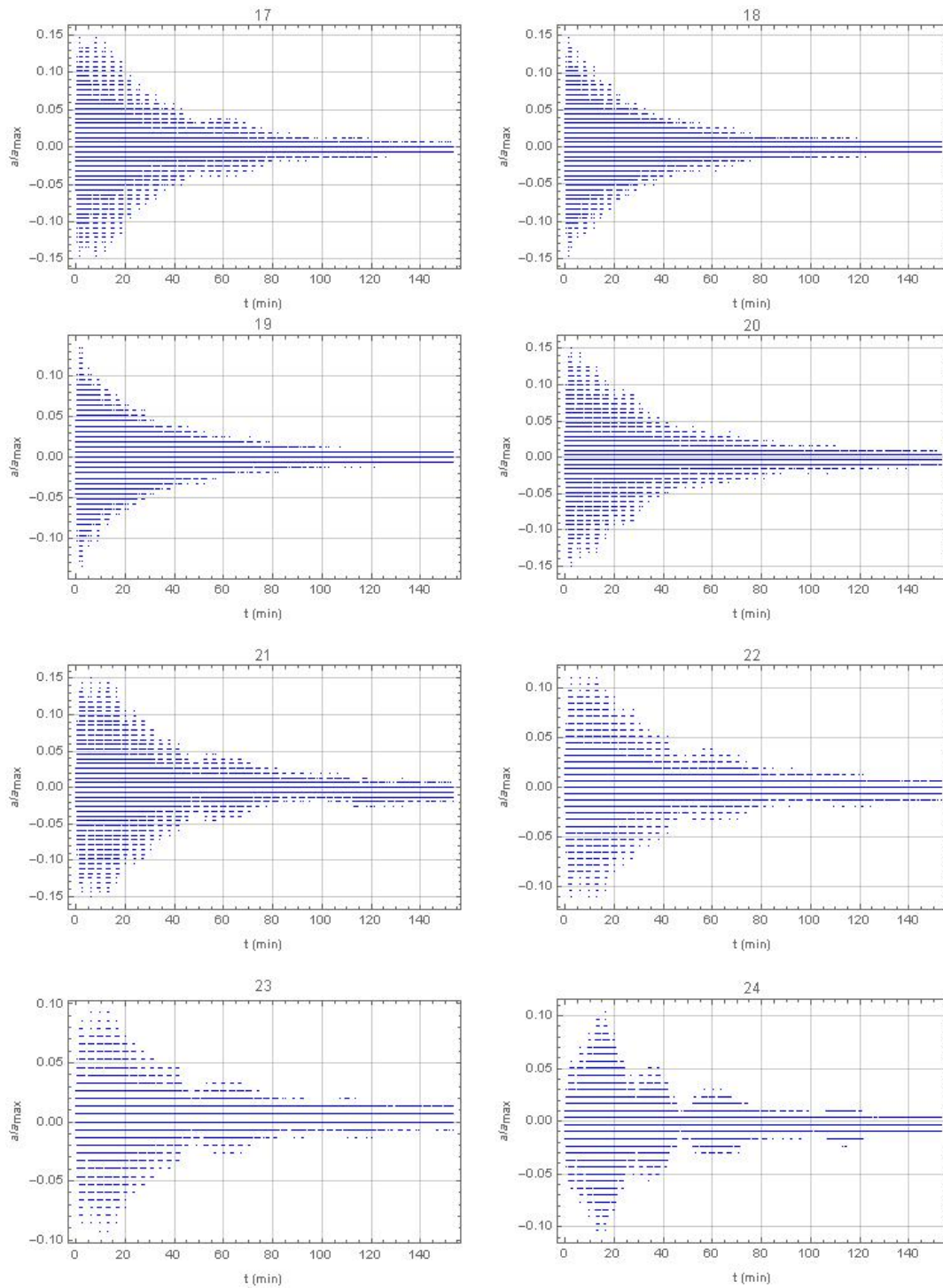


FIGURE 5.7: P08 10°: normalised displacements

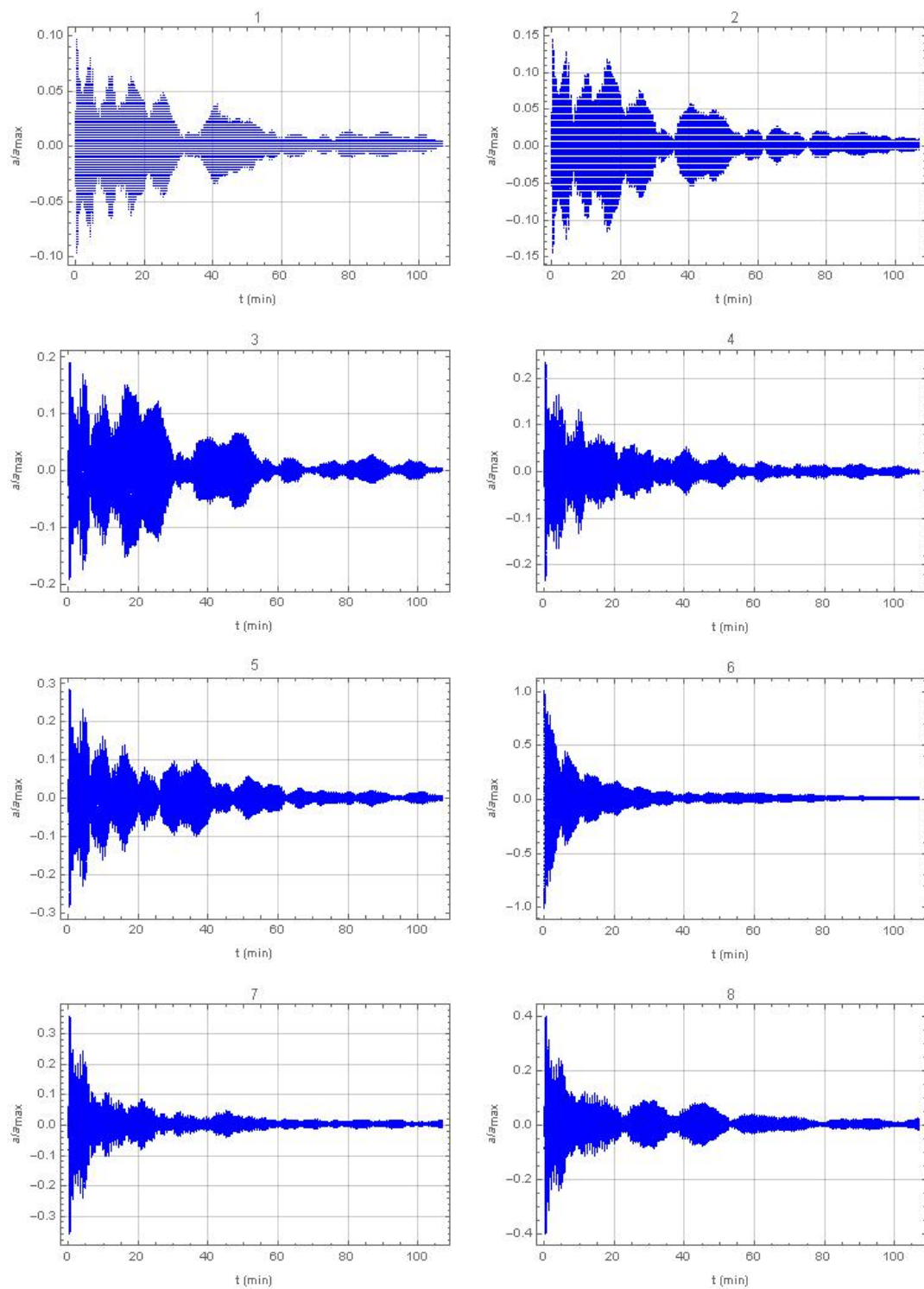


FIGURE 5.8: P06-12-18 50°: normalised displacements

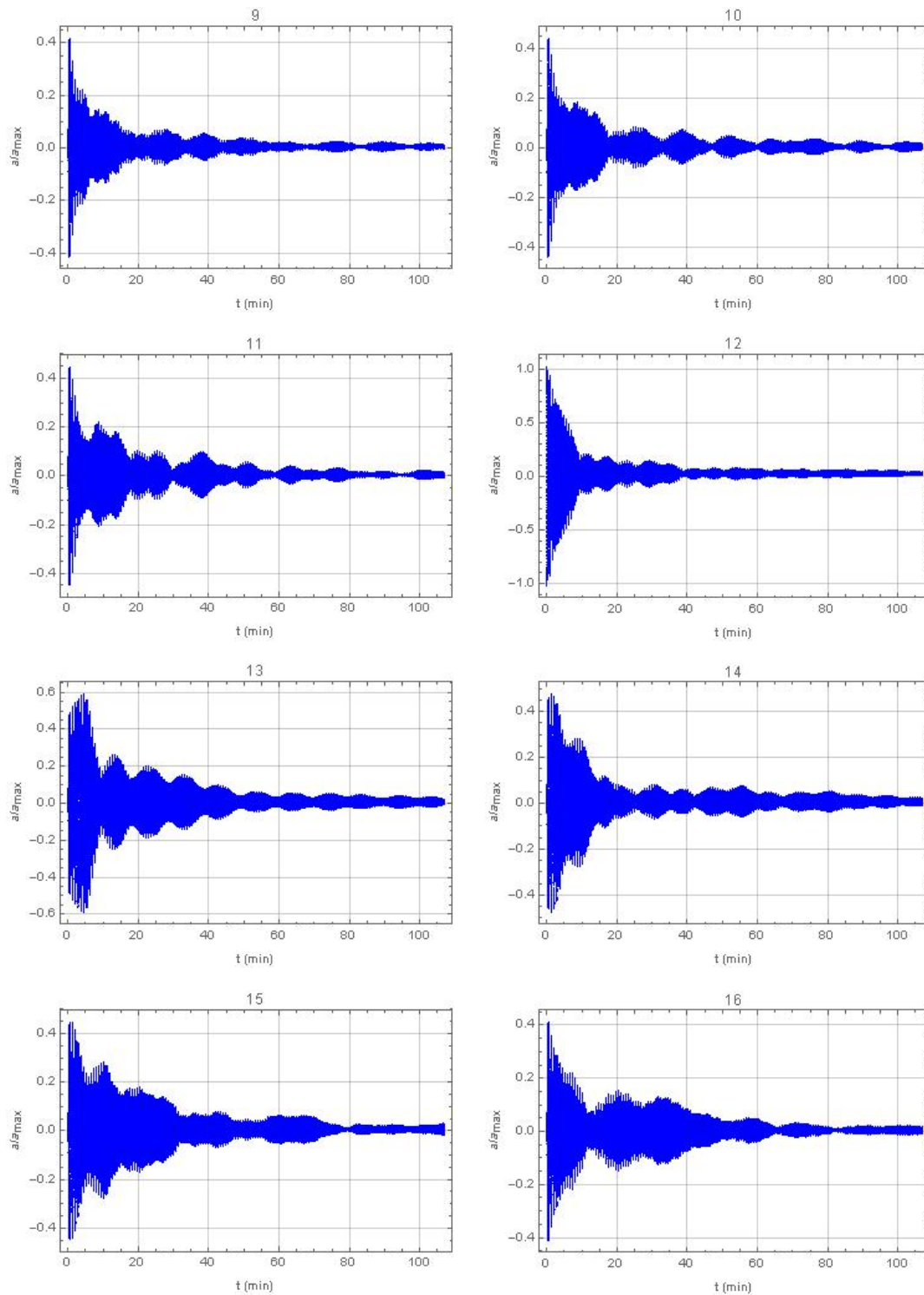


FIGURE 5.9: P06-12-18 50°: normalised displacements

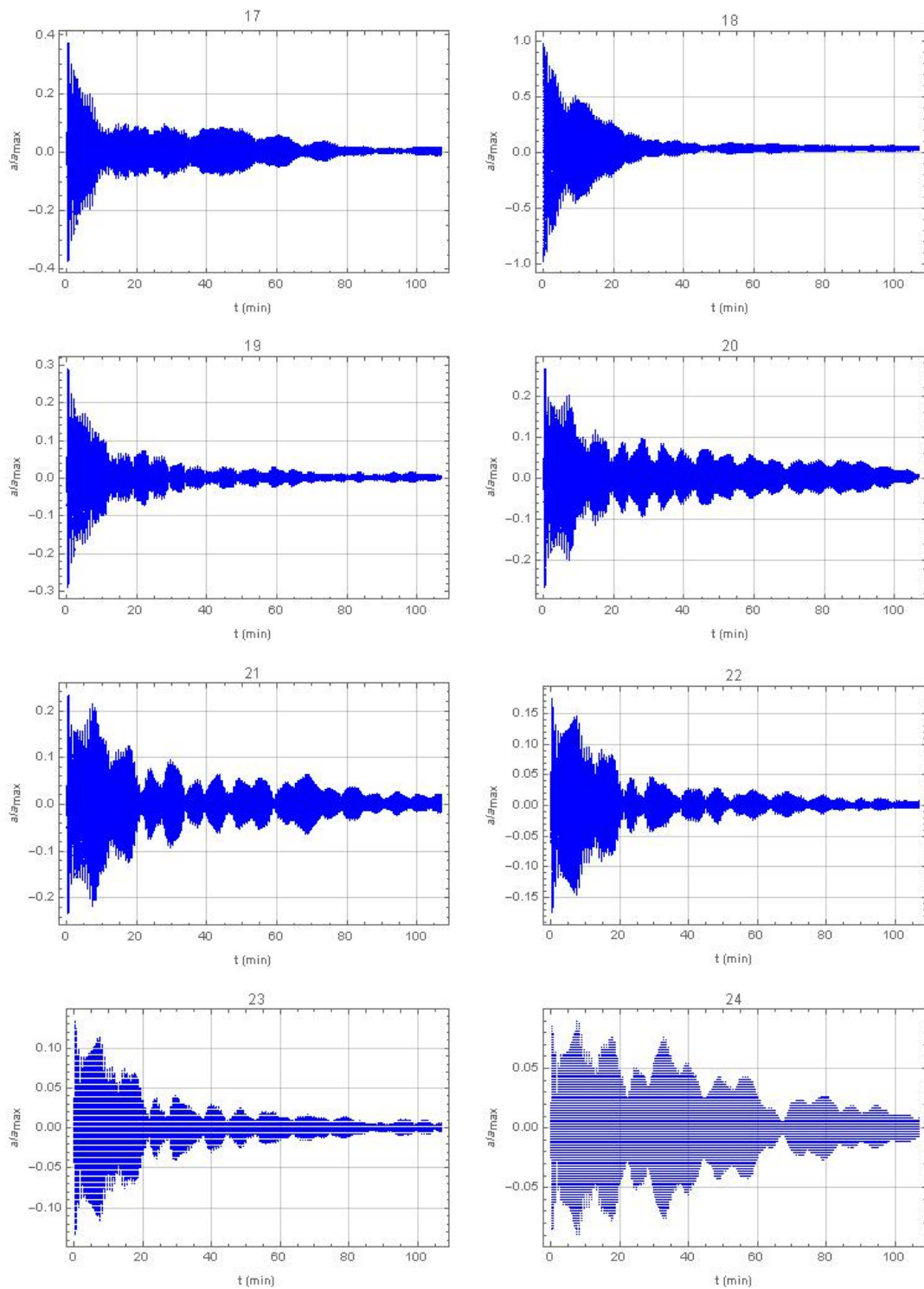


FIGURE 5.10: P06-12-18 50°: normalised displacements

5.2 Chaos outbreak

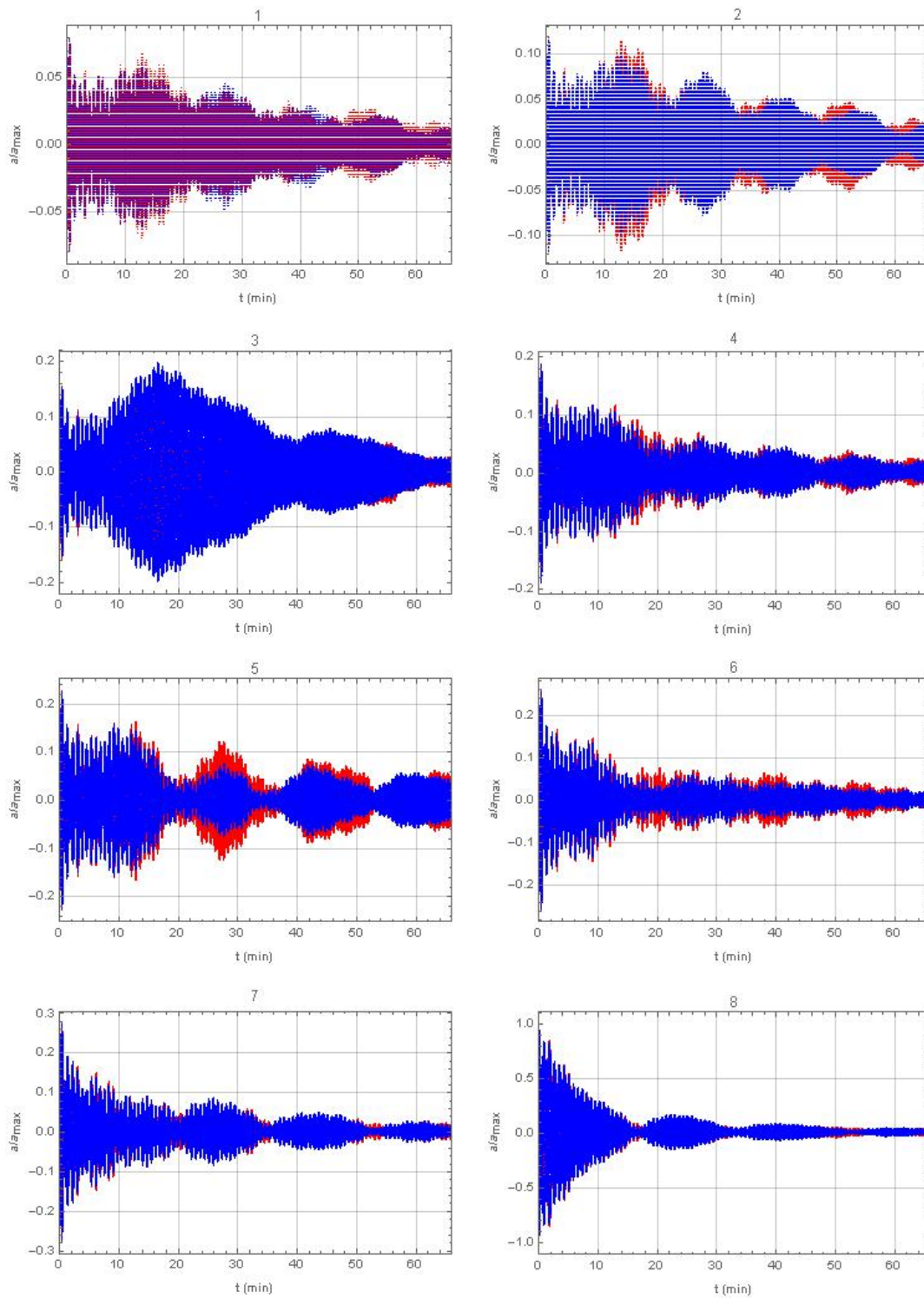


FIGURE 5.11: P08-16 50° : two runs overlap to show chaos outbreak

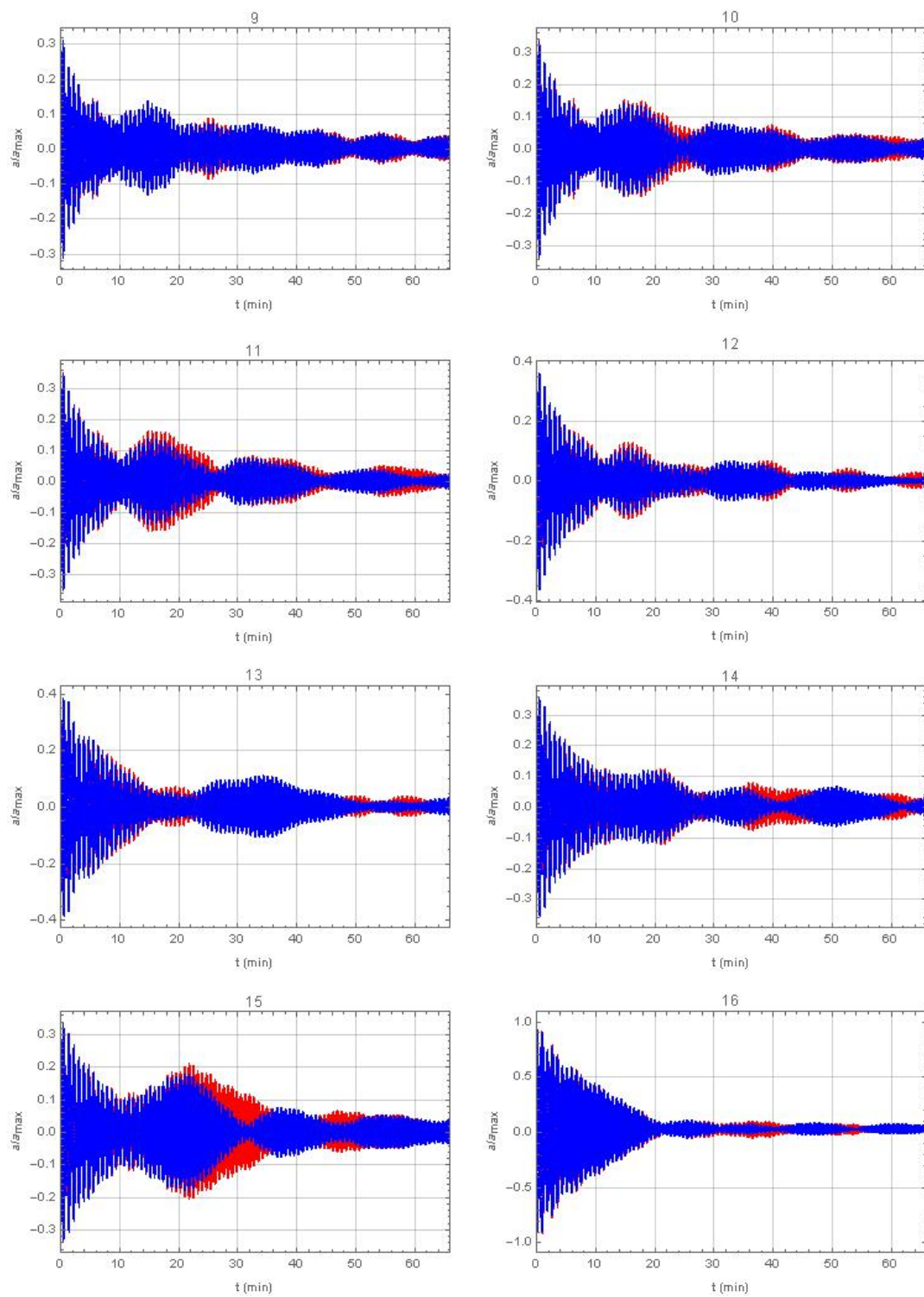


FIGURE 5.12: P08 50°: two runs overlap to show chaos outbreak

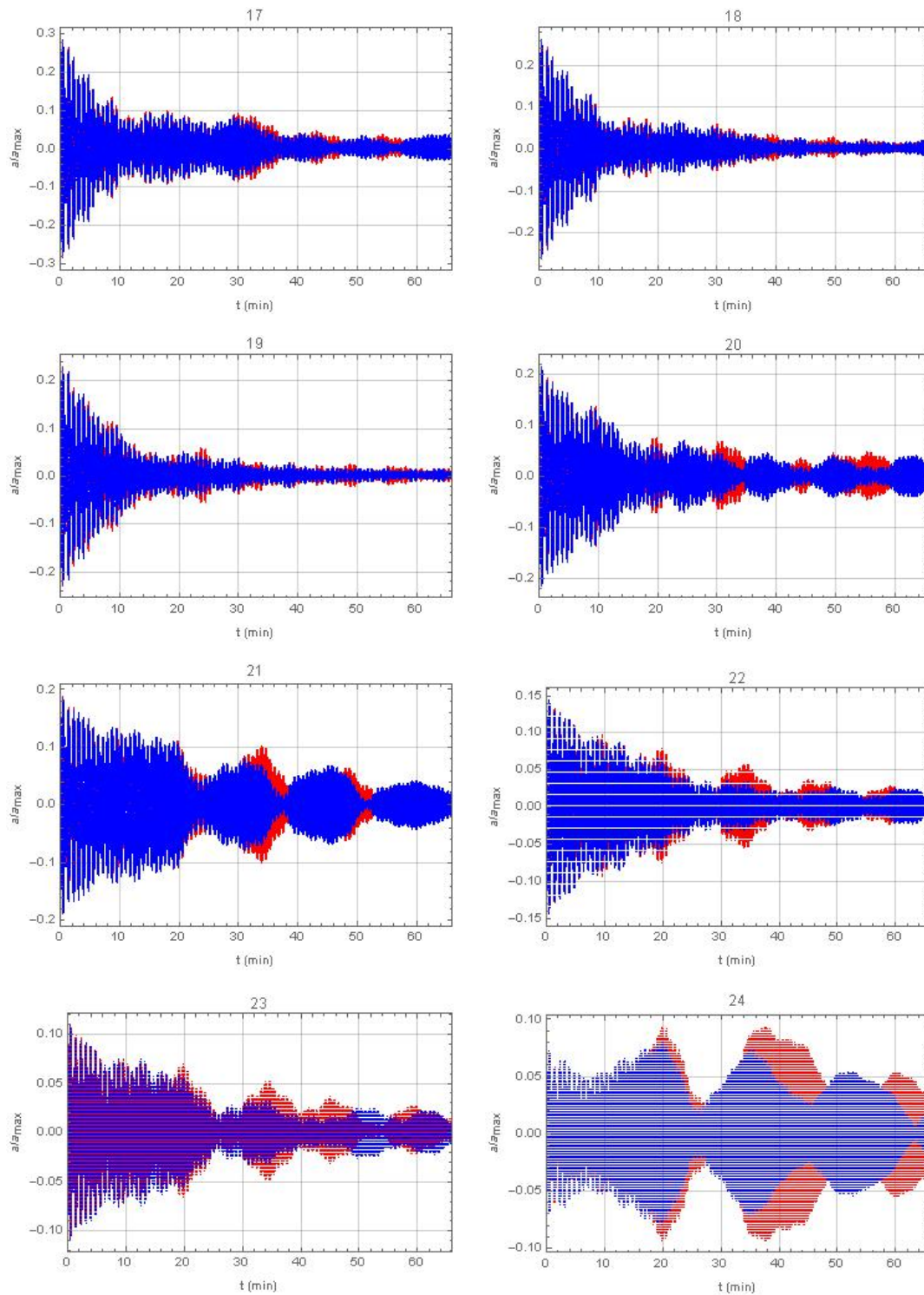


FIGURE 5.13: P08 50°: two runs overlap to show chaos outbreak

5.3 Ω as a function of t

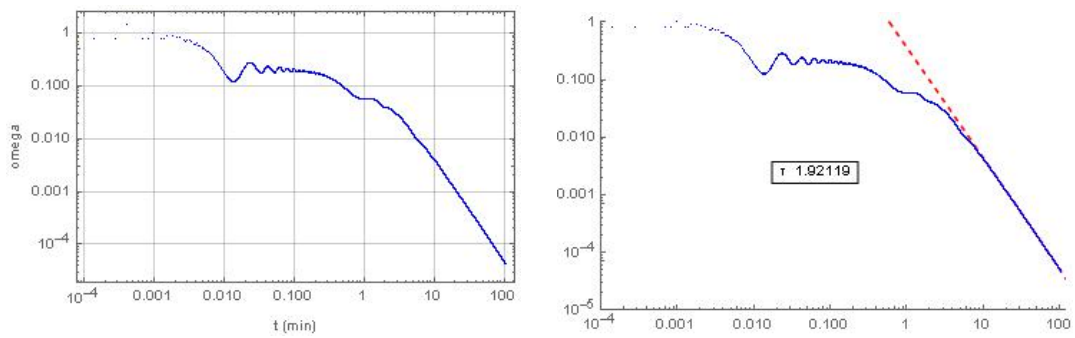


FIGURE 5.14: P08 50°

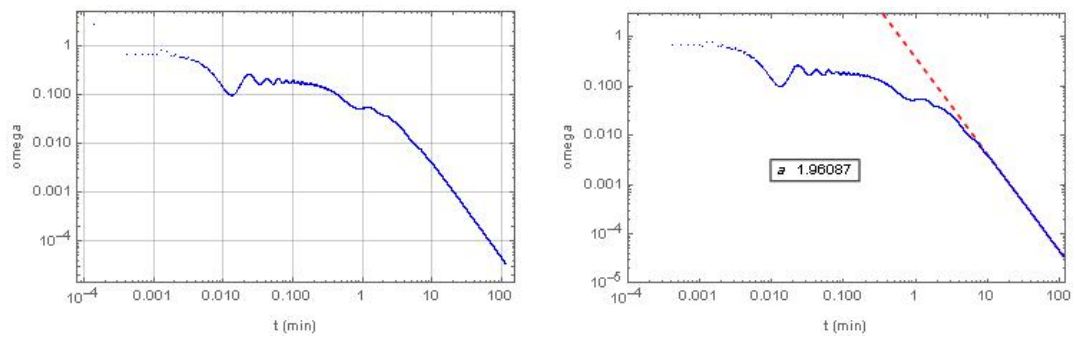


FIGURE 5.15: P16 50°

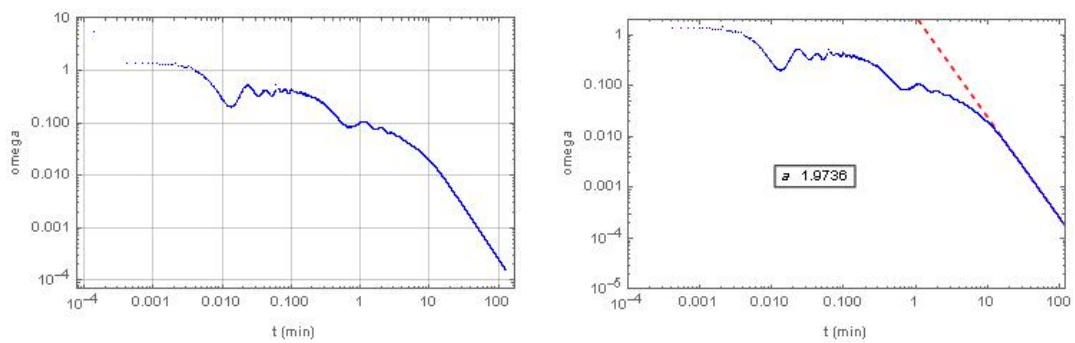


FIGURE 5.16: P08-16 50°

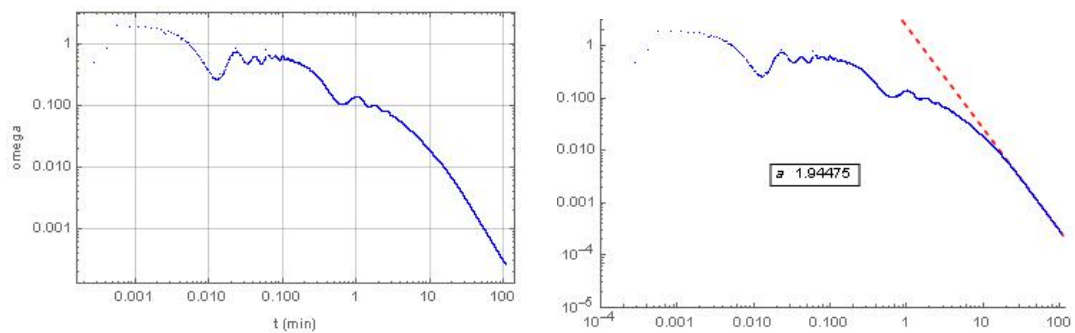


FIGURE 5.17: P06-12-18 50°

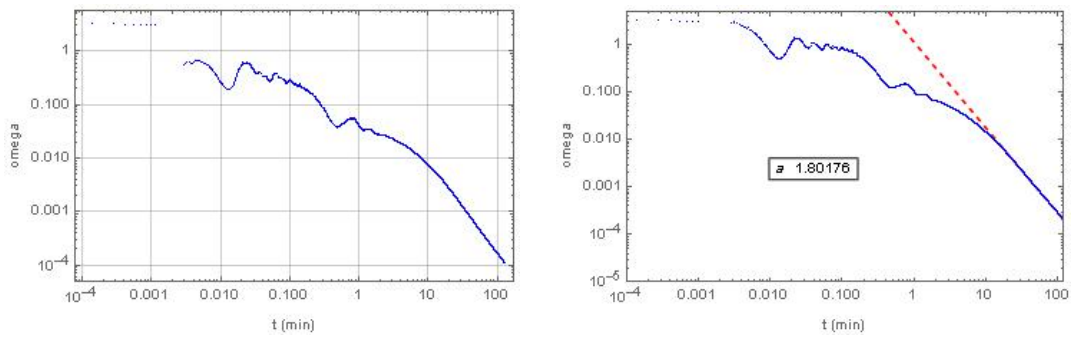


FIGURE 5.18: P3-06-09-12-15-18-21 50°

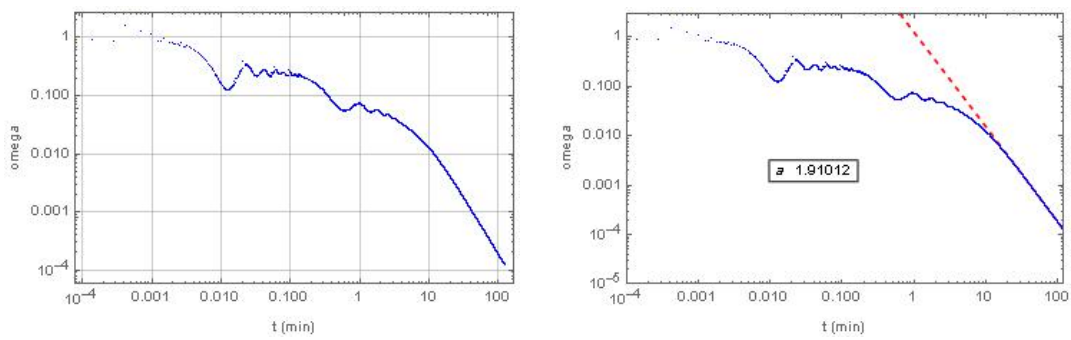


FIGURE 5.19: P06-12-18 40°

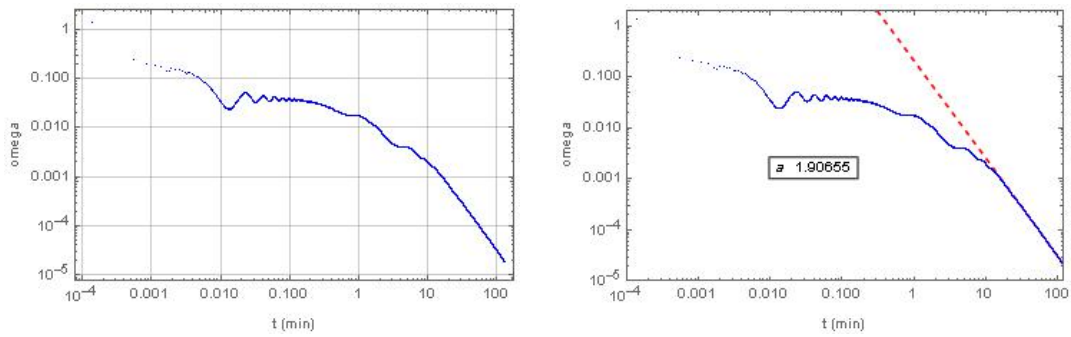


FIGURE 5.20: P08 30°

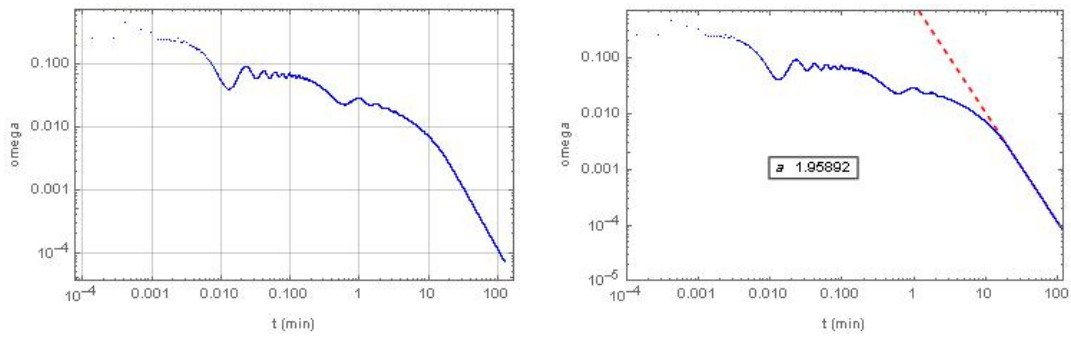


FIGURE 5.21: P08-16 30°

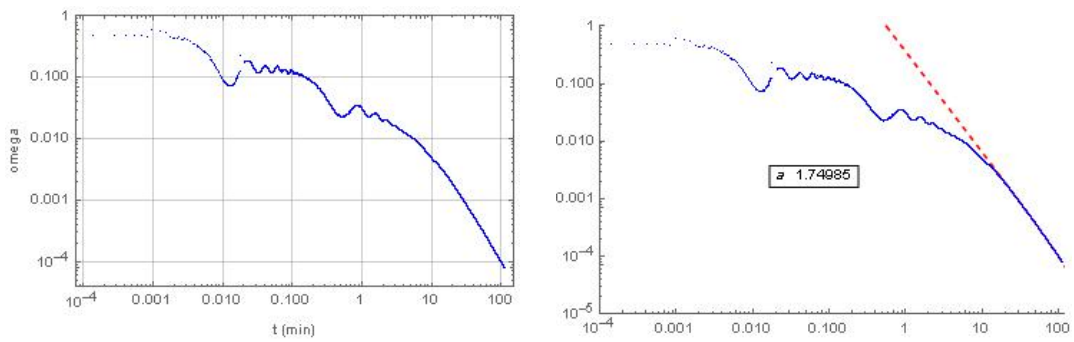


FIGURE 5.22: P04-08-12-16-20 30°

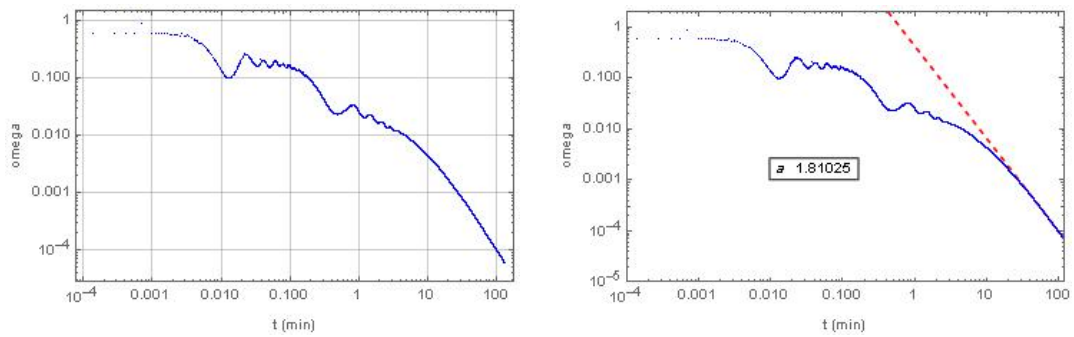


FIGURE 5.23: P03-06-09-12-15-18-21 30°

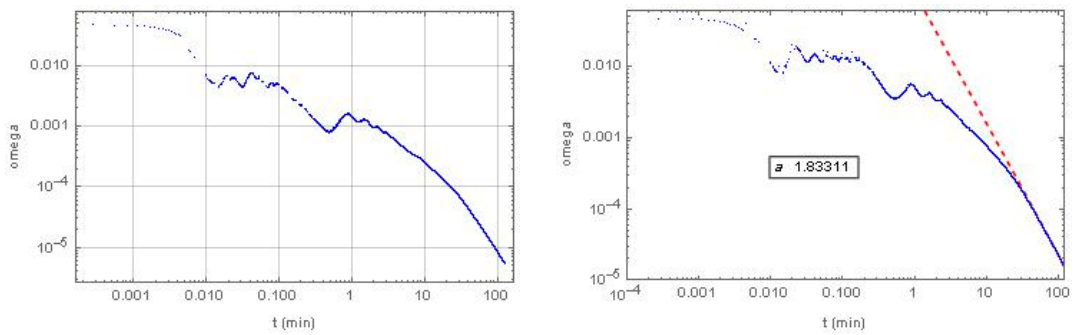


FIGURE 5.24: P09-12-15 20°

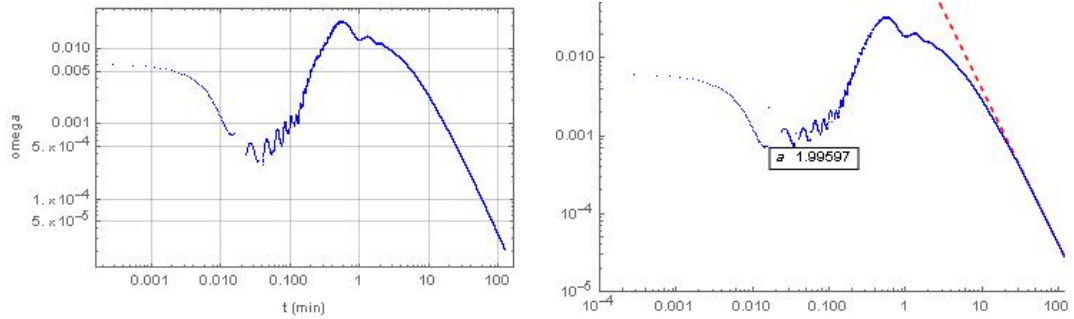


FIGURE 5.25: PA11 20°

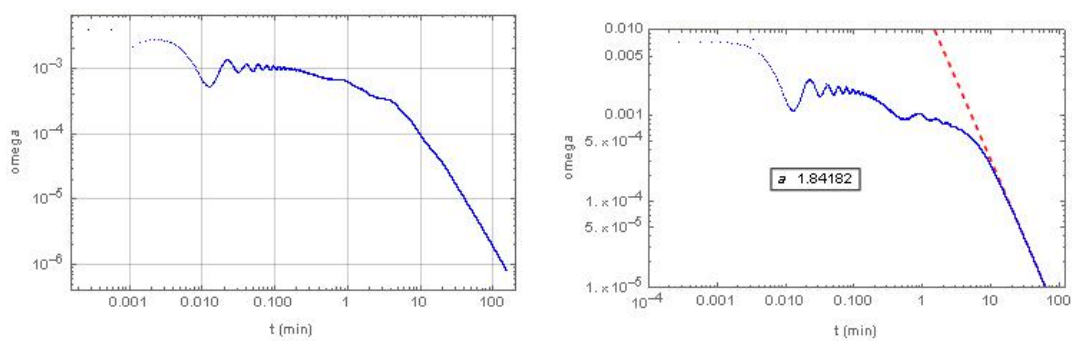


FIGURE 5.26: P08 10°

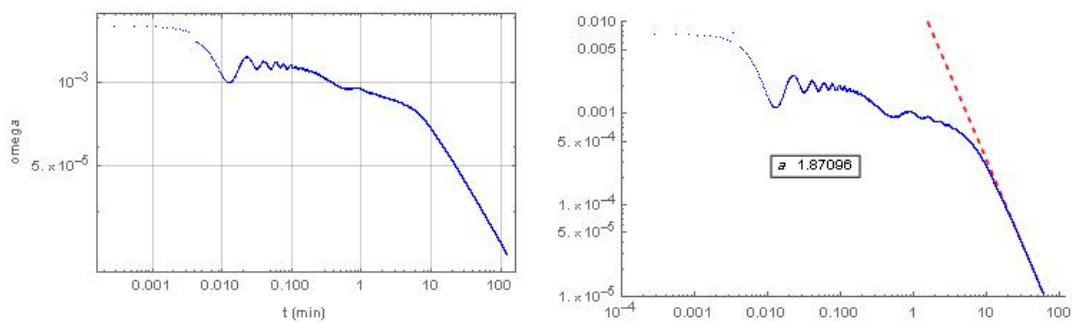


FIGURE 5.27: P08-16 10°

5.4 Envelopes of the time evolution

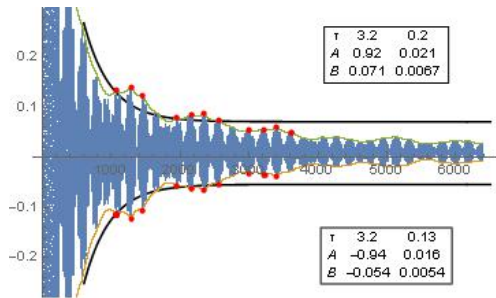


FIGURE 5.28: P08 50°

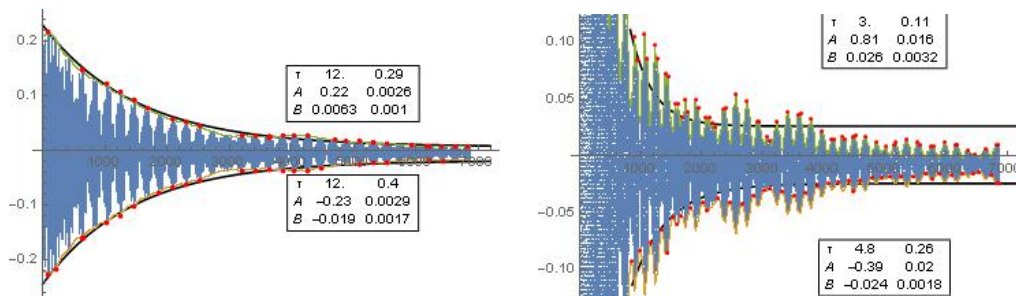


FIGURE 5.29: P16 50°

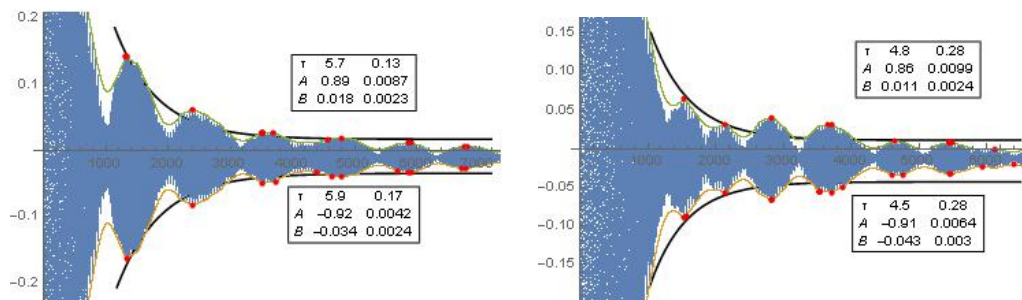


FIGURE 5.30: P08 and P16 50°

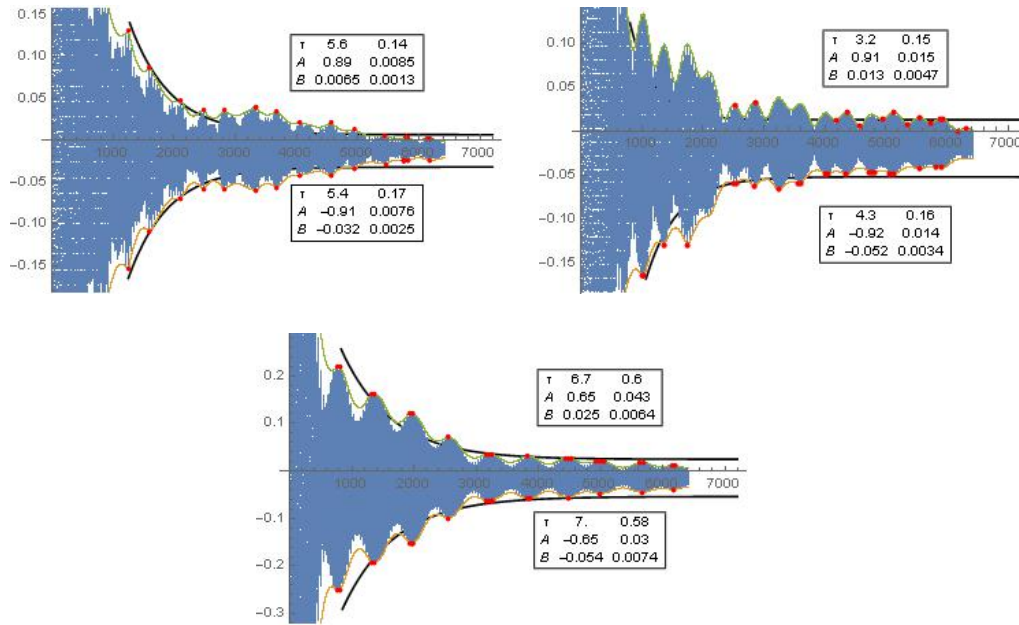


FIGURE 5.31: P06-12-18 50°

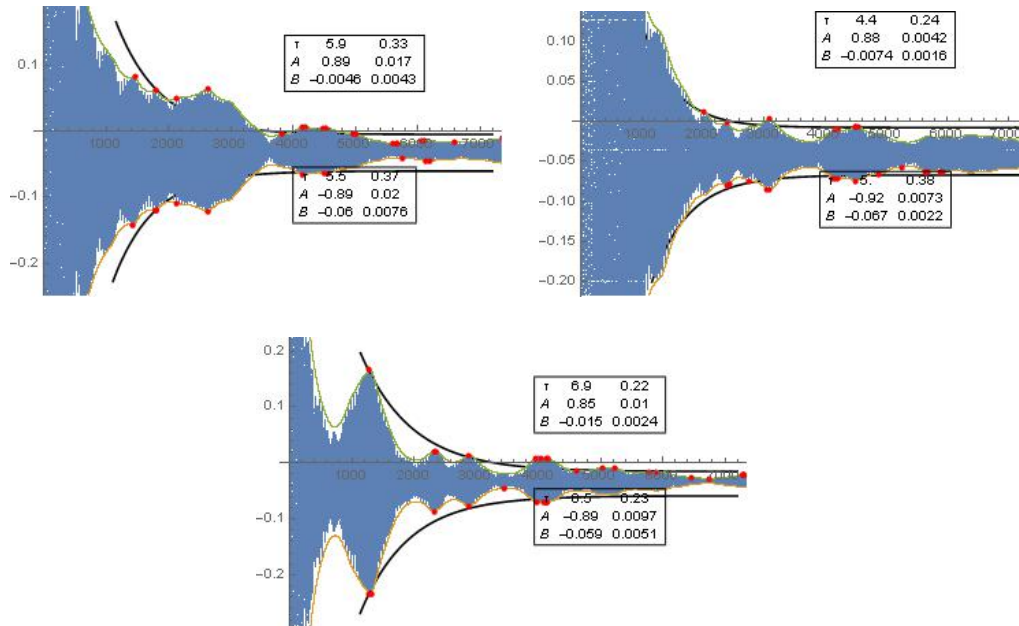


FIGURE 5.32: P03-06-09-12-15-18-21 50°

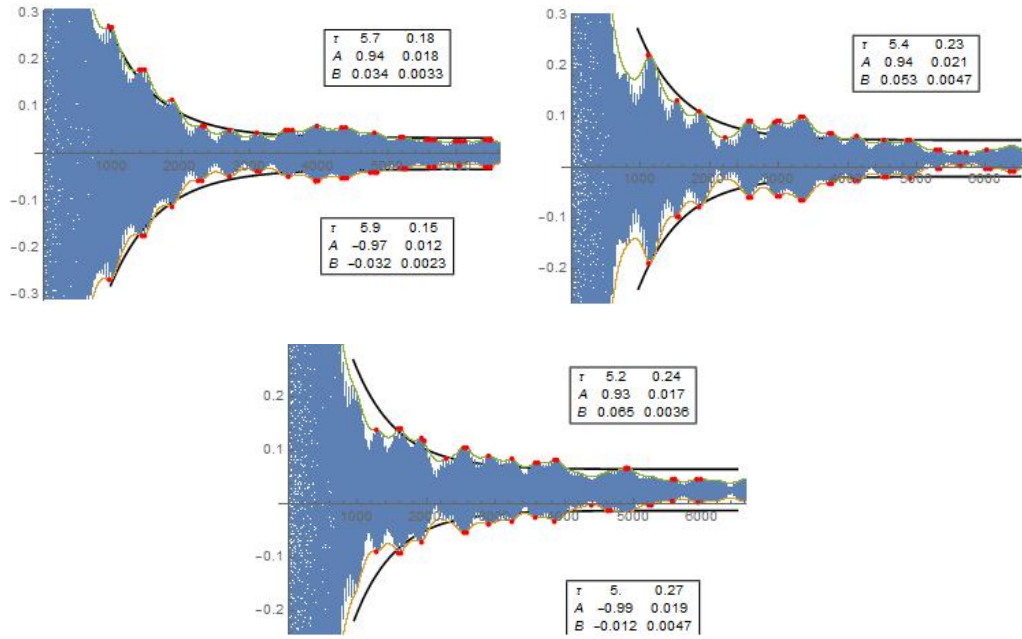


FIGURE 5.33: P06-12-18 40°

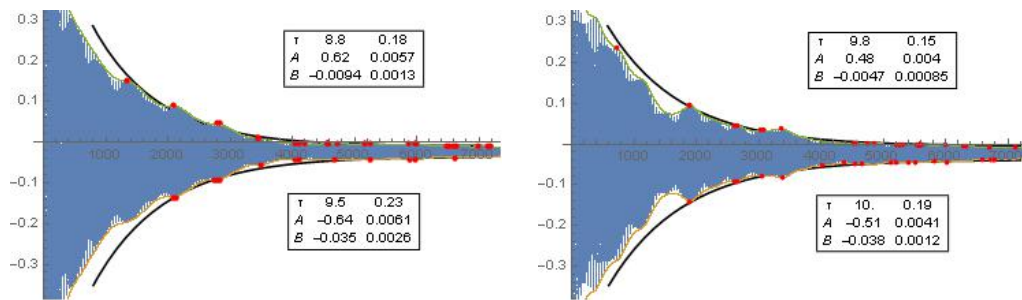


FIGURE 5.34: P03-06-09-12-15-18-21 30°

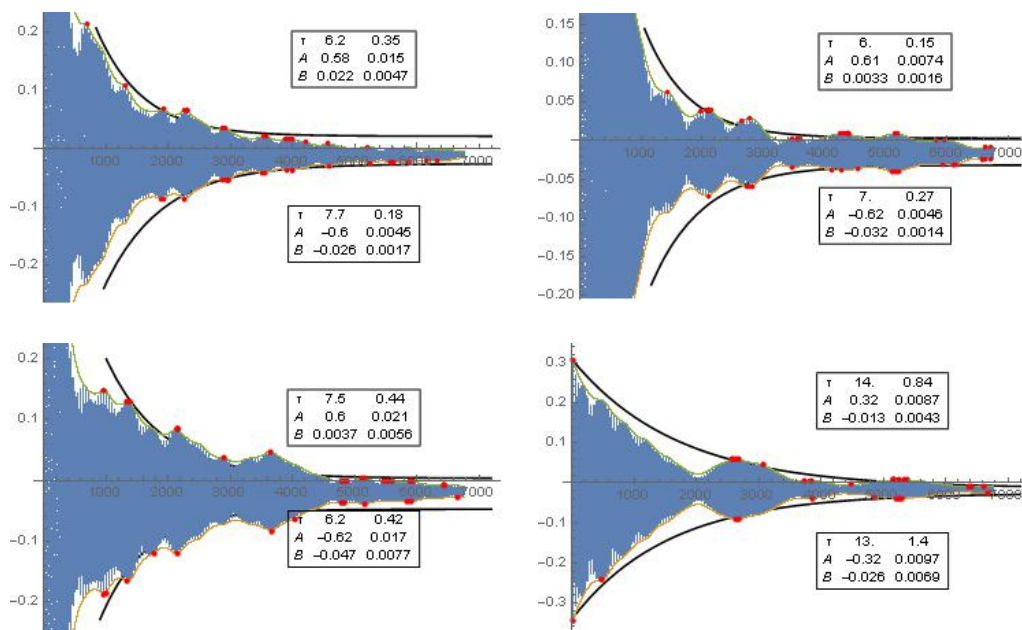


FIGURE 5.35: P04-08-12-16-20 30°

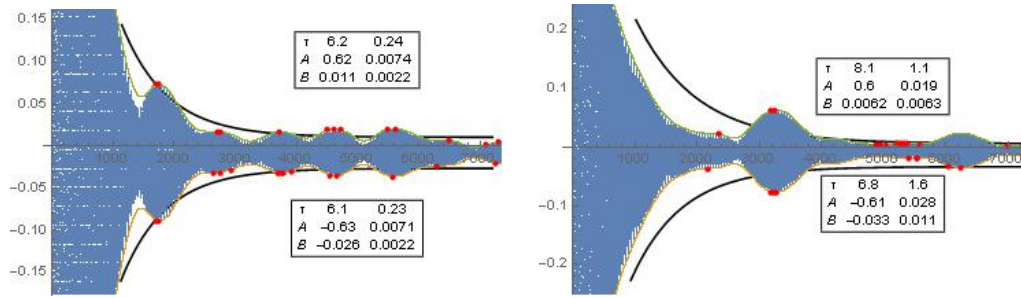


FIGURE 5.36: P08-16 30°

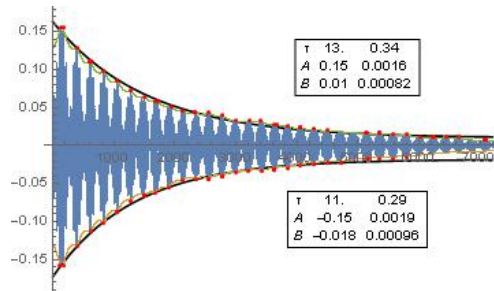


FIGURE 5.37: P08 30°

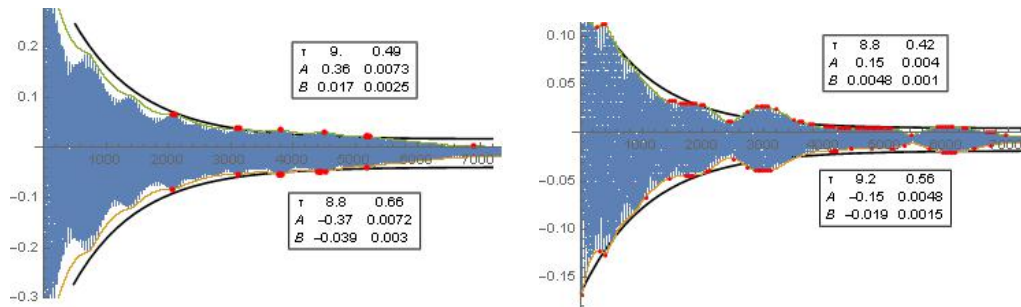


FIGURE 5.38: P09-12-15 20°

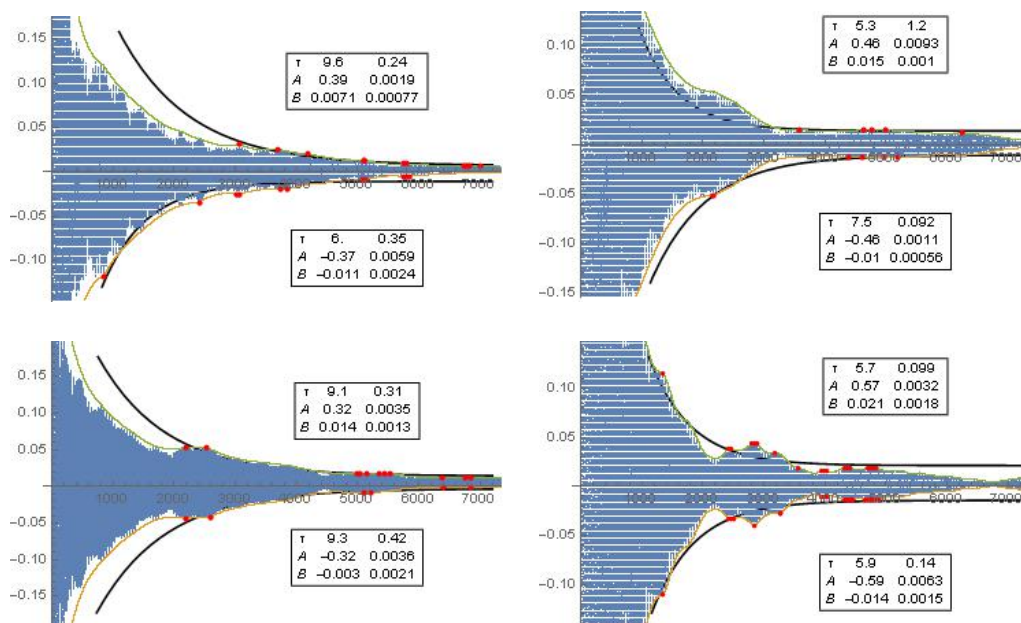


FIGURE 5.39: PA11 20°

5.5 Horizontal analysis: amplitude

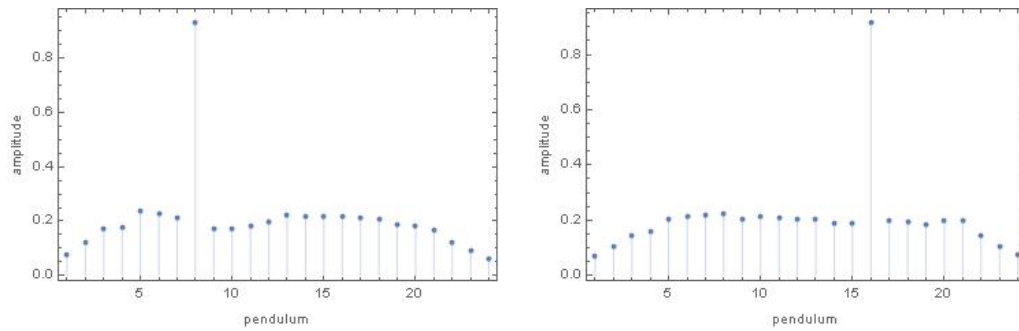


FIGURE 5.40: maximum pendula amplitude
P08 50° (left) - P16 50° (right)

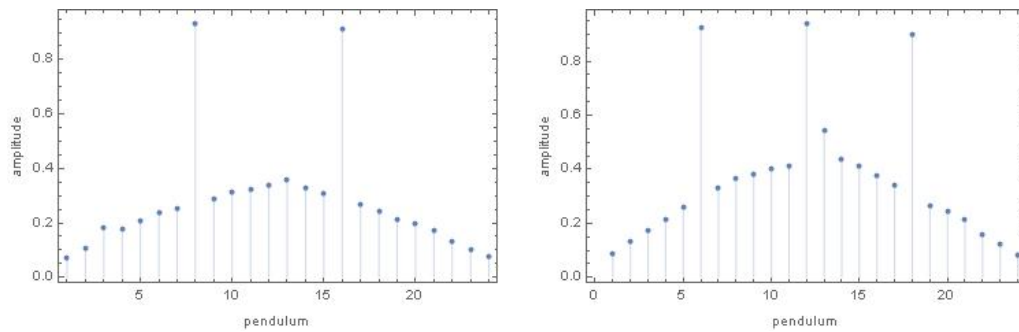


FIGURE 5.41: maximum pendula amplitude
P08-16 50° (left) - P06-12-18 50° (right)

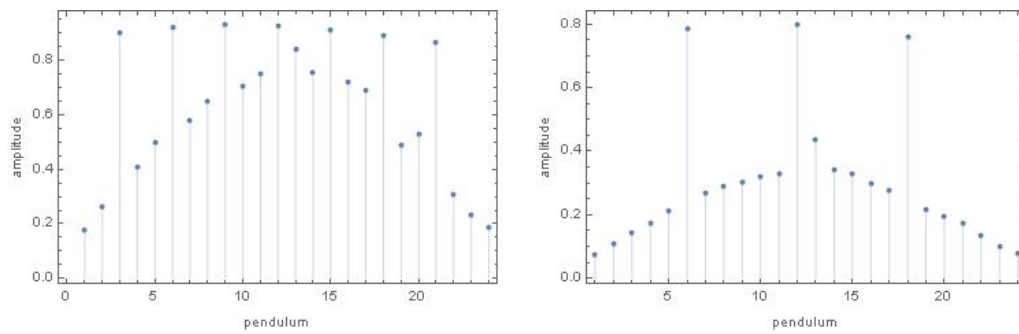


FIGURE 5.42: maximum pendula amplitude
P03-06-09-12-15-18-21 50° (left) - P06-12-18 40° (right)

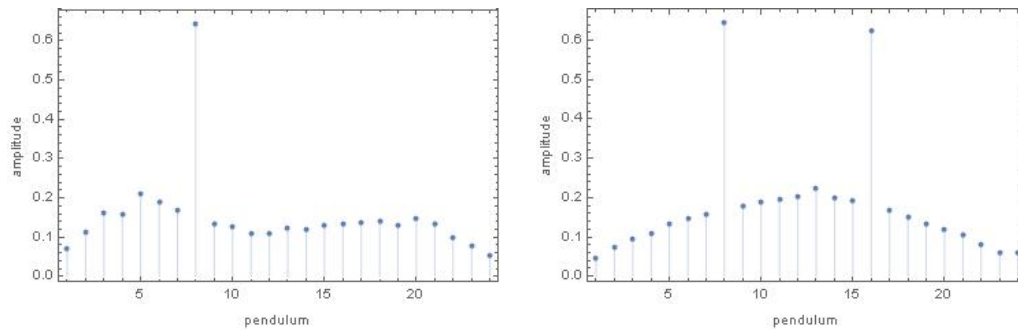


FIGURE 5.43: maximum pendula amplitude
P08 30° (left) - P08-16 30° (right)

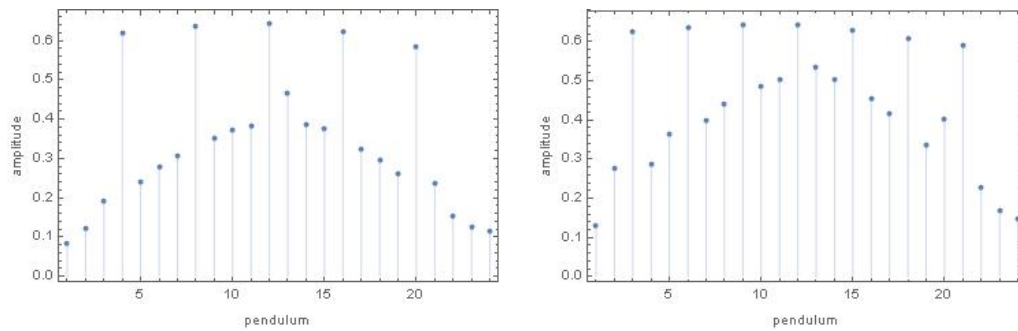


FIGURE 5.44: maximum pendula amplitude
P04-08-12-16-20 30° (left) - P03-06-09-12-15-18-21 30° (right)

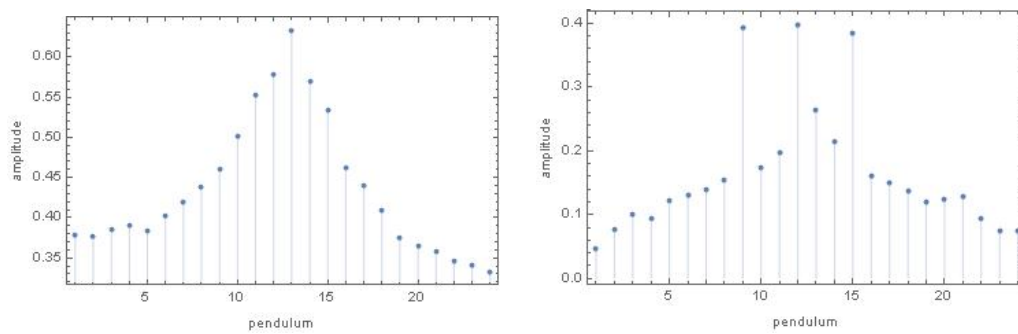


FIGURE 5.45: maximum pendula amplitude
PAll 20° (left) - P09-12-15 20° (right)

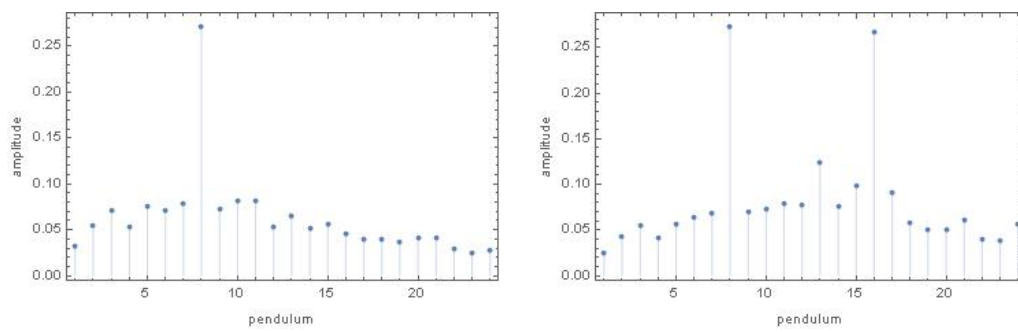


FIGURE 5.46: maximum pendula amplitude
P08 10° (left) - P08-16 10° (right)

5.6 Fourier analysis

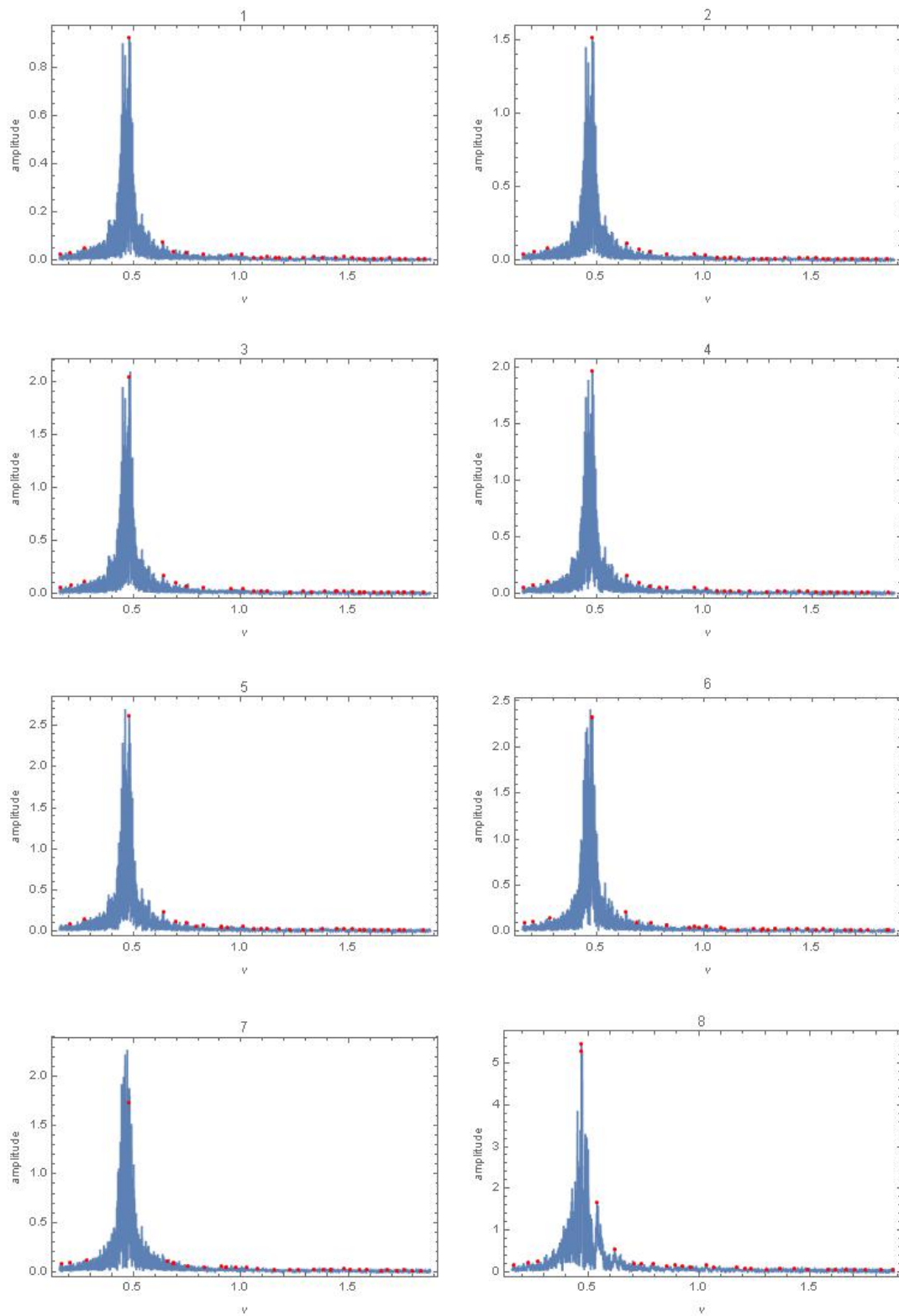


FIGURE 5.47: P08 50°

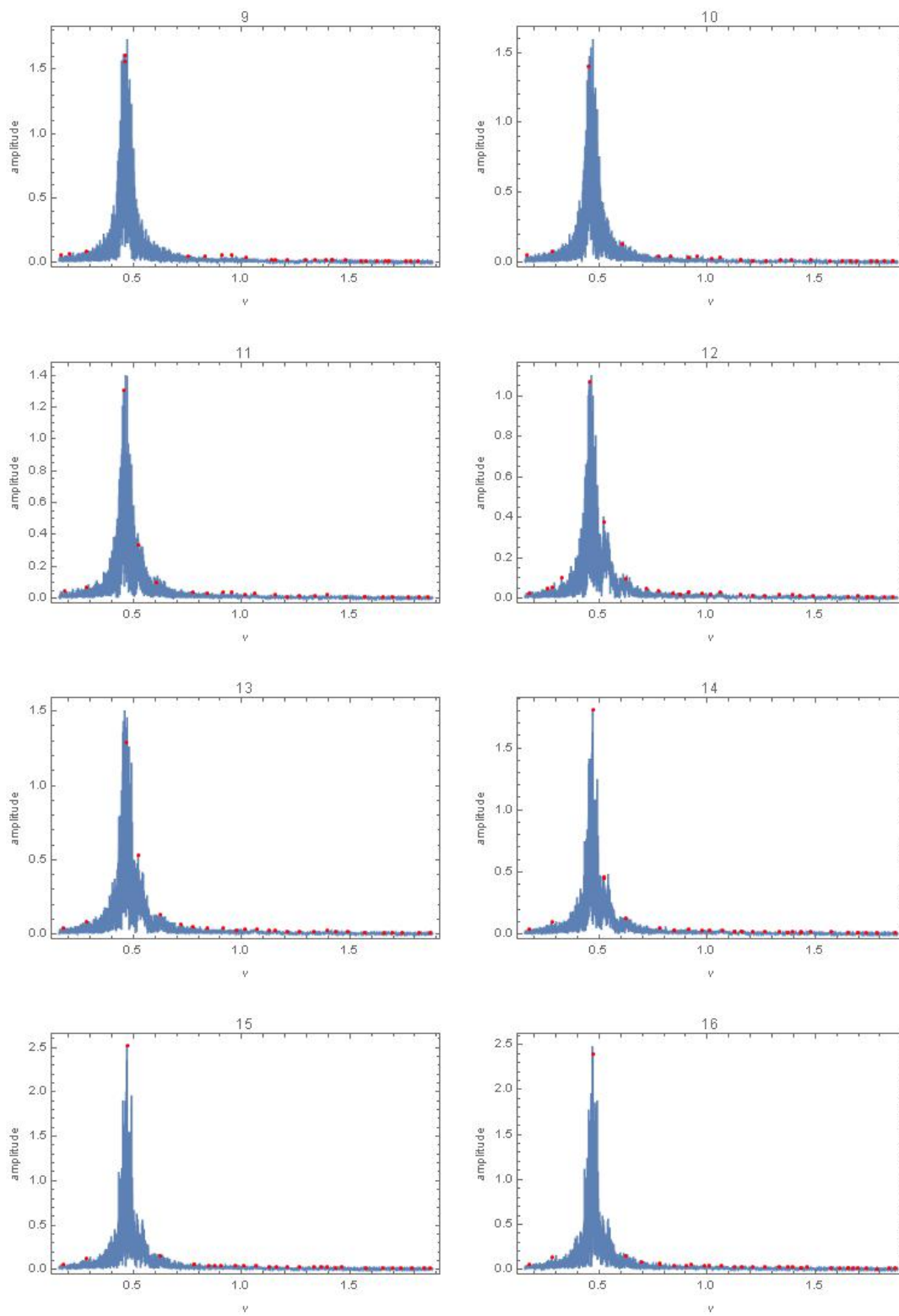


FIGURE 5.48: P08 50°

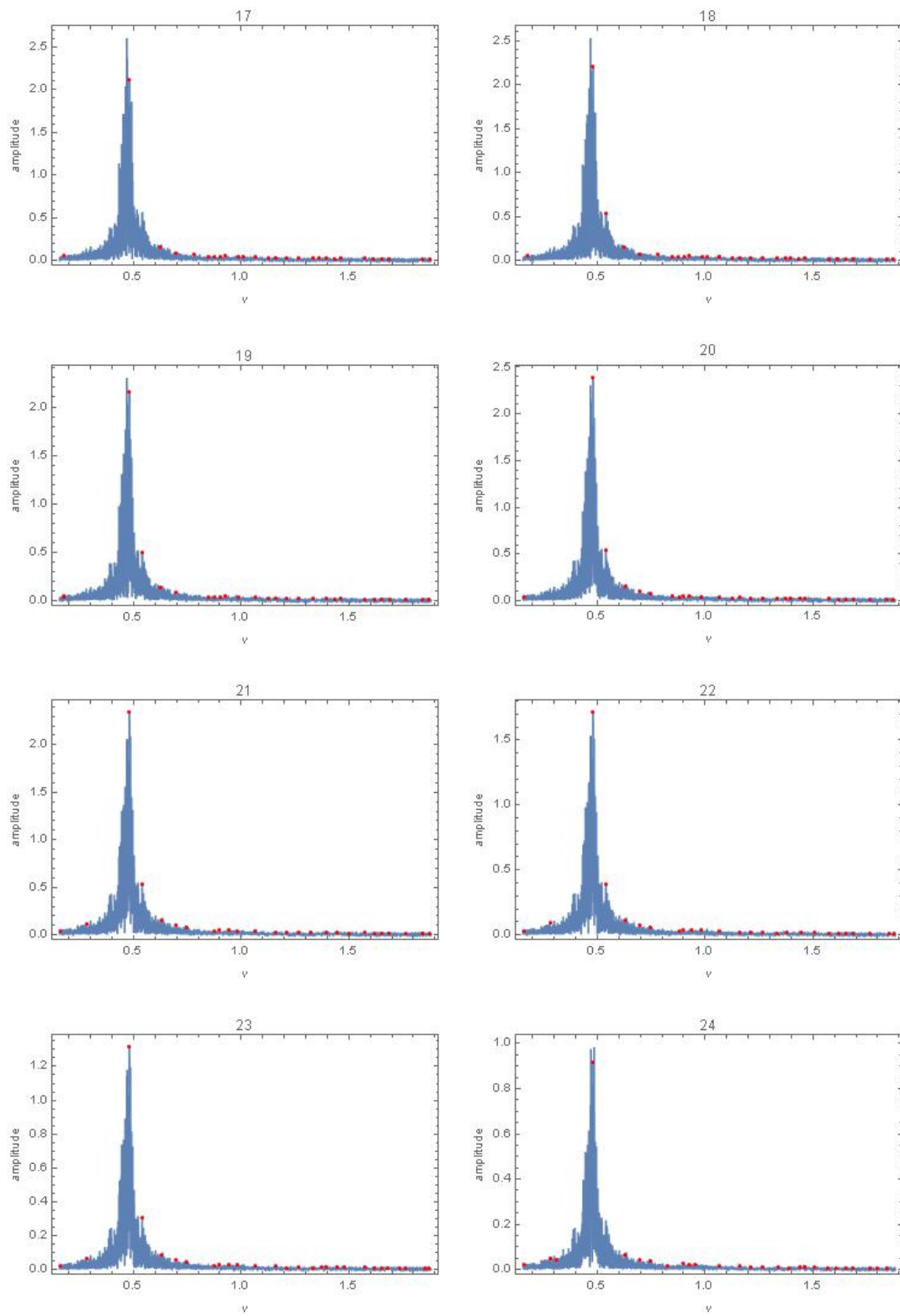


FIGURE 5.49: P08 50°

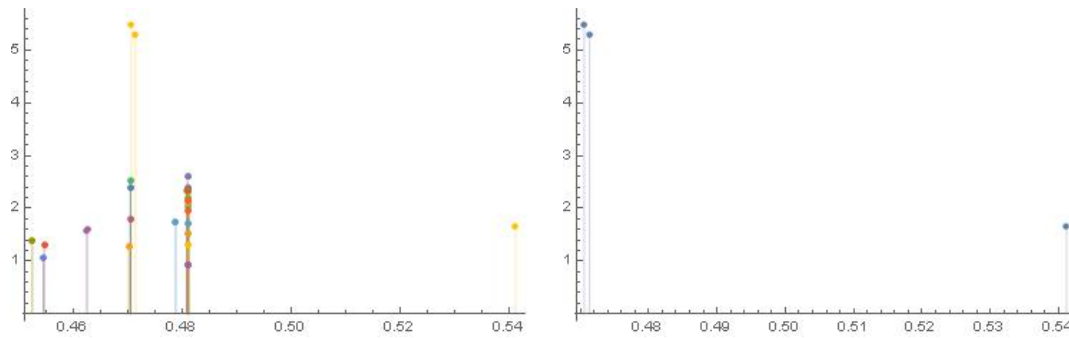


FIGURE 5.50: P08 50°
main Fourier peaks (left) and excited pendula main peaks (right)

TABLE 5.1: P08 50° Main Fourier peaks

pendulum	first	second	third	pendulum	first
1	0.4809			13	0.4701
2	0.4809			14	0.4704
3	0.4811			15	0.4704
4	0.4809			16	0.4704
5	0.4809			17	0.4811
6	0.4808	0.4811		18	0.4811
7	0.4787			19	0.4809
8	0.4706	0.4714	0.5411	20	0.4809
9	0.4626	0.4623		21	0.4809
10	0.4524			22	0.4809
11	0.4546			23	0.4809
12	0.4544			24	0.4809

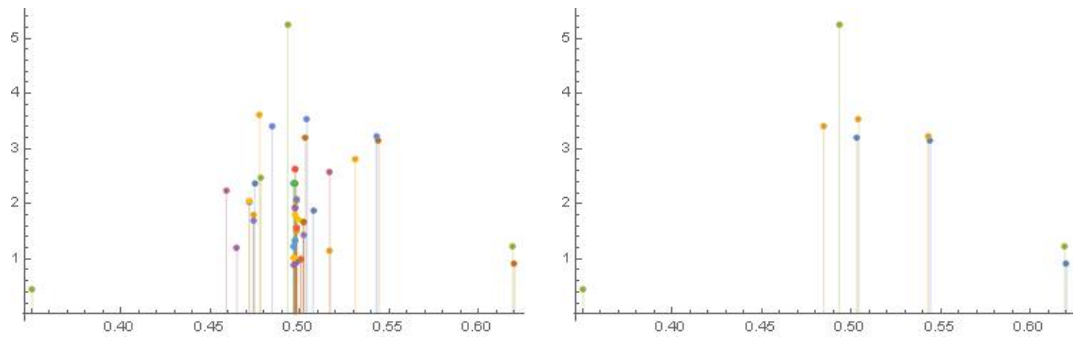


FIGURE 5.51: P06-12-18 50°
main Fourier peaks (left) and excited pendula main peaks (right)

TABLE 5.2: P06-12-18 50° Main Fourier peaks

pendulum	first	second	third	pendulum	first	second	third
1	0.4982			13	0.4777	0.5311	
2	0.4982			14	0.5169	0.4590	
3	0.4783	0.4982		15	0.4968		
4	0.4982			16	0.4748	0.5074	
5	0.4984	0.4719		17	0.4742	0.5170	
6	0.5034	0.5441	0.6202	18	0.4933	0.6193	0.3505
7	0.4974			19	0.5007		
8	0.4719	0.4974	0.4988	20	0.4740	0.5023	
9	0.4976			21	0.5021		
10	0.4976			22	0.4968		
11	0.4976			23	0.4968		
12	0.5042	0.4847	0.5429	24	0.4650	0.4969	

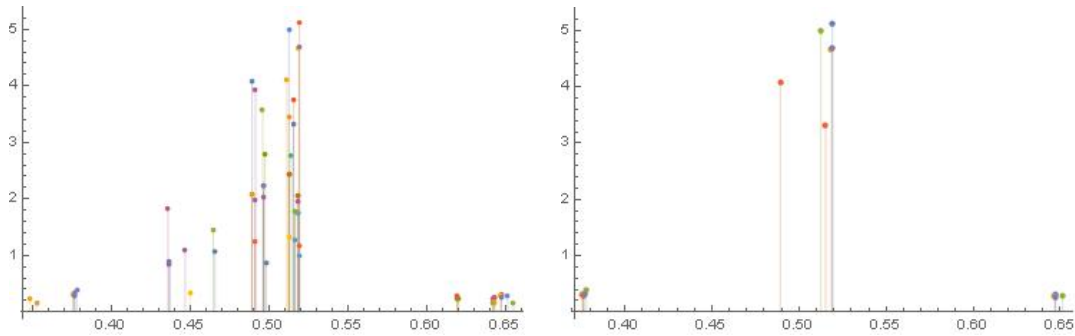


FIGURE 5.52: P04-08-12-16-20 30°
main Fourier peaks (left) and excited pendula main peaks (right)

TABLE 5.3: P04-08-12-16-20 30° Main Fourier peaks

pendulum	first	second	third	pendulum	first	second	third
1	0.4657	0.4368	0.4980	13	0.5112	0.3484	0.6426
2	0.4889			14	0.4913	0.4359	0.6431
3	0.4959	0.4645	0.6550	15	0.5141	0.6419	
4	0.5191	0.3760	0.6471	16	0.4892	0.5153	0.3761
5	0.4963			17	0.5124	0.3523	0.6425
6	0.5185			18	0.5163		
7	0.5185			19	0.4910	0.5188	
8	0.5185	0.3755	0.6467	20	0.5191	0.3767	0.6474
9	0.4910	0.5179	0.4366	21	0.5126		
10	0.4974	0.6194	0.6200	22	0.5160	0.5187	
11	0.5156	0.6191	0.6416	23	0.5126	0.4497	
12	0.5126	0.3779	0.6513	24	0.4963	0.4467	

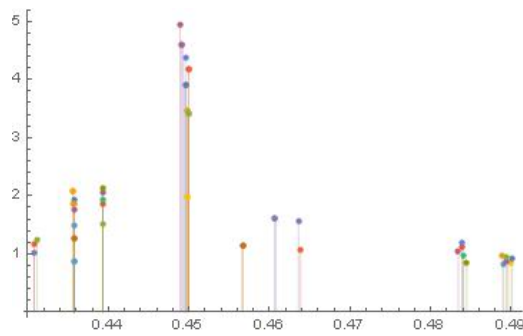


FIGURE 5.53: PAll 20° - main Fourier peaks

TABLE 5.4: PAll 20° Main Fourier peaks

pendulum	first	second	third	pendulum	first	second	third
1	0.4495			13	0.4356		
2	0.4498			14	0.4489	0.4834	
3	0.4499			15	0.4393	0.4841	
4	0.4499			16	0.4358	0.4901	
5	0.4636	0.4308		17	0.4358	0.4889	
6	0.4358			18	0.4393	0.4312	0.4894
7	0.4358	0.4891		19	0.4308	0.4639	
8	0.4356	0.4898		20	0.4607		
9	0.4393	0.4358	0.4894	21	0.4566		
10	0.4393	0.4845		22	0.4358		
11	0.4393	0.4839		23	0.4498		
12	0.4495	0.4839		24	0.4492		

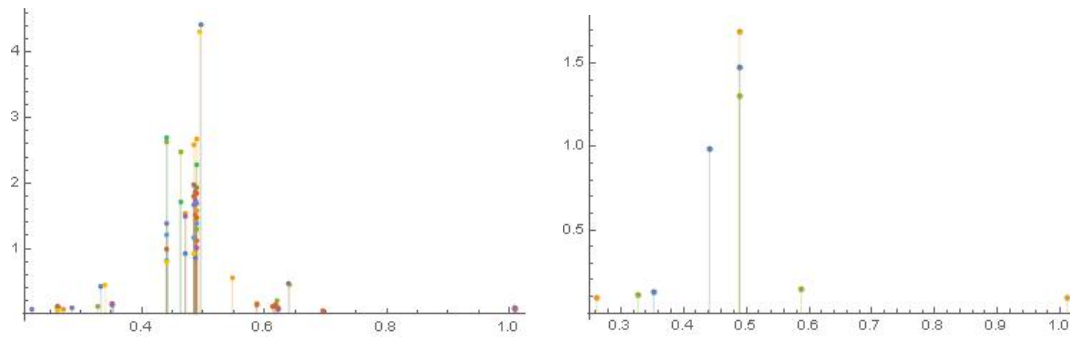


FIGURE 5.54: P08-16 50°
main Fourier peaks (left) and excited pendula main peaks (right)

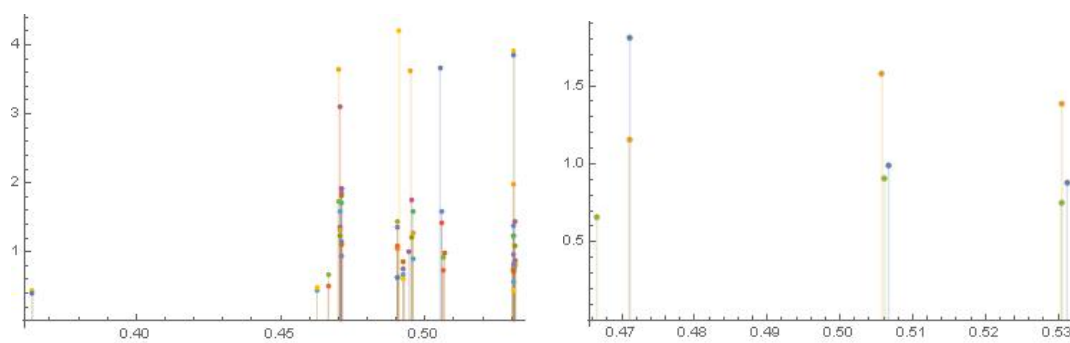


FIGURE 5.55: P08-16 30°
main Fourier peaks (left) and excited pendula main peaks (right)

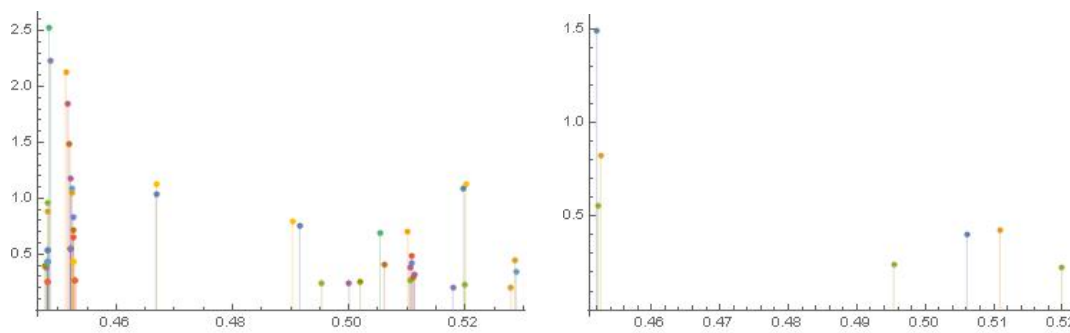


FIGURE 5.56: P08-16 10°
main Fourier peaks (left) and excited pendula main peaks (right)

TABLE 5.5: P08-16 50° Main Fourier peaks

pendulum	first	second	third	pendulum	first	second	third
1	0.4705	0.4863		13	0.4887	0.4854	0.5480
2	0.4705	0.4863	0.6218	14	0.4854		
3	0.4408	0.4632	0.6216	15	0.4411	0.4887	0.4628
4	0.4863	0.6949		16	0.4966	0.6401	0.3335
5	0.4863	0.2856	0.2210	17	0.4890	0.2722	
6	0.4898	0.4412	0.3524	18	0.4890	0.5875	0.3278
7	0.4895	0.4412	0.3524	19	0.4886	0.5872	
8	0.4942	0.6409	0.3404	20	0.4851	0.4412	
9	0.4880	0.3524	0.6171	21	0.4851	0.6142	0.2621
10	0.4886	0.6171	0.2621	22	0.4851	0.4399	0.2621
11	0.4886	0.6171	0.2621	23	0.4851	0.4399	0.2621
12	0.4885	0.2621		24	0.4714	0.4902	0.6220

TABLE 5.6: P08-16 30° Main Fourier peaks

pendulum	first	second	third	pendulum	first	second	third
1	0.4905			13	0.4702	0.4951	0.5305
2	0.4905			14	0.4706	0.4955	0.5309
3	0.4699	0.4905		15	0.4711	0.4956	0.5307
4	0.4905	0.5305		16	0.5308	0.5051	0.3639
5	0.4709	0.4904	0.5305	17	0.4707	0.4959	0.5313
6	0.4711	0.5067	0.5312	18	0.5062	0.5304	0.4666
7	0.4705	0.4956	0.5312	19	0.5062	0.5304	0.4664
8	0.4911	0.5307	0.3639	20	0.4711	0.5304	0.4925
9	0.4705	0.4945	0.5311	21	0.4713	0.4925	0.5305
10	0.4705	0.4955	0.5311	22	0.4925	0.5305	0.4626
11	0.5058	0.5305		23	0.4925	0.4626	0.5305
12	0.5058	0.5305	0.4710	24	0.4709		

TABLE 5.7: P08 10° Main Fourier peaks

pendulum	first	second	third	pendulum	first	second	third
1	0.4483			13	0.4513	0.5102	
2	0.4483	0.5279		14	0.4517	0.5105	
3	0.4483	0.5106		15	0.4484	0.5054	
4	0.4482			16	0.5198	0.4668	0.4915
5	0.4487	0.5179		17	0.4524	0.5286	
6	0.4520	0.5061		18	0.4522	0.4954	0.5199
7	0.4523	0.5287		19	0.4530		
8	0.5201	0.4670	0.4903	20	0.4522		
9	0.4483	0.4480	0.5000	21	0.4527	0.5111	
10	0.4478	0.5020		22	0.4482		
11	0.4526	0.5109		23	0.4526		
12	0.4526	0.5109		24	0.4522	0.5113	

Chapter 6

Physical interpretation of the results

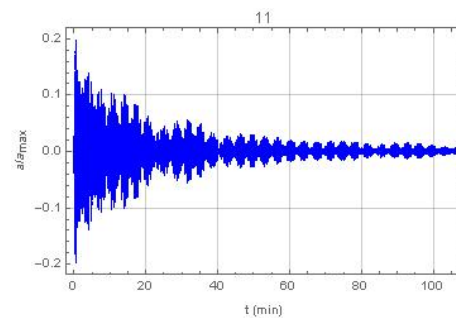
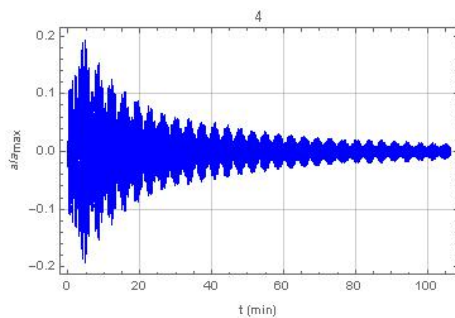
6.1 Measurements

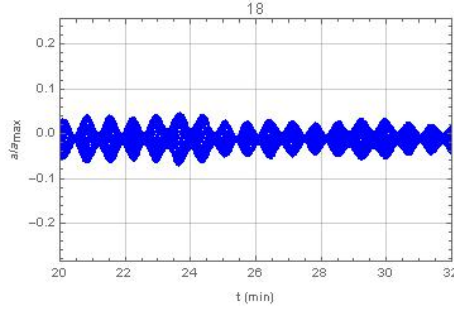
Based on the data obtained through the videotracking algorithm, $\{t_i, x_1(t_i), \dots, x_{24}(t_i)\}$, we calculated the following physical quantities:

- time evolution plot for each pendulum,
- envelope of selected time evolution plots with decay time τ estimate,
- Fourier analysis and main frequency peaks,
- time evolution of total mechanical energy (and potential energy and kinetic energy),
- energy metric evolution for potential energy
- horizontal plot of maximum amplitudes in the chain

6.2 Time evolution of pendulum displacement

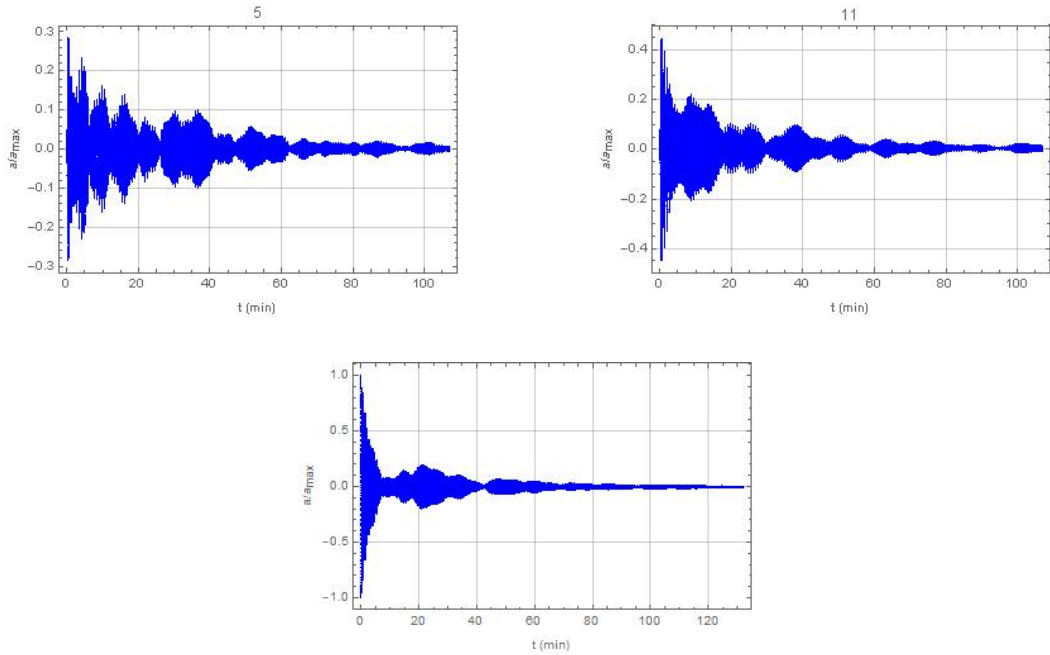
We studied each oscillator motion for the whole run and we plotted the normalised displacement (compared to the initial amplitude of the excited pendula) as a function of time (see 5.1). We found 3 different time scales beats from 1 minute to 30 minutes. If we consider runs with just one excited pendulum (whatever the excitation angle), we recognise pulses of about 4 minutes in the each pendulum (e.g. 4th) plot, but larger scale pulses (20 to 30 minutes) can be noticed in non excited pendulum plots (e.g. 11th).





Shorter beats of about 1 minute can be noticed when zooming in.

More complex structures can be observed when considering runs with higher energy. Those plots also frequently show some serious narrowing of the displacement: in those intervals the considered oscillator is almost stack and almost all its energy has flown to the other pendula, while later on the same pendulum restart acquiring energy and covering wider trajectories.



6.3 Omega

Quantity $\Omega(t)$ provides the thermalisation rate of the system. We define it as the arithmetic mean of the 24 squared difference between the time average (from $t_i = 0$ to the generic instant $t_i = T$) of the potential energy U_j of the j -th oscillator ($\bar{U}_j(T)$) and the arithmetic mean $\langle \bar{U}(T) \rangle$ over the chain, i.e. executed on the 24 time averages of $\bar{U}_j(T)$. In other words $\Omega(T)$ is the squared variance of quantity $\bar{U}_j(T)$. Having said this, Ω can be defined as:

$$\bar{U}_j(T) = \frac{1}{T} \int_0^T U_j(t) dt$$

$$\langle \bar{U}(T) \rangle = \frac{1}{24} \sum_{j=1}^{24} \bar{U}_j(T)$$

$$\Omega(T) = \frac{1}{24} \sum_{j=1}^{24} [\langle \bar{U}(T) \rangle - \bar{U}_j(T)]^2$$

Dealing with time series, we adapt the definition of $\bar{U}_j(T)$ accordingly:

$$\bar{U}_j(T) = \frac{1}{T} \sum_{t_i=0}^{t_i=T} U_j(t_i)[t_{i+1} - t_i]$$

The energy metric Ω just defined derives from the theoretical foundations of multi-particles systems [24, 25, 6] and it is here extended to chain of particles. Starting from the ergodic hypothesis, over a large time scale the phase space average of an observable coincides with its time average. Not knowing the probability distribution, we replaced the probabilistic average with the spacial, horizontal average over the chain (assuming that increasing the number of particles in the chain, all possible states are covered). For the same reason the integral over the phase space is replaced by a sum over the N particles. The energy metric Ω is evaluated using the gravitational potential energy and therefore the oscillation amplitude, because we assume that it gives a good estimate of the oscillator energy.

The energy metric for integrable systems has a constant value and energy is not exchanged between different modes, while for ergodic systems it is expected to go to zero for large values of t . Looking at the bi-logarithmic plots of Ω as a function of t (see 5.3), we recognise an asymptotic phase, starting approximatively after the first 10 to 20 minutes, where the $\Omega(t)$ decreases as a constant power of t . Assume we approximate its behaviour as follows:

$$\Omega \sim t^{-a} + \text{const}$$

where a is an unknown constant. Estimating the best fit of this kind of function, we obtained the following results for parameter a :

angle	excited pendula	a
50	8	1.92
	16	1.96
	8-16	1.97
	6-12-18	1.94
	3-6-9-12-15-18-21	1.80
40	6-12-18	1.91
30	8	1.91
	8-16	1.96
	4-8-12-20	1.75
	3-6-9-12-15-18-21	1.81
20	9-12-15	1.83
	All	2.00
10	8	1.82
	8-16	1.84

Hence the average value is $a = 1.9 \pm 0.1$.

Starting from the definition of Ω we can write it as follows:

$$\Omega \sim t^{-2} t^a$$

where t^α represents the behaviour of the squared variance. Based on our results we can assume that $\alpha \sim 0.1$. This result means that our system experience a high thermalisation rate, due to the system being open and to the energy which rapidly and irreversibly flows from the system to the surrounding environment. In Onorato's paper ([42]) a totally different entropy coefficient is used, but we noticed in the entropy bi-logarithmic plots a similar slope to the one we measured. We roughly estimated a slope of about -2.3 . We also notice that in Onorato work we don't see a complete thermalisation: as a matter of fact those entropy plots show after a long time (corresponding to $s(t) = 10^{-3}$) a maybe temporary stop in thermalisation. At that time entropy starts oscillating around a non zero value.

6.3.1 Thermalization and dissipation

We could conclude that thermalisation is reached more quickly when dissipation occurs: indeed the theoretical models of conservative nonlinear coupling give much longer thermalisation time. The experimental results we gathered show how dissipation or non adiabacity plays a further role in reaching equipartition and thermalisation, as open neural networks and complex multibody systems "degrades" faster that closed ones. As a matter of fact dissipation prevents Poincarè recurrence both from a theoretical standpoint and from an experimental one, but it does not force a priori the energy to be equally distributed on all nodes of the open net.

6.4 Dissipation

Our system turned out to be highly dissipative and the initial energy provided to the excited pendula is quickly transferred to the whole system first and then to the surrounding environment. We first estimate the quick loss of energy was due to the air friction, but a straightforward computation based on Stoke's law was sufficient to understand that this time scale is very long compared to the one experienced by the system. Stokes' law describes the frictional force exerted on spherical objects with very small Reynolds numbers in a viscous fluid. The force of viscosity on a small sphere moving through a viscous fluid is given by:

$$\mathbf{F}_d = 6\pi \eta R \mathbf{v} = \beta \mathbf{v}$$

where:

- \mathbf{F}_d is the frictional force (acting on the interface between the fluid and the particle)
- η is the dynamic viscosity
- R is the radius of the spherical object
- \mathbf{v} is the flow velocity relative to the object and
- $\beta = 6\pi \eta R$

The dynamic viscosity of air at 20°C is $1.81 \cdot 10^{-5} \text{Pa} \cdot \text{s}$ and the radius R of the spheres is 2.5 cm . The work done by this frictional force over the first period $T = 2\pi/\omega = 2\pi\sqrt{l/g}$ can be estimated this way:

$$W = \int_0^T \mathbf{F}_d \cdot d\mathbf{s} = 6\pi\eta R \int_0^T v^2 dt$$

If we consider the forces acting on each sphere: the tension T of the nylon rope, the weight P of the ball itself and the frictional force F_d , we get the following equation of motion:

$$ml\ddot{\theta} = -mgsin\theta - 6\pi\eta Rl\dot{\theta}$$

Solving this second order differential equation and recalling that $v = l\dot{\theta}$, we obtain the following estimate for the work of the frictional force over the first oscillation period:

$$W = 4.8 \cdot 10^{-5} \text{ J}$$

If we compare this quantity with the initial energy of a sphere excited to 50° , $E = 2 \text{ J}$, the overall duration (2h) of each run is not enough to dissipate the whole initial energy: the characteristic oscillation period is 2.2 s and during the run each pendulum can perform about 3600 periods. Moreover consider that the work done on each period decreases as the amplitude decreases. The mechanical energy is expected to exponentially decrease due to air friction with a time constant $\tau = 2m/\beta$ with $\beta = 110^{-5} \text{ Ns/m}$: such a coefficient is of the order of 27h. As a consequence air friction cannot be considered the main reason for the fast energy dissipation our system experiences.

The steel cable does absorb energy, but it stores that energy as elastic potential energy due to the bending of the cable itself (on a direction perpendicular to the cable) where the nylon rope is fastened. If we neglect torsion, traction and compression, this elastic potential energy is stored and released alternatively from and to the oscillator and the overall mechanical energy is conserved, as long as the air friction does dissipate that energy in an irreversible way. This bending force can be considered as the equivalent of the Hooke forces existing in the historical FPU experiment, responsible for coupling. Among others, a difference between the FPU experiment and our experiment is given by the external harmonic force, i.e. weight. For this reason we can talk about oscillators coupled through elastic forces, but subject to forced oscillations in presence of energy loss. The bending frequency $\sqrt{k/m}$ (where m is the effective mass of the segment subject to bending and k is the bending elastic constant) is very high compared to gravitational frequency $\sqrt{g/l}$: if we take a 10 cm segment of a squared section cable we obtain a value of $6 \cdot 10^{10} \text{ N/m}$. As a consequence on a 100 g/m linear density cable the frequency would be of the order of $2 \cdot 10^6 \text{ s}$, 6 orders of magnitude greater than the gravitational frequency. Hence we have not to expect beat phenomena related to those two frequencies.

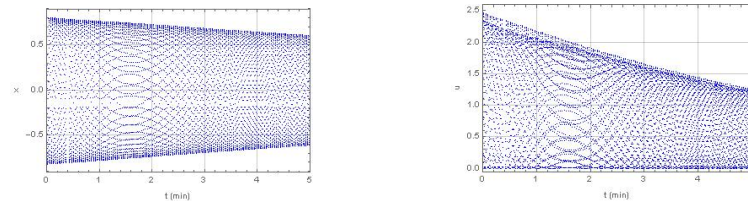
As a consequence the total energy of a given oscillator involves a third term, beyond the gravitational potential energy and the kinetic energy, which is the elastic potential energy. This term is of the order of $\frac{1}{2}k\delta x^2$ and it has an average value higher than zero: neglecting this term entails to underestimate the total energy of the oscillator. We have checked the order of magnitude of this term. For the sake of simplicity we modelled a segment of the cable between neighbour pendula as a rod with a rectangular section (the order of magnitude does not change with a round section) with section bh and length L : this segment is considered to be hooked at the ends. The bending produces an arch and the distance δx of the vertex of the arch from the center is called "arrow" and the bent surface is hL . Exploiting the Young module of the material we can easily obtain the elastic constant k of cable:

$$k = 4bh^3E/L^3$$

Considering that E for steel is of the order of 200 GPa and assuming $b \simeq h \simeq \delta x \simeq 1 \text{ cm}$ and $L = 1 \text{ cm}$, we obtain an elastic potential energy of the order of a Joule.

This is a missing energy we do not take into account when we calculate the total mechanical energy of each pendulum.

For a better understanding of the energy loss process, we then studied the oscillation of a single pendulum oscillating with the same nylon rope length suspended to a concrete wall using a couple of hooks, in order to decouple it from the chain and see the rate of the energy loss of the pendulum. We excited the pendulum at a 40° angle. In the first 5 minutes the elongation lost a 25%, which correspond to a loss of a 50% in height and to an equivalent loss in potential energy as shown in the two following figures.



Comparing those results with the ones we got when we excite a single pendulum of the chain we see a similar loss rate for the chain overall potential energy when considering large angles, while we notice a lower loss rate for small angles as it is shown in the two following figures:

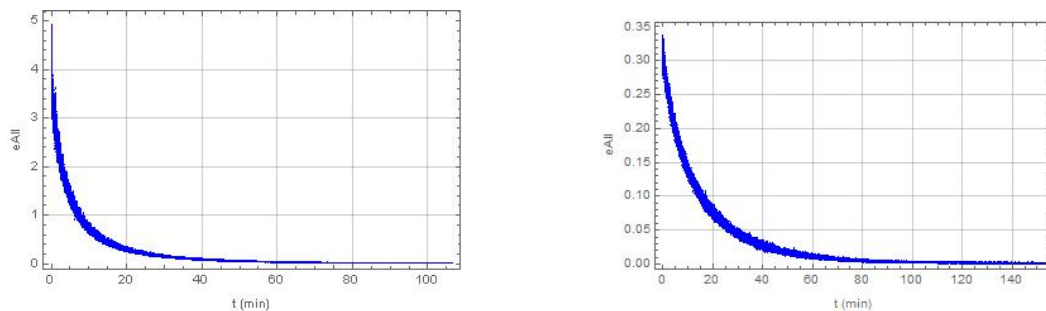
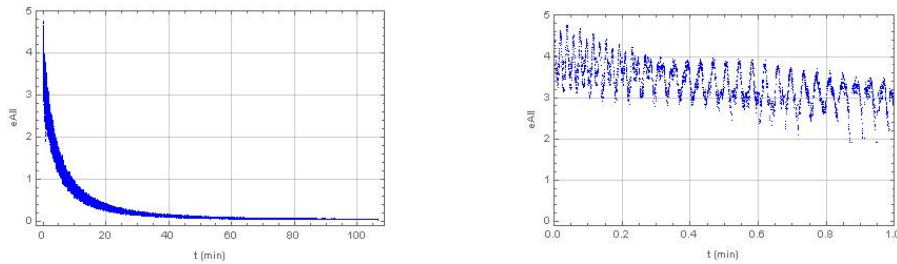


TABLE 6.1: Total energy of the chain as a function of time: 8th pendulum at 50° (left) and at 10° (right)

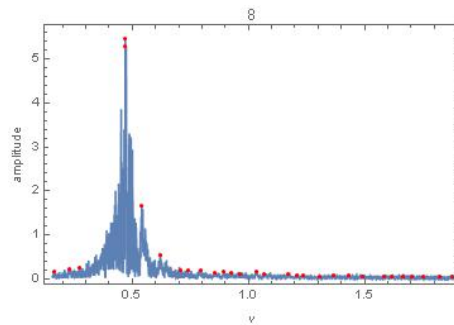
We could conclude that the high dissipation rate is also due to the way nylon rope is fastened to the steel cable. Due to the bending of the cable $k \delta x$ on the horizontal plane, the force acting on the oscillator is not only the tension along the rope (which performs a null work, being perpendicular to the path), but it also has a component along the pendulum trajectory (arch of a circle), due to the bending of that segment of the cable. This component can be calculated as $kx \cos \phi$, where ϕ is the angle of the pendulum with the vertical. This tangent force is responsible for speeding up or slowing down the motion of the oscillator from time to time, even sooner than air friction and other dissipative forces. Moreover the deformation δx also depends on all deformations δx of the remaining segments of the cable where the other pendula are attached: this is due to the coupling of all pendula through the cable. Dissipation plays an important role in our environment, because the initial energy is quickly lost by the excited pendula. Most of it is dissipated at the constraint, because the rope bends at the clamping point. This is shown by the following short term and long term plot for the overall pendula mechanical energy. First plot shows that, when high initial angles are considered, 90% of the initial pendula energy is lost in the first 20 minutes. On the other side the second plot shows the very beginning of the run when the system experiences a periodical energy exchange between the pendula and the catenary, which oscillate as a consequence of the initial excitation.



Probably the main contribution to dissipation is due to both torsion and slipping of the steel cable, at the point where it is fastened to the aluminium cage. As we said the cable is pre-tensioned with two opposite counterweights and it is suspended through two hooks placed on the external side of the framework. Those counterweights balance the pendula weight. When one or more pendula are excited using the electromagnets, the overall stress acting on the cable decreases and the cable tend to stretch, slipping on the hooks. Moreover during the run the cable itself swings and bends at the hook: this phenomenon produces an energy loss from the system to the external environment.

6.5 Fourier Analysis

We obtained the Fourier Spectrum for each oscillator motion, as shown in the related plots (5.6), where oscillation period is provided (inverse of frequency). T_1 indicates the dominant period. The dominant period T_1 is approximately of 2.1 s, corresponding to $2\pi\sqrt{L/g}$, where $L = 1.145$ m, as expected for a simple gravity pendulum. Few other pendula show two relevant secondary peaks. Hereafter we present the table of calculated periods and the Fourier spectrum for one pendulum (7th), where red dots identify the main peaks.



In order to perform Fourier analysis we had to take into account the replica that were removed from the gathered data. This removal affect the highest frequencies that can be detected by the system, which is not 120Hz, but that quantity reduced proportionally to the percentage of detected replica. Hence in practice for a replica percentage of 24% we could detect frequencies in the following range: from $1 \cdot 10^{-6}$ (which corresponds to the 2 hours recording time) up to 46Hz. As it is shown in the plots, the coupling between oscillators impinge on the modes shared between different oscillators. Hence the motion of pendula has a time evolution which is determined by the collective behaviour of the chain, despite the high dissipation of energy. The normal modes of the system do not rule the damping process, but the oscillatory part of the dynamics. All run show also low frequency peak at $2 \cdot 10^{-4}$ Hz that are related to the damping process on a much longer time scale (??).

Close frequencies can be noticed: they are responsible for the different beats seen in the $x(t)$ plots across all runs. For example in figure 6.1, different frequencies

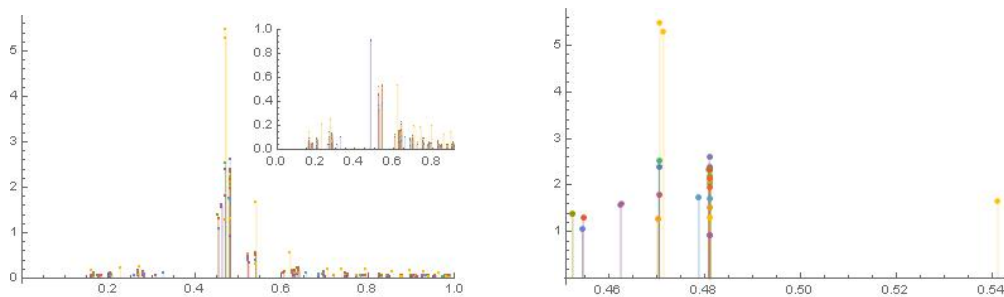
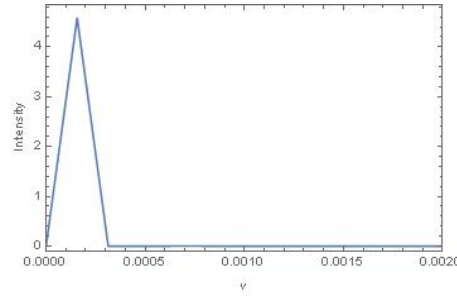


FIGURE 6.1: P08 50° Main Fourier peaks
0 – 1 Hz (left) - 0.45 – 0.54 Hz zoom (right)

TABLE 6.2: P08 50°: Main Fourier peaks

pendulum	first	second	third	pendulum	first
1	0.4809			13	0.4701
2	0.4809			14	0.4704
3	0.4811			15	0.4704
4	0.4809			16	0.4704
5	0.4809			17	0.4811
6	0.4808	0.4811		18	0.4811
7	0.4787			19	0.4809
8	0.4706	0.4714	0.5411	20	0.4809
9	0.4626	0.4623		21	0.4809
10	0.4524			22	0.4809
11	0.4546			23	0.4809
12	0.4544			24	0.4809



with about 10^{-2} Hz distance can be found. Considering the semi-difference between them, we find periods of the order of 3 minutes, while farthest apart frequencies correspond to a period of 25s. Those multiple frequencies can be interpreted as combinatorial frequencies, due to the non-linearity of the coupling between the oscillators. We can deduce that for higher values of the initial energy (i.e. more excited oscillators and/or higher initial angles) more cooperative effects appear and the number of shared modes increases. If this cooperative behaviour would persist, we could encounter Poincaré recurrences, but, having dissipation acting on the system, this can not happen.

6.6 Relaxation time

In order to estimate the relaxation time for the excited pendula, i.e. the time constant of the exponential loss of the initial energy, we evaluated the upper and lower background of the $x(t)$ plot, we identified the local maxima for the upper background or minima for the lower background and we calculated an exponential fit for those two distinct set of points as follows:

$$f(t) = Ae^{-t/(120\tau)} + B$$

where A , B and τ are unknown constants. In related plots (5.4) all involved data are shown: the blue area represents $x(t)$, the green line the upper and lower background, the red points the local maxima (or minima) of those background and finally black lines are the two best fit exponential functions. In the two superimposed tables the fitting parameters are reported.

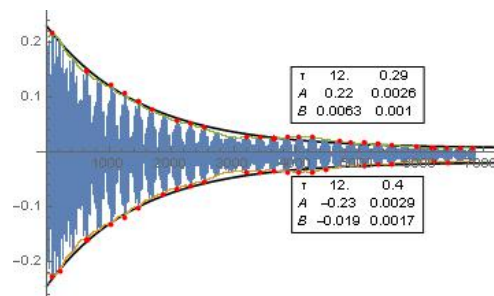


FIGURE 6.2: P16 50°

The values for τ vary from 3 to 14, where $\tau = 3$ corresponds to 6 minutes and $\tau = 14$ to 28 minutes. We also point out that pendula with higher energy get damped more quickly than the others and that the pendula at the end of the chain get less energy than the others. This phenomenon could be related to the nearby constraints. As an example we show the different envelopes for pendulum 4. In the left plot that

angle	excited pendula	n. 4	6	8	9	11	12	13	16	17	18	24
50	8			3.2								
	16			12.0					3.9			
	8 16			5.8					4.8			
	6 12 18		5.5				4.3	6.7				
40	3 6 9 12 15 18 21		5.9				5.0				6.9	
	6 12 18		5.8				5.4				5.1	
30	3 6 9 12 15 18 21				9.5	9.9						
	4 8 12 16 20	7.7		6.5			7.5			14.0		
	8 16			6.2					6.8			
	8 16	13.0										
20	9 12 15				9.0				9.0			
	All	9.6		7.5			5.8					9.2

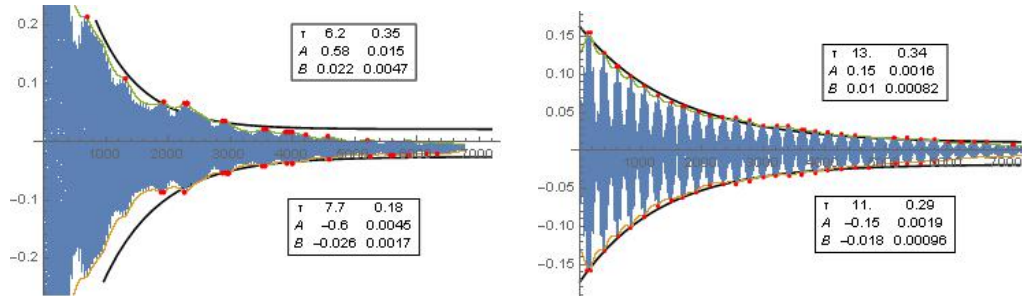
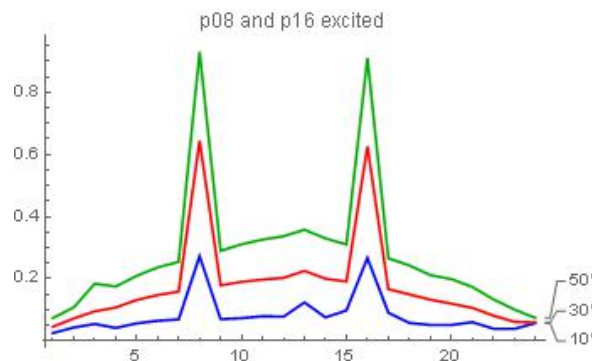


FIGURE 6.3: pendulum 4 damping rate in different runs
P04-08-12-16-20 30° (left) - P08 30° (right)

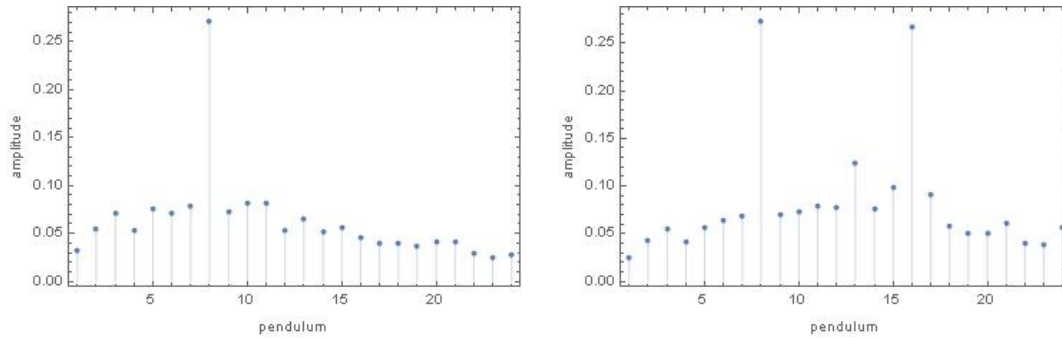
pendulum is one of the excited pendula and it shows a lower value for τ , while in the right one it is not excited and it shows a double value for τ . For most of the pendula ($\tau \simeq 8$) is around 14 minutes, but it also assumes much smaller or larger values for specific pendula.

6.7 Horizontal Analysis

We performed 3 different runs, with the same excited pendula (8th and 16th), but with different initial angles (30°, 40° and 50°). We calculated the maximum amplitude for each pendulum in those different runs: the obtained values are plotted in the following figure using different colours. We can notice that the excited pen-



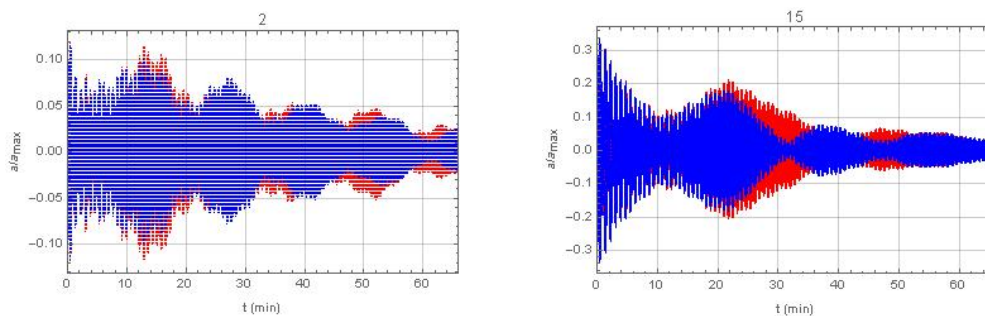
dulum does not transfer most its energy to its next, but rather to the ones next to them. This is shown by local maxima that can be recognised for pendula 3, 13 and 20 or 21. Contrary to what we could expect the not excited pendulum with the highest amplitude is not number 12, but number 13. In [10], using collective excitation on the lattice at high energies and angles, Denardo found similar results. Increas-



ing the available energy and/or the number of pendula the symmetry of the system grows, the cooperative behaviour of the system is amplified and a preferred position is given to the central pendula.

6.8 Chaos

In order to investigate the occurrence of chaos we compared two runs with same initial conditions (see 5.2) and we overlapped the two plots of normalised amplitude as a function of time, as it is shown in the following figure for pendula 2nd and 15th. The difference of the two plots shows that the system is sensitive to small



variations to the initial conditions as it is expected for a chaotic system, but chaos does not arise very early: hence we can conclude that the system has a low Lyapunov exponent, even if a quantitative analysis has not been done. Finally we mention some other chaotic behaviour that was noticed during observation of the system dynamics. For example we noticed in different runs few pendula remaining stack for a minute, while the two neighbours were oscillating with opposite phase. In particular this was observed when exciting pendula on opposite sides of the system. This phenomenon is very relevant, because it shows kind of a potential barrier. The chain as a whole in that case shows modal zones where the energy of the collective motion is almost null, being temporarily transferred to other parts of the chain. We can think that those stack oscillators correspond to a maximum for the interaction forces in the chain.

Chapter 7

Conclusions

7.1 Summary

In the following we summarise the main steps of the present thesis. As a starting phase the FPU literature was widely investigated for the purpose of understanding the reasons of the FPU problem and its historical evolution, the intermediate results and the latest achieved outcomes. As we already mentioned in the Introduction, the first scientists interested in the thermalisation process in order to better understand the open problem of the second law of thermodynamics were Fermi, Pasta and Ulam. Based on a numerical simulation using one of the first computer in history, they deduced the tendency of the system to periodically go back to a very close condition to the initial one where all energy was concentrated in the main oscillation mode. By the way their simulations did not last long enough to allow the achievement of equipartition of energy: as a matter of fact the physical parameters ruling the thermalisation kinetics, i.e. the coupling between oscillators and their number, were not sufficiently large.

Later on Kruskal and Zabusky started again that study and they realised that the Poincarè recurrences observed by their predecessors could be explained if solitons are taken into account. In particular they noticed the characteristic temporal stability of solitons and their tendency to recreate themselves even after interacting with each other. The latest fundamental finding is dated back in 1988 due to Sievers and Takeno, who introduced the concept of ILM, which are do not have to propagate, but can just vibrate maintaining their position.

Despite more than 60 years of research not all theoretical and practical consequences of the FPU problem are completely understood and many questions are still open: in particular the correlation between the second law of thermodynamics and the collective motion with non linear coupling. In this theoretical and experimental frame there are many phenomena to be investigated:

- chaos
- Poincarè recurrence
- solitons, ILM and breathers, beats
- asymptotic synchronisation
- thermalisation and equipartition

In order to deal with an experimental project, several practical problems have to be faced and solved. As it should be clear at this point, many different competences were involved in order to create from scratch the planned setup, to have it working as expected and to analyse the gathered data. In particular the videotracking procedure required the setup to change accordingly:

- in order to reduce the noise detected by the algorithm we were forced to change the original 6 alternating colours of the chain to a single (red) colour and to shade the surrounding with white materials
- to optimise and stabilise the light conditions of the system, which is exposed to both natural and artificial light: we introduced dedicate "soft" lights in the aluminium framework in order to avoid reflection on the spherical surface and we shaded the window with a curtain
- to reduce the synchronisation problems that multiple cooperating webcams face we replaced the 5 previously planned Logitech webcam with a single Go-Pro webcam with a macro lens to better distinguish the pendula at the extreme of the chain
- to take into account the fisheye effect of the webcam we calibrated each single pendulum trajectory with a very delicate and lengthy procedure.

After this long setup procedure, an extensive measurement campaign was carried out: 40 runs were executed, 36 of which having different initial conditions and few others were performed for studying chaos and repeated the same initial conditions. In the meanwhile the data processing was performed: it took a pretty long time, because the video treatment imply huge amount of data to be processed. To summarise the results we can obtain from the elaborated data and plots are the following:

- a) different beats existing at several time scales. In particular we notice "super" beats that last from 20 to 30 minutes, shorter beats which last 4 minutes and third beats that last 1 minutes.
- b) thermalisation of all pendula happens pretty fast and the energy metric Ω decrease regularly as $\Omega \sim t^{-2}$ after the first phase
- c) overall mechanical energy of the pendula is quickly transferred from our open system to the surrounding environment
- d) dissipation at the constraints has a high impact on the system and foster a higher rate in thermalisation of the chain
- e) chaos appears to happens in the first phase of each run and then it is displaced by a quasi-periodic behaviour of the chain in the following

Energy dissipation plays a role in the thermalisation process and speeds up the energy transfer from the excited pendula to the others and then to the environment. As a matter of fact, all real systems are open and this reason makes such an experimental research of a high interest, being much closer to reality.

The results of the research were shared and discussed with the scientific community in different national and international conferences:

- Talk in European Nonlinear Dynamics Conference in Budapest (July 2017)
- Talk in Associazione Italiana di Meccanica Teorica e Applicata Congress in Salerno (September 2017) and publication of the extended abstract in the Conference Proceedings [26]
- Talk in Società Italiana di Fisica National Congress in Trento (September 2017)

7.2 Further research

As a continuation of the present research the videotracking setup could be improved: positioning the GoPro webcam upwards on the floor under the system we could completely avoid the problem due to shadowing of the spheres by the nylon rope that we faced in the actual setup. The experienced replica on the videorecording have to be eliminated: for this reason a faster microSD has to be chosen. For the post-processing activities, a higher level of automation is needed: after the video files are copied to the hard disk where the elaboration takes place, the whole sequence of operations of format conversion, merge of segments, re-conversion and videotracking has to be executed automatically, checking each exit code before launching the following step. All those changes aim to minimise the experimental errors which can be faced during measurement operations. From the mechanical standpoint a second releasing mechanism has to be build and placed on the opposite side of the framework: at that point it will be possible to excite different normal modes of the chain with pendula excited on opposite side of the chain.

In order to generalise the obtained results a more flexible system would be needed: the parameters of interest are mainly

- the coupling
- in the pendulum length
- the pendulum radius
- the number of pendula
- the effective dissipation

This last objective can be obtained setting up a different clamping method for both the chain and the pendula. The best option we could think of is to have a shorter steel cable clamped at the extremes with two grips. Those grips could be connected to an oscillating rolling-element bearing.

From a theoretical standpoint the mathematical model of the physical system has to be further developed and studied in order to better represent the real experimental system. This model could help in extending the research outcomes, changing those parameters in the considered Lagrangian. In particular the cable needs to be modelled as a continuum body rather than as a number of discrete masses. This would help in better understanding the dynamics of the cable. Some experimental tests can be done for this purpose. In order to estimate its damping first of all free vibrations tests have to be done with no pendula involved: cable tension and vibration amplitude have to be considered as parameters of those tests. In order to distinguish the different damping contributions (close to constraints and far from them) forced vibrations tests have to be done. The damping estimate can be done using the Inverse Standing Wave Ratio (ISWR) technique. At Politecnico of Milano the team of prof. Martinelli is working on some simplified models in order to evaluate the structural damping of metal cables based on the energy dissipated during transversal vibrations [39, 18, 11]. Finally the applications of the research to the different technological and theoretical areas have to be exploited: in particular in the technological field the research outcomes can impact both the mechanical and the civil engineering. Other applications can be found in the solid state physics. As an example the results can shed light on polymer studies: as a matter of fact it was recently found by prof. Salesi et al. [8] that their linear chains show oscillatory and

dissipative behaviour and the higher is the energy of the chain the shorter is the related dissipation time.

Appendix A

Equipment specifications

A.1 EclipseMagnetic M52172/24VDC datasheet

Electro-holding magnet
Energise to hold - 25mm diameter
 12VDC or 24VDC Operating voltage

Part numbers
 M52172/12VDC
 M52172/24VDC



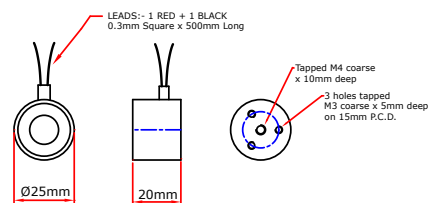
Pull gaps

Air gap (mm)	Magnetic Pull* (N)
0.00	150
0.09	51
0.18	22
0.27	12
0.36	8
0.59	4
1.00	2

* +/- 10% at room temperature

To achieve the optimum pull force 100% contact area must be achieved using the recommended armature plate. The force will be affected if other material specifications, thicknesses and surfaces are used, or if the armature fails to make positive contact over the full diameter of the face of the magnet. Where misalignment is likely to be an issue we recommend that an oversized armature plate is used to ensure 100% full contact, this however will reduce the stated pull force by approximately 10%.

Dimensions



Description

Mountings	Threaded holes in rear face
Finish	Bright nickel plated with machined face
Product weight	66g

Technical Data

Typical holding force	150N
ED rating	100%
IP Rating	54
Standard operating voltage	12VDC (M52172/12VDC) 24VDC (M52172/24VDC)
Current	12V - 180mA 24V - 90mA
Power consumption	2.16W

Connection type

12VDC and 24VDC Free leads (500mm long)

Recommended armature plate

Finish	Bright nickel plated
Diameter	25mm
Height	3mm
Screw	M3
Part No.	M52171/25ARM
Weight	15g



If you have any more questions, require technical assistance and would like a quotation, simply contact us.

www.eclipsesmagnetics.com

Eclipse Magnetics Ltd, Atlas Way, Sheffield, S4 7QQ, England
 T +44 (0)114 225 0600 F +44 (0)114 225 0525 E info@eclipsesmagnetics.com

While every effort has been made to ensure the accuracy of the information in this publication please note that specifications may change without notice.



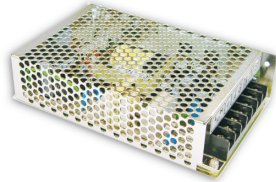
A world leader in magnetic technology



A.2 Mean Well RS-100-24 power supply datasheet

100W Single Output Switching Power Supply

RS-100 series



■ Features :

- Universal AC input / Full range
- Protections: Short circuit / Overload / Over voltage
- Cooling by free air convection
- LED indicator for power on
- 100% full load burn-in test
- All using 105°C long life electrolytic capacitors
- Withstand 300VAC surge input for 5 second
- High operating temperature up to 70°C
- Withstand 5G vibration test
- High efficiency, long life and high reliability



SPECIFICATION

MODEL	RS-100-3.3	RS-100-5	RS-100-12	RS-100-15	RS-100-24	RS-100-48	
OUTPUT	DC VOLTAGE	3.3V	5V	12V	15V	24V	48V
	RATED CURRENT	20A	16A	8.5A	7A	4.5A	2.3A
	CURRENT RANGE	0 ~ 20A	0 ~ 16A	0 ~ 8.5A	0 ~ 7A	0 ~ 4.5A	0 ~ 2.3A
	RATED POWER	66W	80W	102W	105W	108W	110.4W
	RIPPLE & NOISE (max.) Note.2	80mVp-p	80mVp-p	120mVp-p	120mVp-p	120mVp-p	200mVp-p
	VOLTAGE ADJ. RANGE	3.2V ~ 3.5V	4.75 ~ 5.5V	11.4 ~ 13.2V	14.25 ~ 16.5V	22.8 ~ 26.4V	45.6 ~ 52.8V
	VOLTAGE TOLERANCE Note.3	±3.0%	±2.0%	±1.0%	±1.0%	±1.0%	±1.0%
	LINE REGULATION Note.4	±0.5%	±0.5%	±0.5%	±0.5%	±0.5%	±0.5%
	LOAD REGULATION Note.5	±2.0%	±1.0%	±0.5%	±0.5%	±0.5%	±0.5%
	SETUP, RISE TIME	500ms, 20ms/230VAC 1200ms, 30ms/115VAC at full load					
HOLD UP TIME (Typ.)	100ms/230VAC 18ms/115VAC at full load						
INPUT	VOLTAGE RANGE	88 ~ 264VAC 125 ~ 373VDC (Withstand 300VAC surge for 5sec. Without damage)					
	FREQUENCY RANGE	47 ~ 63Hz					
	EFFICIENCY (Typ.)	74%	77%	81%	82%	84%	84%
	AC CURRENT (Typ.)	2.5A/115VAC 1.5A/230VAC					
	INRUSH CURRENT (Typ.)	COLD START 40A/230VAC					
	LEAKAGE CURRENT	<2mA / 240VAC					
PROTECTION	OVERLOAD	110 ~ 150% rated output power Protection type : Hiccup mode, recovers automatically after fault condition is removed					
	OVER VOLTAGE	3.8 ~ 4.45V	5.75 ~ 6.75V	13.8 ~ 16.2V	17.25 ~ 20.25V	27.6 ~ 32.4V	55.2 ~ 64.8V
ENVIRONMENT	WORKING TEMP.	-25 ~ +70°C (Refer to "Derating Curve")					
	WORKING HUMIDITY	20 ~ 90% RH non-condensing					
	STORAGE TEMP., HUMIDITY	-40 ~ +85°C, 10 ~ 95% RH					
	TEMP. COEFFICIENT	±0.03%/°C (0 ~ 50°C)					
	VIBRATION	10 ~ 500Hz, 5G 10min./1cycle, period for 60min. each along X, Y, Z axes					
SAFETY & EMC (Note 6)	SAFETY STANDARDS	UL60950-1, TUV EN60950-1 approved					
	WITHSTAND VOLTAGE	I/P-Q/P:3KVAC I/P-FG:1.5KVAC O/P-FG:0.5KVAC					
	ISOLATION RESISTANCE	I/P-Q/P: I/P-FG, O/P-FG:100M Ohms / 500VDC / 25°C / 70% RH					
	EMC EMISSION	Compliance to EN55022 (CISPR22) Class B, EN61000-3-2, -3					
OTHERS	EMC IMMUNITY	Compliance to EN61000-4-2, 3, 4, 5, 6, 8, 11, EN61000-6-2 (EN50082-2), heavy industry level, criteria A					
	MTBF	260.8Khrs min. MIL-HDBK-217F (25°C)					
NOTE	DIMENSION	159*97*38mm (L*W*H)					
	PACKING	0.6Kg, 24pcs/15.4Kg/0.7CUFT					
<p>1. All parameters NOT specially mentioned are measured at 230VAC input, rated load and 25°C of ambient temperature. 2. Ripple & noise are measured at 20MHz of bandwidth by using a 12" twisted pair-wire terminated with a 0.1uF & 47uF parallel capacitor. 3. Tolerance : includes set up tolerance, line regulation and load regulation. 4. Line regulation is measured from low line to high line at rated load. 5. Load regulation is measured from 0% to 100% rated load. 6. The power supply is considered a component which will be installed into a final equipment. The final equipment must be re-confirmed that it still meets EMC directives. For guidance on how to perform these EMC tests, please refer to "EMI testing of component power supplies." (as available on http://www.meanwell.com) 7. Length of set up time is measured at cold first start. Turning ON/OFF the power supply very quickly may lead to increase of the set up time.</p>							

File Name:RS-100-SPEC 2011-08-19

MeanWell Direct
Tel: +44 (0)118 970 3858 E-mail: sales@meanwelldirect.co.uk

A.3 GoPro Hero4 Black datasheet

HERO4 BLACK

2x the performance. Yet, again.

KEY CAMERA SPECS

- ▶ 4K30 / 2.7K50 / 1440p60 fps
- ▶ 1080p120 / 960p120 / 720p120
- ▶ 12MP / 30 fps Burst
- ▶ Control / View / Share
- ▶ Waterproof to 131' (40m)






Introducing HERO4 Black, the most advanced GoPro ever. Featuring improved image quality and a 2x more powerful processor with 2x faster video frame rates¹, HERO4 Black takes award-winning GoPro performance to a whole new level. Incredible high-resolution 4K30 and high frame-rate 1080p120 video enable stunning, immersive footage of you and your world.

Product Type:	Camera
Available Date:	10.05.14
UPC Code:	818279812767
Model Number:	CHD145-681
Product Name:	HERO4 Black
What's Included:	<ul style="list-style-type: none"> - HERO4 Black Camera - Standard Housing 131' (40m) - Strap-on Backdoor - Rechargeable Battery - Curved Adhesive Mount - Flat Adhesive Mount - Quick Release Buckle - 3-Way FlexArm - USB Cable
Shipping Unit:	Jerrel Case
DIMENSIONS	(H x W x D)
Single Unit:	24.75cm x 18.5cm x 10.25cm
Single Unit:	9.75in x 7.3in x 4.0in
Master Pack (6):	33.0cm x 22.64cm x 20.57cm
Master Pack (6):	13in x 8.9in x 8.1in
WEIGHT	
Single Unit:	575.495g
Single Unit:	1.269 lbs
Master Pack (6):	3455.37g
Master Pack (6):	7.62 lbs

FEATURES + BENEFITS

2x the Performance¹
With improved image quality, a 2x more powerful processor and 2x faster video frame rates, HERO4 Black is the most advanced GoPro ever.

Professional Video up to 4K30
Record vibrant high-resolution, high-frame-rate 4K30, 2.7K50 and 1080p120 video.

Fast, Powerful Photo Capture
Captures high-quality 12MP photos at speeds of up to 30 fps.

Built-in Wi-Fi + Bluetooth²
Delivers enhanced connectivity to the GoPro App, Smart Remote (sold separately) and more.

Protune™—Now for Video + Photos
On-the-fly capture and manual control of Color, ISO, White Balance and more.

Night Photo + Night Lapse
Outstanding exposure settings up to 20 seconds for single and Time Lapse photos.

HLight Tag
Tag & highlight favorite recordings for easy playback, editing and sharing.

QuickCapture
Power on and record automatically with the press of a button.

SuperView™
Captures the world from an extreme wide-angle view.

Auto Low Light
Automatically adjusts frame rate for optimal low-light performance.

High-Performance Audio
Enhanced audio system captures increased dynamic range with reduced distortion.³

Improved Camera Control⁴
New dedicated buttons deliver quick access to camera settings. Simplified menus make navigating menus easier than ever.

Ultra-Wide Angle Glass Lens
Optical engineering, innovative housing design and your world.

Selectable FOV
Three FOV settings—UltraWide, Medium and Narrow—allow for a broad range of perspectives.

Durable + Waterproof to 131' (40m)
Made to withstand extreme environments and conditions.

Wearable + Mountable
Enables immersive self-capture during your favorite activities.

Compatible with all GoPro Mounts
Adventure and accessories—and countless—for capturing a wide range of perspectives and activities.

GoPro App + Software
Control your camera remotely. View and share your content. Daily create, preview, GoPro style ideas.

FIGURE A.1: datasheet page 1/2

HERO4
BLACK
GoPro
Be a HERO

PROFESSIONAL VIDEO



RESOLUTION	FPS (NTSC/PAL)	VIEW ANGLE
4K	30, 25, 24	Ultra Wide
4K SuperView	24	Ultra Wide
2.7K	30, 28, 25, 24	Ultra Wide, Med
2.7K SuperView	30, 25	Ultra Wide
2.7K 4:3	30, 25	Ultra Wide
1440p	60, 48, 30, 48, 24, 25, 24	Ultra Wide
1080p	120, 90, 40, 30, 48, 24, 25, 24	Ultra Wide, Med ¹ , Narrow
1080p SuperView	60, 48, 30, 48, 24, 25, 24	Ultra Wide
840p	120, 60, 50	Ultra Wide
720p	120, 60, 50, 30, 25	Ultra Wide, Med, Narrow
720p SuperView	120, 60, 50	Ultra Wide
WVGA	24.8	Ultra Wide

KEY SPECS

- Video: 4K30 / 2.7K50 / 1440p80 / 1080p120 / 960p120 / 720p120
- Photo: 12MP @ 30 fps Burst
- Built-in Wi-Fi + Bluetooth*
- Protune™—now for photo + video
- HiLight Tag
- SuperView™
- Auto Low Light
- Night Photo + Night Lapse
- QuikCapture
- Built-in microphone
- Waterproof to 131' (40m)

PHOTOS

PHOTO
12MP

BLURST
12MP @
28 fps

TIME-LAPSE
0.5, 1, 2, 5, 10,
30, 60 second
intervals

NIGHT PHOTO
10, 15, 20, 30
second exposure
times

NIGHT LAPSE
10, 15, 20, 30 second
exposure times / Up to
60s in interval

FEATURED SETTINGS

protune™

Cinema-quality capture and advanced manual control for video and photos.

SUPER VIEW

Capture the world's most immersive field of view.

AUTO LOW LIGHT

Automatically adjusts frame rate for optimal low light performance.

CAPTURE. CREATE. SHARE.

GOPRO APP + SOFTWARE
Do more with your GoPro than ever before. Control your camera remotely. View and share your content. Easily create gopro.com, GoPro-style videos.



* Get Started at gopro.com/getstarted

IMAGE ASSETS




All product assets are available via secure site. Contact your GoPro channel manager for access information and usage terms.

Footnote
* Compared to the HERO3+ Black Edition.
¹ 180° and 180°+ are available upon request.

See more at partner.gopro.com
3333 Cleanse Way | San Mateo, CA 94402
©2014 GoPro, Inc. All rights reserved. GoPro, the GoPro logo, and other marks contained herein are trademarks of GoPro, Inc. in the United States and other countries. All other trademarks are the property of their respective owners. Copyright © 2014. GoPro, Inc. All rights reserved.

FIGURE A.2: datasheet page 2/2

Appendix B

SphereTracking Software

The following code was used to process videos produced by GoPro webcam in order to track the motion of the pendula.

B.1 file AutoColorFilter.cpp

```

1 //Originally written by Kyle Hounslow and modified for Marta Greselin with
  GoPro
2
3 #include "opencv\highgui.h"
4 #include "opencv\cv.h"
5 #include <sstream>
6 #include <string>
7 #include <iostream>
8 #include <fstream>
9 #include <vector>
10 #include <windows.h>
11 #include <memory>
12 #include "Sphere.h"
13
14 using namespace cv;
15 using std::ofstream;
16
17 //initial min and max HSV filter values.
18 int HMIN = 0;
19 int HMAX = 217;//179;
20 int S_MIN = 86;// 59;
21 int S_MAX = 255;//199;
22 int V_MIN = 101;//67;
23 int V_MAX = 227;// 129;
24 //default capture width and height
25 const int FRAME_WIDTH = 1920;
26 const int FRAME_HEIGHT = 1080;
27 //max number of objects to be detected in frame
28 const int MAX_NUM_OBJECTS = 80;
29 //minimum and maximum object area
30 const int MIN_OBJECT_AREA = 16 * 16;// 18 * 18;// 20 * 20;
31 const int MAX_OBJECT_AREA = FRAME_HEIGHT*FRAME_WIDTH / 1.5;
32 //names that will appear at the top of each window
33 const string windowName = "GoPro";
34 const string windowName2 = "Thresholded Image";
35 SYSTEMTIME systime;
36 string strTemp;
37 string StrDay;
38 VideoWriter oVideoWriter;
39 string filename;
40
41 // Sphere tracking procedure

```

```

42 string wordToString(WORD number) {
43     std::stringstream ss;
44     ss << number;
45     return ss.str();
46 }
47 string intToString(int number) {
48     std::stringstream ss;
49     ss << number;
50     return ss.str();
51 }
52 void drawObject(vector<Sphere> theSpheres, Mat &frame) {
53     for (int i = 0; i<theSpheres.size(); i++) {
54         cv::circle(frame, cv::Point(theSpheres.at(i).getXPos(), theSpheres.at(i).getYPos()), 14, cv::Scalar(0, 0, 255));
55         cv::putText(frame, intToString(theSpheres.at(i).getXPos()), cv::Point(theSpheres.at(i).getXPos() + 15, theSpheres.at(i).getYPos() + 0), 1, 1, Scalar(0, 255, 0));
56         cv::putText(frame, intToString(theSpheres.at(i).getYPos()), cv::Point(theSpheres.at(i).getXPos() + 15, theSpheres.at(i).getYPos() + 15), 1, 1, Scalar(0, 255, 0));
57     }
58 }
59 void morphOps(Mat &thresh) {
60     //create structuring element that will be used to "dilate" and "erode" image.
61     //the element chosen here is a 2px by 2px rectangle
62     Mat erodeElement = getStructuringElement(MORPH_RECT, Size(2, 2));
63     //dilate with larger element so make sure object is nicely visible
64     Mat dilateElement = getStructuringElement(MORPH_RECT, Size(4, 4));
65     erode(thresh, thresh, erodeElement);
66     erode(thresh, thresh, erodeElement);
67     dilate(thresh, thresh, dilateElement);
68     dilate(thresh, thresh, dilateElement);
69 }
70 void trackFilteredObject(Sphere theSphere, Mat threshold, Mat HSV, Mat & cameraFeed, shared_ptr<ofstream> &file, int frame) {
71     string strFrame;
72     vector<Sphere> spheres;
73     Mat temp;
74     threshold.copyTo(temp);
75     //these two vectors needed for output of findContours
76     vector<vector<Point>> contours;
77     vector<Vec4i> hierarchy;
78     //find contours of filtered image using openCV findContours function
79     findContours(temp, contours, hierarchy, CV_RETR_CCOMP, CV_CHAIN_APPROX_SIMPLE);
80     //use moments method to find our filtered object
81     double refArea = 0;
82     bool objectFound = false;
83     if (hierarchy.size() > 0) {
84         int numObjects = hierarchy.size();
85         //if number of objects greater than MAX_NUM_OBJECTS we have a noisy filter
86         if (numObjects<MAX_NUM_OBJECTS) {
87             for (int index = 0; index <= numObjects - 1; index = hierarchy[index][0]) {
88                 Moments moment = moments((cv::Mat)contours[index]);
89                 double area = moment.m00;
90                 //if the area is less than 20 px by 20px then it is probably just noise
91                 //if the area is the same as the 3/2 of the image size, probably just a bad filter
92                 //we only want the object with the largest area so we save a reference area each

```

```

93     //iteration and compare it to the area in the next iteration.
94     if (area>MIN.OBJECT_AREA) {
95         Sphere sphere;
96         sphere.setXPos(moment.m10 / area);
97         sphere.setYPos(moment.m01 / area);
98         sphere.setType(theSphere.getType());
99         sphere.setColour(theSphere.getColour());
100        spheres.push_back(sphere);
101        objectFound = true;
102    }
103 }
104
105 strFrame = to_string(frame);
106 putText(cameraFeed, strFrame, Point(0, 15), 1, 1, Scalar(0, 0, 255),
107 2);
108
109 //let user know you found an object
110 if (objectFound) {
111     (*file) << strFrame;
112     for (int i = 0; i < spheres.size(); i++) {
113         (*file) << " " + intToString(spheres.at(i).getXPos()) + " " +
114         intToString(spheres.at(i).getYPos());
115     }
116     (*file) << endl;
117     drawObject(spheres, cameraFeed);
118 }
119 else putText(cameraFeed, "TOO MUCH NOISE! ADJUST FILTER", Point(0, 40)
120 , 1, 2, Scalar(0, 0, 255), 2);
121 }
122
123 int main(int argc, char* argv[])
124 {
125     vector<shared_ptr<ofstream>> files;
126     int frame;
127     Mat cameraFeed;
128     Mat HSV;
129     Mat threshold;
130     VideoCapture capture("C:/Users/Docente/Videos/GoPro270617.mp4");
131     //set height and width of capture frame
132     capture.set(CV_CAP_PROP_FRAME_WIDTH, FRAME_WIDTH);
133     capture.set(CV_CAP_PROP_FRAME_HEIGHT, FRAME_HEIGHT);
134     //set framesize for videoWriter
135     Size frameSize(FRAME_WIDTH, FRAME_HEIGHT);
136     cv::namedWindow(windowName, WINDOW_NORMAL);
137
138     cout << "Recording started" << std::endl;
139     GetLocalTime(&systime);
140     StrDay = wordToString(systime.wYear) + "-";
141     strTemp = wordToString(systime.wMonth);
142     if (strTemp.size() == 1) StrDay += "0" + strTemp + "-";
143     else StrDay += strTemp + "-";
144     strTemp = wordToString(systime.wDay);
145     if (strTemp.size() == 1) StrDay += "0" + strTemp + "-";
146     else StrDay += strTemp + "-";
147     strTemp = wordToString(systime.wHour);
148     if (strTemp.size() == 1) StrDay += "0" + strTemp + "-";
149     else StrDay += strTemp + "-";
150     strTemp = wordToString(systime.wMinute);
151     if (strTemp.size() == 1) StrDay += "0" + strTemp;
152     else StrDay += strTemp;
153     // Impostazione dei file dati

```

```

153 files.clear();
154 filename = "C:/TrackingVideo/" + StrDay + "-GoProData.txt";
155 files.push_back(shared_ptr<ofstream>(new ofstream(filename.c_str())));
156 // Impostazione del file video
157 oVideoWriter = VideoWriter("C:/TrackingVideo/" + StrDay + "-GoPro.avi",
158     CV_FOURCC('D', 'I', 'V', '4'), 120, frameSize, true);
159 //initialize the VideoWriter object
160 if (!oVideoWriter.isOpened())
161 {
162     cout << "ERROR: Failed to initialize video writing" << endl;
163     //char cExit;
164     //std::cin >> cExit;
165     //PostQuitMessage(1);
166 }
167 //start an infinite loop where video is copied to cameraFeed matrix
168 frame = 0;
169 while(1)
170 {
171     //store image to matrix
172     bool bSuccess = capture.read(cameraFeed);
173     if (!bSuccess) {
174         cout << "ERROR: Cannot read a frame from video file" << endl;
175         break;
176     }
177     //convert frame from RGB to HSB colorspace
178     cvtColor(cameraFeed, HSV, COLOR_BGR2HSV);
179     //set HSV values from user selected region
180     Sphere sphere("");
181     inRange(HSV, Scalar(H_MIN, S_MIN, V_MIN), Scalar(H_MAX, S_MAX, V_MAX),
182         threshold);
183     morphOps(threshold);
184     //find spheres
185     trackFilteredObject(sphere, threshold, HSV, cameraFeed, files[0],
186         frame++);
187     oVideoWriter.write(cameraFeed);
188     imshow(windowName, cameraFeed);
189     if (waitKey(5) == 27) break; // 'esc' exit program
190 }
191 destroyWindow(windowName);
192 oVideoWriter.release();
193 return 0;
194 }

```

B.2 file Sphere.cpp

```
1
2 #include "Sphere.h"
3
4 Sphere::Sphere()
5 {
6     //set values for default constructor
7     setType("null");
8     setColour(Scalar(0,0,0));
9 }
10
11 Sphere::Sphere(string name){
12
13     setType(name);
14
15     if(name=="sphere"){
16         setHSVmin(Scalar(0, 59, 67));
17         setHSVmax(Scalar(179, 199, 129));
18         //RGB value for green:
19         setColour(Scalar(0,0,255));
20     }
21 }
22
23 Sphere::~Sphere(void)
24 {
25 }
26
27 int Sphere::getXPos(){
28
29     return Sphere::xPos;
30 }
31 }
32
33 void Sphere::setXPos(int x){
34
35     Sphere::xPos = x;
36 }
37 }
38
39 int Sphere::getYPos(){
40
41     return Sphere::yPos;
42 }
43 }
44
45 void Sphere::setYPos(int y){
46
47     Sphere::yPos = y;
48 }
49 }
50
51 Scalar Sphere::getHSVmin(){
52
53     return Sphere::HSVmin;
54 }
55 }
56 Scalar Sphere::getHSVmax(){
57
58     return Sphere::HSVmax;
59 }
60 }
```

```
61 void Sphere::setHSVmin(Scalar min){
62
63     Sphere::HSVmin = min;
64 }
65
66 void Sphere::setHSVmax(Scalar max){
67
68     Sphere::HSVmax = max;
69 }
70 }
```


B.3 file Sphere.h (to be included for the compilation in C code)

```
1 #pragma once
2 #include <string>
3 #include "opencv\cv.h"
4 #include "opencv\highgui.h"
5 using namespace std;
6 using namespace cv;
7
8 class Sphere
9 {
10 public:
11     Sphere();
12     ~Sphere(void);
13
14     Sphere(string name);
15
16     int getXPos();
17     void setXPos(int x);
18
19     int getYPos();
20     void setYPos(int y);
21
22     Scalar getHSVmin();
23     Scalar getHSVmax();
24
25     void setHSVmin(Scalar min);
26     void setHSVmax(Scalar max);
27
28     string getType(){return type;}
29     void setType(string t){type = t;}
30
31     Scalar getColour(){
32         return Colour;
33     }
34     void setColour(Scalar c){
35
36         Colour = c;
37     }
38
39 private:
40
41     int xPos, yPos;
42     string type;
43     Scalar HSVmin, HSVmax;
44     Scalar Colour;
45 };
```


Appendix C

Mathematica code

The following code was used to calculate all the physical quantities of interest based on the data produced by the videotracking algorithm.

C.1 Load data

```
SetDirectory["C:\\FPU\\elab.FPU"];
```

```
L = 1.145;
```

```
g = 9.81;
```

```
fps = 120;
```

```
excPend = {8, 16};
```

```
GoProData = Import["GoProData.txt", "Table"];
```

```
InitialFrame = GoProData[[1, 1]] - 1;
```

```
yTrajectory[sphere_, pixel_] :=
```

```
Which [sphere==1, 1075.5876927974166 - 0.18870066427474577pixel + 0.00006599017741519634pixel2 + 1.818711566426105410(-8)pixel3,
sphere==2, 1052.9584678309586 - 0.19232907168373092pixel + 0.00005934422577072623pixel2 + 1.883190437885620710(-8)pixel3,
sphere==3, 1060.3524415001448 - 0.3286802665468743pixel + 0.0001947978699867646pixel2 - 2.490249666040940410(-8)pixel3,
sphere==4, 1015.7761525312723 - 0.2926508533900111pixel + 0.0001605467622795486pixel2 - 1.430379544325046510(-8)pixel3,
sphere==5, 973.3843397593116 - 0.317603745426182pixel + 0.00020462430677967595pixel2 - 3.55019074920459110(-8)pixel3,
sphere==6, 916.302206158762 - 0.24284225884879887pixel + 0.00013241129228379548pixel2 - 1.158837072579349810(-8)pixel3,
sphere==7, 851.9876076102589 - 0.16464840130395222pixel + 0.00006920662057300188pixel2 + 1.37262447933850810(-9)pixel3,
sphere==8, 831.1487077846357 - 0.20556699971490672pixel + 0.00010059828497002864pixel2 - 8.04908483546979510(-9)pixel3,
sphere==9, 744.9310374741791 - 0.10519272778655803pixel + 0.000025314603235718588pixel2 + 1.198309034530638410(-8)pixel3,
sphere==10, 685.9889859127799 - 0.06279941581873275pixel + 5.7612110302412710(-6)pixel2 + 9.3096318219362910(-9)pixel3,
sphere==11, 642.92701641342 - 0.08062974618563501pixel + 0.00003266070237496218pixel2 - 1.293304140127793210(-10)pixel3,
sphere==12, 560.4645306139125 + 0.029674990695285015pixel - 0.00004970775679033956pixel2 + 1.533235941924001310(-8)pixel3,
sphere==13, 504.8069725900765 + 0.06187314001185479pixel - 0.000067802124891285pixel2 + 1.650398149135626310(-8)pixel3,
sphere==14, 442.11798379333675 + 0.12252552075825367pixel - 0.00011362399569603218pixel2 + 2.74787490152028110(-8)pixel3,
sphere==15, 388.7757341551241 + 0.11342219324790266pixel - 0.00007198727552449685pixel2 + 6.27615556705457710(-9)pixel3,
sphere==16, 326.77704910261565 + 0.1576838099213499pixel - 0.00010196972724133125pixel2 + 1.317833818283237210(-8)pixel3,
sphere==17, 254.47933066255098 + 0.23276993397831905pixel - 0.0001541283072764384pixel2 + 2.344105219275677810(-8)pixel3,
sphere==18, 223.50656190183724 + 0.2007816812988414pixel - 0.0001136792332753662pixel2 + 7.00957774844677910(-9)pixel3,
sphere==19, 138.65636136913827 + 0.29369637192360226pixel - 0.00018238312399019804pixel2 + 2.38290182618732410(-8)pixel3,
sphere==20, 112.25697293941553 + 0.2586162190308203pixel - 0.00014247068055456567pixel2 + 9.4879192309134410(-9)pixel3,
```

```

sphere==21, 63.829975806095824 + 0.25886563590781525pixel - 0.00011899342912254382pixel2 - 3.25757052471081810(-9)pixel3,
sphere==22, -16.413090518786678 + 0.35250715882528666pixel - 0.0001949924264625299pixel2 + 1.833489266742507410(-8)pixel3
sphere==23, -44.77575212746545 + 0.3493348701936882pixel - 0.00020187483993629467pixel2 + 2.364680495335863410(-8)pixel3,
sphere==24, -91.69389667021399 + 0.2874225118862467pixel - 0.00008695482157617094pixel2 - 2.009457292403858310(-8)pixel3]

initPix = Flatten[Table[Take[Flatten[Take[GoProData, 1]], {2n}], {n, 1, 24}]];

initPix[[8]] = Round [  $\frac{\text{initPix}[[7]] + \text{initPix}[[9]]}{2}$  ];
initPix[[16]] = Round [  $\frac{\text{initPix}[[15]] + \text{initPix}[[17]]}{2}$  ];

a1 = -0.0019367089632610765Part[initPix, 1];
a2 = -0.0018767495907569033Part[initPix, 2];
a3 = -0.0018509133203608076Part[initPix, 3];
a4 = -0.0018219686068335701Part[initPix, 4];
a5 = -0.0017671597800040316Part[initPix, 5];
a6 = -0.0017999580672171897Part[initPix, 6];
a7 = -0.0017734124373084716Part[initPix, 7];
a8 = -0.0017593549683131036Part[initPix, 8];
a9 = -0.001745207984827598Part[initPix, 9];
a10 = -0.0017434384385143385Part[initPix, 10];
a11 = -0.0017244128384490845Part[initPix, 11];
a12 = -0.001732645744717328Part[initPix, 12];
a13 = -0.0017207078280285452Part[initPix, 13];
a14 = -0.0016829333378576715Part[initPix, 14];
a15 = -0.0017053806178472261Part[initPix, 15];
a16 = -0.0017153610704472265Part[initPix, 16];
a17 = -0.0017260381114903283Part[initPix, 17];
a18 = -0.00172987921989900 Part[initPix, 18];
a19 = -0.001734915448719971Part[initPix, 19];
a20 = -0.00173735384841998Part[initPix, 20];
a21 = -0.0017744353782386893Part[initPix, 21];
a22 = -0.0017551559517549476Part[initPix, 22];
a23 = -0.0017901023418946675Part[initPix, 23];
a24 = -0.0018095883556454354Part[initPix, 24];

PixelToMx[sphere_, pixel_] := Which[sphere==1, a1 + 0.0019367089632610765pixel,
sphere==2, a2 + 0.0018767495907569033pixel,
sphere==3, a3 + 0.0018509133203608076pixel,
sphere==4, a4 + 0.0018219686068335701pixel,
sphere==5, a5 + 0.0017671597800040316pixel,
sphere==6, a6 + 0.0017999580672171897pixel,
sphere==7, a7 + 0.0017734124373084716pixel,
sphere==8, a8 + 0.0017593549683131036pixel,
sphere==9, a9 + 0.001745207984827598pixel,
sphere==10, a10 + 0.0017434384385143385pixel,
sphere==11, a11 + 0.0017244128384490845pixel,

```

```

sphere==12, a12 + 0.001732645744717328pixel,
sphere==13, a13 + 0.0017207078280285452pixel,
sphere==14, a14 + 0.0016829333378576715pixel,
sphere==15, a15 + 0.0017053806178472261pixel,
sphere==16, a16 + 0.0017153610704472265pixel,
sphere==17, a17 + 0.0017260381114903283pixel,
sphere==18, a18 + 0.001729879219899008pixel,
sphere==19, a19 + 0.001734915448719971pixel,
sphere==20, a20 + 0.001737353848419982pixel,
sphere==21, a21 + 0.0017744353782386893pixel,
sphere==22, a22 + 0.0017551559517549476pixel,
sphere==23, a23 + 0.0017901023418946675pixel,
sphere==24, a24 + 0.0018095883556454354pixel];

t = ParallelMap [ #-InitialFrame
                 fps &, GoProData[[All, 1]] ];
xp = Table[GoProData[[All, 2sphere]], {sphere, 24}];
yp = Table[GoProData[[All, 2sphere + 1]], {sphere, 24}];
swap = {};
Do[If[Abs[yTrajectory[sphere + 1, xp[[sphere, i]]] - yp[[sphere, i]]] ≤ Abs[yTrajectory[sphere, xp[[sphere, i]]] - yp[[sphere, i]]]&&
Abs[yTrajectory[sphere, xp[[sphere + 1, i]]] - yp[[sphere + 1, i]]] ≤
Abs[yTrajectory[sphere + 1, xp[[sphere + 1, i]]] - yp[[sphere + 1, i]]], AppendTo[swap, {i, sphere}];
p = xp[[sphere, i]];
xp[[sphere, i]] = xp[[sphere + 1, i]];
xp[[sphere + 1, i]] = p], {i, Length[t]}, {sphere, 23}];
replica = {};
Do[j = 0; Do[If[xp[[sphere, i]]==xp[[sphere, i + 1]], j++], {sphere, 24
}];
If[j == 24, AppendTo[replica, i]], {i, Length[t] - 1}];

replicaPer = Length[replica]/Length[t] * 100.

26.5469

tOld = t;
xpOld = xp;

replica = Partition[replica, 1];
Clear[t, xp]
t = Delete[tOld, replica];

xp = Transpose[Delete[Transpose[xpOld], replica]];

x = Table[ParallelMap[PixelToMx[sphere, #]&, xp[[sphere]]], {sphere, 24}];

amp = Table [  $\frac{\text{Max}[x[[u]]]-\text{Min}[x[[u]]]}{2}$ , {u, 24} ] ;
med = Table [  $\frac{\text{Max}[x[[u]]]+\text{Min}[x[[u]]]}{2}$ , {u, 24} ] ;

```

C.2 Potential energy U, mechanical energy E, energy metrics Omega

```

u = Table [gL (1 - Sqrt [1 - (x[[sphere,i]]/L)^2]), {sphere, 24}, {i, Length[t] - 1}];
e = Table [1/2 ( (x[[sphere,i+8]] - x[[sphere,i-8]]) / (t[[i+8]] - t[[i-8]]) )^2 + u[[sphere, i]], {sphere, 24}, {i, 9, Length[t] - 8}];
eT = Transpose[e];
e0 = Flatten[Take[eT, 1]];
pP[list.]:=Prepend[list, e0];
eT = Flatten[Take[NestList[pP, eT, 8], -1], 1];
eN = Flatten[Take[eT, -1]];
aP[list.]:=Append[list, eN];
eT = Flatten[Take[NestList[aP, eT, 7], -1], 1];
e = Transpose[eT];

eAll = Table[Sum[e[[sphere, i]], {sphere, 24}], {i, Length[t] - 1}];
uAcc = Transpose[Accumulate[Transpose[Table[u[[sphere, i]](t[[i + 1]] - t[[i]]), {sphere, 24}, {i, Length[t] - 1}]]];
uMedia = Table [uAcc[[sphere, i]]t[[i]]^-1, {sphere, 24}, {i, Length[t] - 1}];
omega = Variance[uMedia];

ListLogLogPlotT[time_, list_, label.]:=ListLogLogPlot [Transpose [ { {time/60, list} } ], Joined -> False, Axes -> False, Frame -> True,
FrameLabel -> {"t (min)", label}, PlotStyle->{Blue}, GridLines -> Automatic, PlotRange -> All];

ListLogLogPlotT[Take[t, {1, -2}], omega, "omega"];

Export["LogLogPlotomega.jpg", %, "JPEG"]

tEnd = Drop[t, fps * 60 * 20];
omegaEnd = Drop[omega, fps * 60 * 20];

funfitomega[s.]:=As^(-a) + B;
fit = NonlinearModelFit[Transpose[{Take[tEnd, {1, -2}]/60, omegaEnd}], funfitomega[s], {a, A, B}, s, MaxIterations -> 1000000];
exp = fit["ParameterTableEntries"];

LogLogPlot[fit[s], {s, 0, 120}, PlotStyle -> {Red, Dashed}, PlotRange -> {{.0001, 120}, {.00001, 3}}, FrameLabel -> {"t (min)", "omega"},
Epilog -> {Inset[Grid[Thread[{a, Map[NumberForm[#, 2]&, exp[[1, {1}]], {2}]}], Frame -> True]], Frame -> True]

Show[%, ListLogLogPlotT[Take[t, {1, -2}], omega, "omega"]]

Export["omega_tangente.jpg", %, "JPEG"];

eAll = Table[Sum[e[[sphere, i]], {sphere, 24}], {i, Length[t] - 1}];
uAll = Table[Sum[u[[sphere, i]], {sphere, 24}], {i, Length[t] - 1}];

amp = Table [ (Max[x[[sphere]]] - Min[x[[sphere]]) / 2, {sphere, 24} ];
med = Table [ (Max[x[[sphere]]] + Min[x[[sphere]]) / 2, {sphere, 24} ];

ListLinePlot[amp, PlotRange -> All]

Export["ampiezze.jpg", %, "JPEG"]

```

```
ListPlotT[time_, list_, label_, sphere_]:=ListPlot [Transpose [ {  $\frac{\text{time}}$ , list } ], Joined → False, Axes → False, Frame → True,
FrameLabel → { "t (min)", label }, PlotStyle->{Red, Blue}, GridLines → Automatic, PlotRange → {{0, 3}, All}, PlotLabel → sphere];
lpx[sphere_]:=ListPlotT [t, x[[sphere]], "a/amax", sphere];
lpe[sphere_]:=ListPlotT[Take[t, {2, -1}], e[[sphere]], e];
lpk[sphere_]:=ListPlotT[Take[t, {2, -1}], e[[sphere]] - u[[sphere]], k];
lpu[sphere_]:=ListPlotT[Take[t, {2, -1}], u[[sphere]], u];
```

C.3 Plots export

```
For[sphere = 1, sphere ≤ 24, sphere++, Print[lpx[sphere]]];

For[sphere = 1, sphere ≤ 24, sphere++,
Export[p <> IntegerString[sphere] <> "x(t).jpg", lpx[sphere], "JPEG"];
]

For[sphere = 1, sphere ≤ 24, sphere++, Print[lpe[sphere]]];

For[sphere = 1, sphere ≤ 24, sphere++,
Export[p <> IntegerString[sphere] <> "e(t).jpg", lpe[sphere], "JPEG"];]

For[sphere = 1, sphere ≤ 24, sphere++,
Export[p <> IntegerString[sphere] <> "k(t).jpg", lpk[sphere], "JPEG"];
]

For[sphere = 1, sphere ≤ 24, sphere++,
Export[p <> IntegerString[sphere] <> "u(t).jpg", lpu[sphere], "JPEG"];
]

Export["eAll.jpg", ListPlotT[Take[t, {1, -2}], eAll, "eAll", "JPEG"];
Export["uAll.jpg", ListPlotT[Take[t, {1, -2}], uAll, "uAll", "JPEG"];
Export["kAll.jpg", ListPlotT[Take[t, {1, -2}], eAll - uAll, "kAll", "JPEG"];
```

C.4 Fourier analysis

```
n = Length[t];
Solo se n è dispari
t = Drop[t, -1];
x = Transpose[Drop[Transpose[x], -1]];

n = Length[t];

x1 = Take[x, 1];
x2 = Take[x, {2}];
x3 = Take[x, {3}];
x4 = Take[x, {4}];
x5 = Take[x, {5}];
```

```
x6 = Take[x, {6}];
x7 = Take[x, {7}];
x8 = Take[x, {8}];
x9 = Take[x, {9}];
x10 = Take[x, {10}];
x11 = Take[x, {11}];
x12 = Take[x, {12}];
x13 = Take[x, {13}];
x14 = Take[x, {14}];
x15 = Take[x, {15}];
x16 = Take[x, {16}];
x17 = Take[x, {17}];
x18 = Take[x, {18}];
x19 = Take[x, {19}];
x20 = Take[x, {20}];
x21 = Take[x, {21}];
x22 = Take[x, {22}];
x23 = Take[x, {23}];
x24 = Take[x, {24}];

tx1 = Transpose[Prepend[Part[x, {1}], t]];
tx2 = Transpose[Prepend[Part[x, {2}], t]];
tx3 = Transpose[Prepend[Part[x, {3}], t]];
tx4 = Transpose[Prepend[Part[x, {4}], t]];
tx5 = Transpose[Prepend[Part[x, {5}], t]];
tx6 = Transpose[Prepend[Part[x, {6}], t]];
tx7 = Transpose[Prepend[Part[x, {7}], t]];
tx8 = Transpose[Prepend[Part[x, {8}], t]];
tx9 = Transpose[Prepend[Part[x, {9}], t]];
tx10 = Transpose[Prepend[Part[x, {10}], t]];
tx11 = Transpose[Prepend[Part[x, {11}], t]];
tx12 = Transpose[Prepend[Part[x, {12}], t]];
tx13 = Transpose[Prepend[Part[x, {13}], t]];
tx14 = Transpose[Prepend[Part[x, {14}], t]];
tx15 = Transpose[Prepend[Part[x, {15}], t]];
tx16 = Transpose[Prepend[Part[x, {16}], t]];
tx17 = Transpose[Prepend[Part[x, {17}], t]];
tx18 = Transpose[Prepend[Part[x, {18}], t]];
tx19 = Transpose[Prepend[Part[x, {19}], t]];
tx20 = Transpose[Prepend[Part[x, {20}], t]];
tx21 = Transpose[Prepend[Part[x, {21}], t]];
tx22 = Transpose[Prepend[Part[x, {22}], t]];
tx23 = Transpose[Prepend[Part[x, {23}], t]];
tx24 = Transpose[Prepend[Part[x, {24}], t]];
```



```

If[i == 6, FFTV6,
If[i == 7, FFTV7, If[i == 8, FFTV8,
If[i == 9, FFTV9, If[i == 10, FFTV10, If[i == 11, FFTV11,
If[i == 12, FFTV12, If[i == 13, FFTV13, If[i == 14, FFTV14, If[i == 15, FFTV15,
If[i == 16, FFTV16, If[i == 17, FFTV17, If[i == 18, FFTV18, If[i == 19, FFTV19, If[i == 20, FFTV20,
If[i == 21, FFTV21, If[i == 22, FFTV22, If[i == 23, FFTV23, FFTV24]]]]]]]]]]]]]]]]]]]]];

deltaNu =  $\frac{f_{ps}}{n}$  (1 - replicaPer/100.)

0.000130228

frequencyValues = Table[deltaNu * (i - n/2), {i, 1, n}];

pPeaks = Table[FindPeaks[Table[Abs[FFTV[sphere]][[i]], {i, n/2 + 1000, n/2 + 12000}], 60], {sphere, 24}];

fapPeaks[sphere.]:=Table[{frequencyValues[[pPeaks[[sphere, i, 1]] + n/2 + 1000]], pPeaks[[sphere, i, 2]]},
{i, Length[pPeaks[[sphere]]}]

po = Table[fapPeaks[sphere], {sphere, 24}];

ListPlot[po, PlotRange -> All, Filling -> Axis];

Export["horizontal_Fourier.jpg", %, "JPEG"]

ListLinePlotPunti[sphere.]:=ListLinePlot[Table[{frequencyValues[[i]], Abs[FFTV[sphere]][[i]]}, {i, n/2 + 1000, n/2 + 12000}],
PlotRange -> All, Epilog -> {Red, PointSize[0.01], Point[po[[sphere]]]}]

For[sphere = 1, sphere <= 24, sphere++, Print[ListLinePlotPunti[sphere]]]

For[sphere = 1, sphere <= 24, sphere++,
Export[p <> IntegerString[sphere] <> "ftPEAKS.jpg", ListLinePlotPunti[sphere], "JPEG"];
]

ListPlot[po, PlotRange->All, Filling -> Axis, Epilog -> Inset[ListPlot[po, PlotRange -> {{0.4, .8}, {0, 5}}, Filling -> Axis], {2, 4.5}]]

poOrdered = Table[Sort[po[[i]], #1[[2]] > #2[[2]]&], {i, 24}];

first3po = Table[Take[poOrdered[[i]], 3], {i, 24}];

poTable = Table[Partition[Flatten[Select[first3po[[i]], #[[2]] > 0.2&]], 2], {i, 24}];

ListPlot[first3po, PlotRange -> All, Filling -> Axis]

Export["horizontal_Fourier_3picchi.jpg", %, "JPEG"]

horizontal_Fourier_3picchi.jpg

ListPlot[poTable, PlotRange -> All, Filling -> Axis]

Export["horizontal_Fourier_upto3picchialti.jpg", %, "JPEG"]

horizontal_Fourier_upto3picchialti.jpg

ListPlot[{poTable[[8]], poTable[[16]]}, PlotRange -> All, Filling -> Axis]

Export["horizontal_Fourier_upto3picchialti_soloexc.jpg", %, "JPEG"]

```

horizontal_Fourier_upto3picchialti_soloexc.jpg

```
Export["poTable.txt", poTable, "Table"]
```

```
ListPlot[po, PlotRange → All, Filling → Axis]
```

```
For[sphere = 1, sphere ≤ 24, sphere++, Print[ListPlotFFT[sphere]]]
```


Bibliography

- [1] VI Arnold. "Generation of quasi-periodic motion from a family of periodic motions". In: *Dokl. Akad. Nauk SSSR*. Vol. 138. 1. 1961, pp. 13–15.
- [2] P Bocchieri et al. "Anharmonic chain with Lennard-Jones interaction". In: *Physical Review A* 2.5 (1970), p. 2013.
- [3] A Carati, L Galgani, and A Giorgilli. "The Fermi–Pasta–Ulam problem as a challenge for the foundations of physics". In: *Chaos: An Interdisciplinary Journal of Nonlinear Science* 15.1 (2005), p. 015105.
- [4] A Carati et al. "The Fermi-Pasta-Ulam problem". In: *NUOVO CIMENTO-SOCIETA ITALIANA DI FISICA SEZIONE B* 117.9/11 (2002), pp. 1017–1026.
- [5] C Cercignani, Luigi Galgani, and A Scotti. "Zero-point energy in classical nonlinear mechanics". In: *Physics Letters A* 38.6 (1972), pp. 403–404.
- [6] Wolfgang Christian. *Open source physics: A user's guide with examples*. Pearson Education, 2007.
- [7] Eddie GD Cohen. "The FPU problem and statistical mechanics". In: *APS March Meeting Abstracts*. 2005.
- [8] Claudio Colleoni et al. "Delayed luminescence induced by complex domains in water and in TEOS aqueous solutions". In: *Physical Chemistry Chemical Physics* 18.2 (2016), pp. 772–780.
- [9] T Dauxois, M Peyrard, and S Ruffo. "The Fermi–Pasta–Ulam "numerical experiment": history and pedagogical perspectives". In: *European Journal of Physics* 26.5 (2005), S3. URL: <http://stacks.iop.org/0143-0807/26/i=5/a=S01>.
- [10] B Denardo et al. "Observations of localized structures in nonlinear lattices: Domain walls and kinks". In: *Physical review letters* 68.11 (1992), p. 1730.
- [11] Giorgio Diana et al. "On the measurement of overhead transmission lines conductor self-damping". In: *IEEE Transactions on Power Delivery* 15.1 (2000), pp. 285–292.
- [12] M Eleftheriou and S Flach. "Discrete breathers in thermal equilibrium: distributions and energy gaps". In: *Physica D: Nonlinear Phenomena* 202.1 (2005), pp. 142–154.
- [13] Massimo Falcioni and Angelo Vulpiani. "Il contributo di Enrico Fermi ai sistemi non lineari: l'influenza di un articolo mai pubblicato". In: *Conoscere Fermi nel centenario della nascita* 29 (1901).
- [14] E Fermi, J Pasta, and S Ulam. *E. Fermi Collected Papers*. 1965.
- [15] E Fermi, J Pasta, and S Ulam. "Los Alamos Sci. Lab. Rep". In: *LA-1940* (1955).
- [16] Enrico Fermi. *Collected Papers:(Note E Memorie)*. Vol. 2. University of Chicago Press, 1962.

- [17] IE Fermi et al. *Studies of the nonlinear problems*. Tech. rep. Los Alamos Scientific Lab., N. Mex., 1955.
- [18] Francesco Foti and Luca Martinelli. “Finite element modeling of cable galloping vibrations. Part II: Application to an iced cable in 1: 2 multiple internal resonance”. In: *Journal of Vibration and Control* (2016), p. 1077546316660017.
- [19] F Fucito et al. “Approach to equilibrium in a chain of nonlinear oscillators”. In: *Journal de Physique* 43.5 (1982), pp. 707–713.
- [20] L Galgani and A Scott. “Planck-like distributions in classical nonlinear mechanics”. In: *Physical Review Letters* 28.18 (1972), p. 1173.
- [21] L Galgani and A Scotti. “Recent progress in classical nonlinear dynamics”. In: *La Rivista del Nuovo Cimento* (1971-1977) 2.2 (1972), pp. 189–209.
- [22] L Galgani et al. “On the problem of energy equipartition for large systems of the Fermi-Pasta-Ulam type: analytical and numerical estimates”. In: *Physica D: Nonlinear Phenomena* 59.4 (1992), pp. 334–348.
- [23] Antonio Giorgilli and Luigi Galgani. “Rigorous estimates for the series expansions of Hamiltonian perturbation theory”. In: *Celestial mechanics* 37.2 (1985), pp. 95–112.
- [24] Harvey Gould et al. *STP Fermi-Pasta-Ulam Program*. 2009. URL: <https://www.compadre.org/osp/items/detail.cfm?ID=8643>.
- [25] Harvey Gould et al. *The Fermi-Pasta-Ulam problem*. 2009. URL: <http://stp.clarku.edu/simulations/fpu/index.html>.
- [26] Marta Greselin, Giovanni Salesi, and Roberto Leporini. “Thermalisation of a coupled pendulum chain”. In: *AIMETA 2017. XXIII Conference of the Italian Association of Theoretical and Applied Mechanics*. Vol. 3, pp. 972–978.
- [27] H Guoxiang and X Zaixin. “Kinks and solitons in coupled pendulum lattices”. In: *Chinese Physics Letters* 9.12 (1992), p. 659.
- [28] Andreas Henrici and Thomas Kappeler. “Results on normal forms for FPU chains”. In: *Communications in Mathematical Physics* 278.1 (2008), pp. 145–177.
- [29] Kyle Hounslow. *OpenCV Tutorial: Adding an Automatic Colour Filter for Object Tracking*. 2015. URL: <https://www.youtube.com/watch?v=s5ROKdRUkuI&t=41s>.
- [30] Kyle Hounslow. *OpenCV Tutorial: Multiple Object Tracking in Real Time (1/3)*. 2013. URL: https://www.youtube.com/watch?v=RS_uQGOQIdg&t=504s.
- [31] Kyle Hounslow. *OpenCV Tutorial: Multiple Object Tracking in Real Time (2/3)*. 2013. URL: <https://www.youtube.com/watch?v=ASci7J5W1FM&t=116s>.
- [32] Kyle Hounslow. *OpenCV Tutorial: Multiple Object Tracking in Real Time (3/3)*. 2013. URL: <https://www.youtube.com/watch?v=4KY1HgQQAts>.
- [33] Kyle Hounslow. *Tutorial: Real-Time Object Tracking Using OpenCV*. 2013. URL: <https://www.youtube.com/watch?v=bSeFrPrqZ2A>.
- [34] FM Izrailev and BV Chirikov. “Statistical properties of a nonlinear string”. In: *Sov. Phys. Dokl.* Vol. 11. 1. 1966, pp. 30–32.
- [35] Eyal Kenig et al. “Intrinsic localized modes in parametrically driven arrays of nonlinear resonators”. In: *Physical Review E* 80.4 (2009), p. 046202.

- [36] AN Kolmogorov. "On preservation of conditionally periodic motions under a small change in the Hamiltonian function". In: *Dokl. Akad. Nauk SSSR*. Vol. 98. 4. 1954, pp. 527–530.
- [37] MD Kruskal and NJ Zabusky. "Stroboscopic-Perturbation Procedure for Treating a Class of Nonlinear Wave Equations". In: *Journal of Mathematical Physics* 5.2 (1964), pp. 231–244.
- [38] LD Landau, EM Lifshitz, and RJ Donnelly. "Mechanics, Vol. I of Course on Theoretical Physics". In: *American Journal of Physics* 40.7 (1972), pp. 1050–1051.
- [39] Luca Martinelli and Federico Perotti. "Numerical analysis of the non-linear dynamic behaviour of suspended cables under turbulent wind excitation". In: *International Journal of Structural Stability and Dynamics* 1.02 (2001), pp. 207–233.
- [40] J Möser. "On invariant curves of area-preserving mappings of an annulus". In: *Nachr. Akad. Wiss. Göttingen, II* (1962), pp. 1–20.
- [41] Nikolai Nikolaevich Nekhoroshev. "An exponential estimate of the time of stability of nearly-integrable Hamiltonian systems". In: *Russian Mathematical Surveys* 32.6 (1977), pp. 1–65.
- [42] M Onorato et al. "Route to thermalization in the α -Fermi–Pasta–Ulam system". In: *Proceedings of the National Academy of Sciences* 112.14 (2015), pp. 4208–4213.
- [43] Mason A Porter et al. "Fermi, Pasta, Ulam and the Birth of Experimental Mathematics: A numerical experiment that Enrico Fermi, John Pasta, and Stanislaw Ulam reported 54 years ago continues to inspire discovery". In: *American Scientist* 97.3 (2009), pp. 214–221.
- [44] Bob Rink. "Proof of Nishida's conjecture on anharmonic lattices". In: *Communications in mathematical physics* 261.3 (2006), pp. 613–627.
- [45] Bob Rink. "Symmetry and resonance in periodic FPU chains". In: *Communications in Mathematical Physics* 218.3 (2001), pp. 665–685.
- [46] Emilio Segrè. *Enrico Fermi, fisico: una biografia scientifica*. Zanichelli, 1971.
- [47] DL Shepelyansky. "Low-energy chaos in the Fermi-Pasta-Ulam problem". In: *Nonlinearity* 10.5 (1997), p. 1331.
- [48] AJ Sievers and S Takeno. "Intrinsic localized modes in anharmonic crystals". In: *Physical Review Letters* 61.8 (1988), p. 970.
- [49] NJ Zabusky and MD Kruskal. "Interaction of "solitons" in a collisionless plasma and the recurrence of initial states". In: *Physical review letters* 15.6 (1965), p. 240.
- [50] VE Zakharov, VS L'vov, and G Falkovich. *Kolmogorov spectra of turbulence I: Wave turbulence*. Springer Science & Business Media, 2012.